A Comparative Cradle-to-Gate Life Cycle Assessment of Titanium Slag Production with Hydrogen and Coal based Pre-Reduction

Tora Eidsmoen

Master Thesis in Energy

University of Bergen
Geophysical Institute

June 2023

Supervisor: Velaug Myrseth Oltedal
Co-supervisors: Geoffrey Sean Gilpin & Asgeir Sorteberg

Acknowledgments

This thesis concludes my Master of Science in Energy from the University of Bergen (UiB) and was carried out during my fifth and final year of studies.

Bergen, June 2023

Tora Eidsmoen
....
Tora Eidsmoen

Abstract

In light of the pressing challenge of global warming and climate change, emission-intensive industries and sectors seek ways to reduce their environmental footprint and ensure long-term viability in a zero-emission future. This thesis investigates the novel approach of substituting coal with hydrogen as a reducing agent in the production of titanium slag and high purity pig iron from ilmenite in collaboration with Eramet Titanium and Iron AS.

While the environmental impacts of employing hydrogen as a fuel for transportation or reductant in the steel industry have been extensively covered in the literature, its application in the titanium industry remains unexplored, creating a knowledge gap that this thesis seeks to address. Hence, the primary objective of this study is to investigate the environmental impacts of a current and future production process of titanium slag and high purity pig iron using coal and hydrogen as alternative reducing agents. Additionally, three different hydrogen production methods (green, blue, and grey) and their influence on the overall environmental performance of the hydrogen-based production process are investigated. Finally, the environmental impact of titanium slag produced through the traditional direct smelting method is compared with the results obtained in this study.

To assess these objectives, this thesis employs the Life Cycle Assessment (LCA) methodology, with ReCiPe midpoint (H) as the impact assessment method. The functional unit is defined as *one kilogram of chloride slag*. Additionally, results are presented for the co-production of sulfate slag and high purity pig iron.

The LCIA results are presented for eight impact categories, with a particular emphasis on the global warming potential. For the current process utilizing coal as a reductant, 1.52 kg of CO_2 equivalents per kg of chloride slag is obtained. In contrast, employing green, blue, and grey hydrogen as reductants result in 0.46, 0.54, and 0.67 kg of CO_2 equivalents per kg of chloride slag, respectively. Notably, a reduction potential of 69% per kg of chloride slag is achieved when employing green hydrogen as the reductant. Overall, the results demonstrate reduced impacts across all included impact categories for the hydrogen-based processing route compared to the coal-based processing route, with the most significant reduction potential observed when utilizing green H_2.

Table of Contents

List of Abbreviations

GHG	Greenhouse gas
ETI	Eramet Titanium and Iron AS
H2	Hydrogen
CO_2	Carbon dioxide
eq	equivalents
LCA	Life cycle assessment
HPPI	High purity pig iron
TiO_2	Titanium dioxide
wt.%	Weight percent
EAF	Electric arc furnace
Fe	Metallic iron
CO	Carbon monoxide
BF	Blast furnace
BOF	Basic oxygen furnace
DRI	Direct reduced iron
CCS	Carbon capture and storage
GWP	Global warming potential
C-PR	Carbon-based processing route
H-PR	Hydrogen-based processing route
LCI	Life cycle inventory
LCIA	Life cycle impact assesment
ISO	International standardization organization
IPCC	Intergovernmental Panel on Climate Change
NO_x	Nitrogen oxides
SO_2	Sulfate dioxide
1,4-DCB	1,4 dichlorobenzene
MPT	Mining, processing and transportation
GCO	Grand Côte Operations
RoW	Rest of world
tkm	ton kilometer
STP	Standard conditions
VOC	Volatile organic compunds
PAH	Polyaromatic hydrocarbons
PM	Particulate matter
HM	Heavy metals
AEL	Alkaline electrolysis
LHV	Lower heating value
SMR	Steam methane reforming
MDEA	Methyl diethanolamine
WGS	Water gas shift reaction
HT + LT	High temperature + Low temperature
SSB	Norway Statistics

1 Introduction

1.1 Motivation and background

In our commitment to mitigating climate change bound by the Paris Agreement, Norway has committed to reduce emissions of greenhouse gases (GHG) by at least 55% by 2030 compared to the 1990 levels and reach net-zero by 2050 [1]. By the end of 2021, emissions had been reduced by 4.7% [2]. To achieve the emission reduction target, large-scale structural changes must be implemented across all economic sectors rapidly.

The most significant decrease in GHG emissions since 1990 has been seen in the land-based industrial sector, which currently accounts for approximately 24% of the Norwegian GHG emissions [2]. Due to several driving forces, such as the EU Emissions Trading System, CO_2 taxation, and increased environmental regulations [3], the majority of the potential for reductions in GHG emissions in the industrial sector using available technology has been exhausted [4]. To ensure further emission reduction and the long-term viability of emission-intensive industries, innovative low-emission technologies must be developed and implemented.

"We want to be here in 20 years."

- Harald Grande, Former Managing Director at ETI[1]

Eramet Titanium and Iron AS (ETI), located in Tyssedal, is pioneering one such innovative project. ETI aims to substitute coal with hydrogen (H_2) as the reducing agent in the production of titanium slag and high purity pig iron (HPPI) from ilmenite, consequently achieving a substantial reduction in carbon dioxide (CO_2) emissions [6]. ETI currently contributes to 0.56% of the national GHG emissions through its production process [7]. Decarbonization is essential to ensure the survival of carbon-intensive industrial operations such as ETI in a low-emission society, as pointed out by Harald Grande (former managing director at ETI).

ETI's H_2 project is the first attempt to commercialize hydrogen-based reduction of ilmenite at a global level, which has led to great attention both nationally and internationally. It has been approved as an "*Important project of common European interest*" (IPCEI) in the H_2-technology value chain and granted financial support from Enova [6]. The multi-year development project has been under research for several years. Its current stage involves testing in a lab-scaled facility, which is planned to be scaled to an on-site process pilot in Tyssedal by 2026.

---

[1] Kloden Brenner – Hva må gjøres? (Heikki Eidsvoll Holmås, 2021) [5]

In light of the urgency to achieve substantial reductions in GHG emissions, the importance of investigating the environmental impacts of new technology is emphasized. To make informed decisions, it is essential to understand the potential environmental benefits and trade-offs of new technology over its lifecycle prior to being implemented. This thesis sets out to do just so for the hydrogen-based reduction of ilmenite by employing the life cycle assessment (LCA) methodology in collaboration with Eramet Titanium and Iron AS.

The following sections provide the necessary background for the research question posed in this thesis, which is presented at the end of Chapter 1.

1.1.1 Introduction to the titanium industry

ETI primarily produces titanium slag and HPPI through the beneficiation of ilmenite ($FeTiO_3$) [6]. Ilmenite is predominately comprised of titanium- and iron oxides and is the most abundant naturally occurring titanium compound [8]. The primary application of titanium slag is as feedstock in producing titanium dioxide (TiO_2) pigment and certain production processes for titanium metal [9]. Both products play an important role in modern society due to their unique properties and versatile applications in various industries, ranging from aerospace and biomedical to cosmetics and building materials.

Several alternative production routes exist to produce TiO_2 pigment and titanium metal, some of which are illustrated in Figure 1.
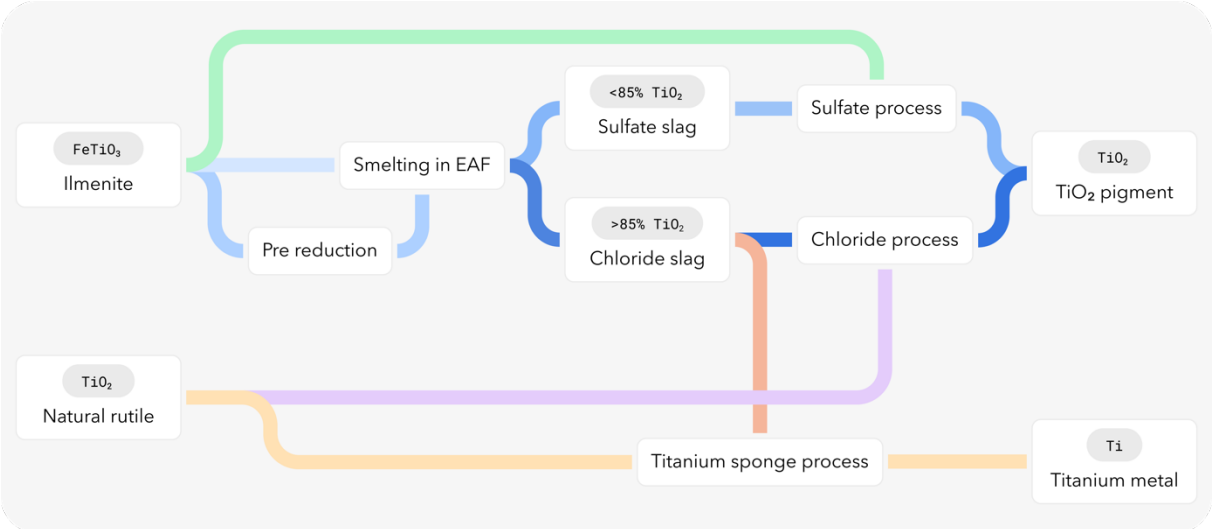
Figure 1 Alternative production routes for TiO₂ pigment and titanium metal. EAF = electric arc furnace.

Two commercial processes currently exist for producing TiO_2 pigment: the sulfate and chloride processes, as illustrated in Figure 1. These differ in both raw material requirements and process chemistry [9]. While it is possible to use ilmenite directly as feedstock in the sulfate process, the chloride process requires feedstock containing higher percentages of TiO_2 than what is found in natural ilmenite. This can be achieved through the beneficiation

of ilmenite to titanium slag, as done at ETI in Tyssedal. The TiO_2 content of titanium slag varies. To be suitable for the chloride process, it must contain above 85% TiO_2. Conversely, the sulfate process allows for the use of titanium slag with lower TiO_2 percentages, as well as ilmenite directly. Hence, the distinction between chloride slag and sulfate slag arises from the different subsequent processes in which they are utilized, and the percentage of TiO_2 serves as a distinguishing factor. The term *titanium slag* encompasses both chloride slag and sulfate slag. Chloride slag is also utilized as feedstock in titanium sponge production for titanium metal [10].

Alternatively, natural rutile can be used as feedstock in the chloride process, and titanium metal production [11]. Natural rutile contains close to 100% TiO_2, making it the preferred feedstock in terms of chemical composition. However, it is a far scarcer resource than ilmenite [12], and this production route alone could not sustain the current consumption rate of TiO_2 pigment. Hence, titanium slag poses a sustainable alternative in terms of resource utilization.

1.1.2 Introduction to titanium slag production

To extract the titanium from ilmenite, a reduction reaction is initiated, where a reducing agent is utilized to form a stronger chemical bond with oxygen and thereby remove oxygen from the compound [13]. A reducing agent is defined by its ability to donate electrons (i.e., its reduction potential), causing a reduction in the oxidation state [14]. Carbon inhabits a high reduction potential and is commonly utilized reductant in various industrial applications.

Titanium slag is most commonly produced, in short, by smelting of ilmenite in electric arc furnaces (EAF) using carbon-based reductants [15], [16]. An endothermic reduction reaction is induced by the presence of carbon and heat generated within the EAF, and the iron oxides contained in the ilmenite are reduced to metallic iron that can be separated from the TiO_2. The following simplified reaction equation describes the overall process:

$$FeTiO_3(s) + C(s) \rightarrow Fe(l) + TiO_2(l) + CO(g) \qquad (1.1)$$

As described by eq. (1.1), smelting of ilmenite yields metallic iron (Fe) and carbon monoxide (CO), in addition to titanium slag containing 70-94% TiO_2. The molten iron can be further refined to HPPI, which is produced as a valuable co-product. The resulting CO gas is highly toxic and typically managed through thermal oxidation to form CO_2, which is subsequently emitted into the atmosphere. Hence, the current production of titanium slag is associated with a significant carbon footprint.

The ilmenite charged to the EAF can either be raw or pre-reduced, meaning that the iron oxides contained in the ilmenite undergo a solid-state reduction reaction prior to being

charged to the EAF [17]. Pre-reduction is found to increase the efficiency in the smelting phase, as the primary endothermic reduction process is shifted upstream [13], [18]. ETI is currently the only titanium slag facility that operates with a pre-reduction phase, which is also known as the "*Tyssedal process*".

1.1.3 Hydrogen as a reducing agent

H_2 inhibits good reduction properties and is posed as an alternative to reduce carbon emissions in industrial processes which are currently carbon-intensive, such as the steel industry [19]-[20]. Steel is predominantly produced through a combination of a blast furnace (BF) and a basic oxygen furnace (BOF). Due to its dependence on carbon, this processing route is not compatible with the net-zero emission target. Utilizing H_2 as a reductant in a direct reduction process (DRI) is found to be the most promising alternative steel production route [21], [22]. The Circored technology is currently the most developed DRI process, which involves a solid-state reduction process of the iron ore in a fluidized bed reactor [22]. Several studies suggest that similar technology is applicable to titanium slag, as both processes involve the reduction of iron oxides [13], [24]. Utilizing H_2 in such a process has been shown to reduce up to 90% of the iron oxides contained in the ilmenite in a solid state reduction [23], following eq. (1.2):

$$FeTiO_3(s) + H_2(g) \rightarrow Fe(l) + TiO_2(l) + H_2O(g) \tag{1.2}$$
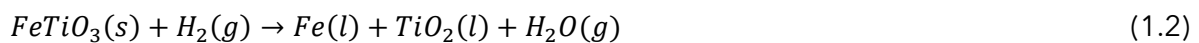
Using H_2 to reduce ilmenite offers clear environmental benefits, as it does not generate CO_2 emissions. Additionally, studies suggest that feeding hot and pre-reduced ilmenite into the EAF increases the efficiency of the smelting phase, yielding a reduced electricity consumption [25], [24].

1.1.4 Introduction to hydrogen production

Availability and utilization of low-emission H_2 is a vital part of the decarbonization of several sectors both in a Norwegian and European context, which is strongly emphasized by the European Green Deal with the European Hydrogen Strategy [20], as well as the Norwegian Hydrogen strategy [26]. The objective of the European Commission is to increase the share of low-emission H_2 in the European energy mix from the current rate of 1% to 14% by 2050 to reach the net-zero target. Currently, 85% of the H_2 produced is generated on-site for specific industrial applications [27]. As a result, the open market for H_2 remains relatively small.

The European Hydrogen Strategy aims to establish a more robust H_2 economy, including infrastructure for H_2 production, transportation, and storage, as well as supporting the development of H_2-based technologies [20]. However, to establish H_2 as a feasible decarbonization solution, the production must be sustainable. Currently, 96% of all H_2 is produced from natural gas [28], commonly referred to as *grey* H_2, which is associated with

substantial CO_2 emissions. The remaining four percent is produced through water electrolysis, where electricity separates the H_2 and oxygen (O) in water molecules. H_2 produced through water electrolysis employing renewable electricity, commonly referred to as *green* H_2, is associated with a low environmental footprint compared to grey H_2.

The urgency of large-scale low-emission H_2 production has been further accelerated by the RePowerEU plan [29], published in response to the recent energy crisis resulting from the Russian invasion of Ukraine. While the European Hydrogen strategy emphasizes the preference for green H_2, meeting the estimated demand for H_2 through water electrolysis will require a significant capacity expansion of renewable energy at a rapid pace. In light of this, *blue* H_2 production has gained attention as a transitional alternative. Blue H_2 is produced through the same method as grey H_2 but utilizes carbon capture and storage (CCS) technology to capture CO_2 emissions and thus lowering the carbon footprint [20]. As the production technology and infrastructure are already operable from grey H_2 production, it can be argued that blue H_2 can provide a more immediate solution to decarbonizing industries requiring large amounts of H_2.

1.1.5 Introduction to life cycle assessment

This thesis LCA, which is a structured and comprehensive methodology used to evaluate the environmental impacts associated with a product or process throughout its life cycle [30]. The life cycle of a product spans from raw material extraction, processing, production, distribution, use-phase and end-of-life treatment, recycling, and disposal, as illustrated in Figure 2. This is commonly referred to as a cradle-to-grave perspective.
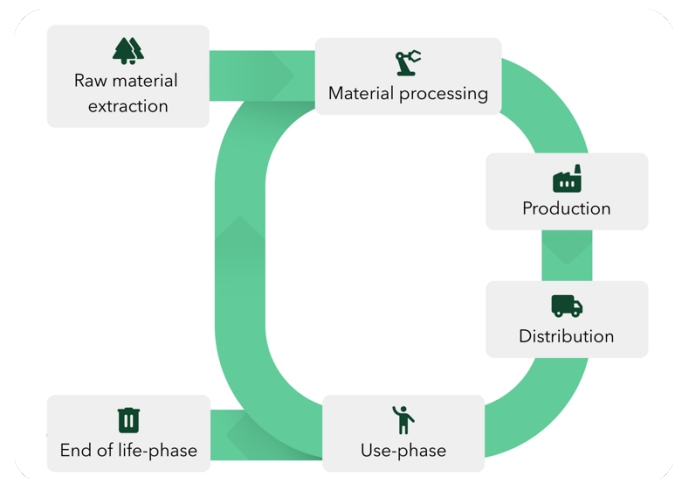
Figure 2 Illustration of the life cycle of a product.

LCA is increasingly used by engineers to evaluate the environmental impacts and performance of different technologies. In doing so, an enhanced understanding of the benefits and potential trade-offs of implementing technology can be facilitated, enabling a more informed decision-making process for stakeholders. Chapter 2 provides an in-depth description of the LCA methodology.

1.2 The environmental impacts of titanium slag production (literature review)

A literature review of relevant studies covering the environmental impact of titanium slag has been conducted. No LCA study explicitly focusing on titanium slag has been found in the literature. Titanium slag production is, however, included as part of the system boundary in studies covering TiO_2 pigment and titanium metal production, which are presented in the following sections. First, the reviewed studies covering titanium slag production using carbon as a reductant in an EAF are presented. Then, one study assessing the environmental impacts of titanium slag using H_2 as a reductant is introduced.

1.2.1 Studies on commercial carbon-based titanium slag production processes

The first LCA on TiO_2 pigment production was conducted by Reck and Richards et al. [31], and investigated six different production routes utilizing various feedstocks, including the use of titanium slag in the sulfate and chloride route. No results specifically pertaining to titanium slag are presented. Of the investigated processing routes, utilizing titanium slag as feedstock was found to have the largest gross energy requirements. Additionally, it was found that titanium slag generated the least waste of the assessed feedstock alternatives due to the co-production of HPPI.

Liao et al. [32] published an LCA case study of TiO_2 pigment production, which assessed the resource use in the sulfate and chloride production route using titaniferous magnetite upgraded to titanium slag as feedstock. The study provides no results specifically pertaining to titanium slag production.

Middlemas et al. [33] published an LCA study comparing the energy requirements and CO_2 emissions from an emerging processing option, alkaline roasting to upgrade titanium slag, with the traditional processing options to produce TiO_2 pigment from titanium slag. The study presents a CO_2 emission rate of 2.25 kg CO_2 per kg titanium slag. The percentage of TiO_2 contained in the titanium slag is not specified.

Gao et al. [10] published the most recent LCA study that includes titanium slag production. The study investigated the production of titanium sponge (i.e., raw material for manufacturing titanium alloys) through the Kroll process in China using hard rock ilmenite. The study is the most comprehensive LCA of the reviewed literature, offering a complete LCI alongside detailed and transparent results. The ReCiPe method was employed, and results are presented for eight midpoint categories. The concentration of TiO_2 in the titanium slag is not specified by percentage. It is, however, described as "high-grade titanium slag" and therefore assumed to contain >85% TiO_2. Co-production of HPPI is not included in the system boundary. A GWP of 2.23 kg CO_2equivalents (eq) per kg chloride slag is displayed, including the mining and processing of ilmenite.

Charikinya et al. [34] published an LCI report on the primary production of precious and scarce metals in South Africa in collaboration with the ecoinvent Association, which includes the beneficiation of ilmenite to titanium slag at 85% TiO_2 (i.e., chloride slag). The report applies the LCA methodology with a cradle-to-gate approach, using data from the Rio Tinto RBM operations, which accounts for 25% of the global titanium slag production. Rutile and zircon concentrate is produced as co-products from the beneficiation of heavy mineral sands, and HPPI is produced as a by-product from the smelting of ilmenite. The multifunctionality is solved by allocation based on the weight percent (wt.%) of the produced products (i.e., mass allocation). The LCI is employed as a dataset in the ecoinvent database. When assessing the LCIA of this dataset using the ReCiPe midpoint (H) method, a GWP of 1.56 kg CO_2eq per kg chloride slag is obtained.

1.2.2 Studies on novel hydrogen-based titanium slag production processes

Orth et al. [24] published a study covering energy savings and CO_2 emissions from a hydrogen-based titanium slag production process [24]. The data is obtained from a demonstration plant of the Circosmelt® process, patented by Outotec, which is based on a pre-reduction of ilmenite in a circulating fluidized bed and smelting in an EAF. The study does not employ the LCA method. An emission rate of 1.54 kg CO_2 per kg titanium slag is presented, where 53% of this is associated with electricity production.

1.3 Objectives and scope of the study

Several studies investigating the environmental impacts of steel production using H_2 as a reductant have been conducted [22], [35]-[36]. However, as seen in the literature review, only one study investigating the environmental impacts of titanium slag production using H_2 has been found in the existing literature [24], which is perceived to be limited in its scope and data availability. To evaluate the environmental impacts of titanium slag production using H_2 as a reducing agent, a more comprehensive analysis needs to be conducted. For this, LCA is considered to be the most appropriate method.

To address the current research gap, this thesis employs LCA methodology to assess and compare the environmental impacts of titanium slag produced through a carbon-based processing route (C-PR) and hydrogen-based processing route (H-PR), using data provided by Eramet Titanium and Iron AS. The following research question is raised:

How does titanium slag produced through pre-reduction of ilmenite using coal (C-PR) and hydrogen (H-PR) as alternative reducing agents compare in terms of environmental impacts?

Hence, the primary objective of the study is to generate quantitative life cycle data on titanium slag produced through the current production process at ETI (i.e., C-PR) and future

process (i.e., H-PR) and assess the environmental impact associated with each production route through the LCA methodology.

Given the discrepancies in environmental impacts of H_2 production methods, the effect of utilizing H_2 produced through different methods should also be assessed. Green H_2 is primarily intended at ETI, but given the ongoing debate on blue H_2, the effect of employing both alternatives should be considered. Additionally, grey H_2 should be assessed as this is currently the production method for nearly all H_2 available for purchase.

Furthermore, Eramet Titanium and Iron AS is currently the sole facility incorporating an additional pre-reduction phase in its operations, and investigating the environmental impacts associated with this production route compared to the direct smelting route would provide valuable insights.

Hence, two secondary objectives are presented:

The first secondary objective of the study is to *explore the environmental impacts associated with green, blue, and grey H_2 and incorporate this into the LCI of titanium slag produced through the H-PR*. By considering different H_2 production methods, this objective aims to enhance the value and comprehensiveness of the environmental assessment.

The last secondary objective is *to examine the environmental impact of titanium slag produced through the traditional method of direct smelting without the pre-reduction process and compare these with the results obtained from this study*. This comparison will contribute valuable insights into the environmental performance of the additional pre-reduction process for titanium slag production.

Through these objectives, this study aims to enhance the understanding of established and emerging technologies within the titanium industry regarding environmental sustainability.

1.4 Structure of work and outline of the thesis

An overview of the workflow is provided in Figure 3.

Conceptualization
Identify knowledge gaps in literture.
Proposal of project to ETI.

Research
The titanium slag industry.
H_2 as a reducing agent.
Investigate ETI's current process

Data collection
Acquisition and compiling of LCI data.
Revising of data in conjunction with ETI.

Building of LCI model
Build LCI model in Simapro.

Analysis
Evaluation of data quality.
Contribution and sensitivity analysis.

Figure 3 Illustration and description of the workflow of the thesis.

The initial phase involved the conceptualization of the master thesis, which encompassed research to identify knowledge gaps in the literature pertaining to the environmental impact of hydrogen applications. As a result, ETI's hydrogen project was recognized as a potential project, and an LCA study was proposed to ETI. During this master thesis, considerable effort was dedicated to developing an understanding of the industrial process and the acquisition and compiling of process data from ETI, both of which was essential to establish a robust and representative life cycle inventory (LCI). This involved multiple on-site visits to ETI in Tyssedal. During this work, detailed process schemes were developed and revised by representatives from ETI.

The thesis is structured according to the phases of an LCA study, which includes the following:

- o Goal and scope
- o Life cycle inventory (LCI)
- o Life cycle impact assessment (LCIA)
- o Interpretation of results

Hence, the structure of this thesis deviates from the IMRaD structure. Notably, the methodology chapter (Chapter 2) provides a theoretic explanation of the LCA methodology, while the method used in this thesis is outlined in the goal and scope (Chapter 3) and the LCI (Chapter 4). Additionally, the interpretation chapter is referred to as *discussion*.

2 Methodology

The following chapter presents the LCA methodology used to assess the research question posed in this thesis.

2.1 Life Cycle Assessment methodology

The LCA methodology is standardized by the International Organization for Standardization (ISO) in the ISO 14040:2006 [30] and 14044:2006 [37], and is defined as a method that:

"…*assesses, in a systematic way, the environmental aspects and potential environmental impacts of a product throughout its life cycle from raw material acquisition to final disposal*."

Essentially, an LCA quantifies the effect on the biosphere (i.e., the natural environment) resulting from changes in the technosphere (i.e., human activities) [38]. Conducting an LCA involves defining a product, process, or service through models that describe the elements of its physical system [30], [39]. To assess the environmental impact, the investigated system is divided into unit processes that describe the smallest elements considered in the study. For each unit process, input- and output flows, such as energy, materials, emissions, and waste streams, are identified and compiled into a complete LCI. From the LCI data, a model representing the life cycle of the system is constructed using LCA software. The computational structure of LCA is based on linear algebra, and the environmental impacts associated with the analyzed system are quantified by applying a set of mathematical equations that translate the LCI data into related environmental impact categories depending on the selected impact assessment method.

A functional unit is defined in each LCA study, which enables a better comparison of the environmental performance of different product systems [38]. The functional unit is based on the provided functions of the system under investigation and is the reference unit upon which the environmental impact of the system is expressed. It is essential to acknowledge that the LCA methodology does not predict absolute or precise environmental impacts but rather emphasizes consistency when comparing different alternatives [39].

The LCA methodology consists of four separate phases [30]: goal and scope definition, life cycle inventory (LCI), life cycle Impact assessment (LCIA), and interpretation of results, as illustrated in Figure 4.
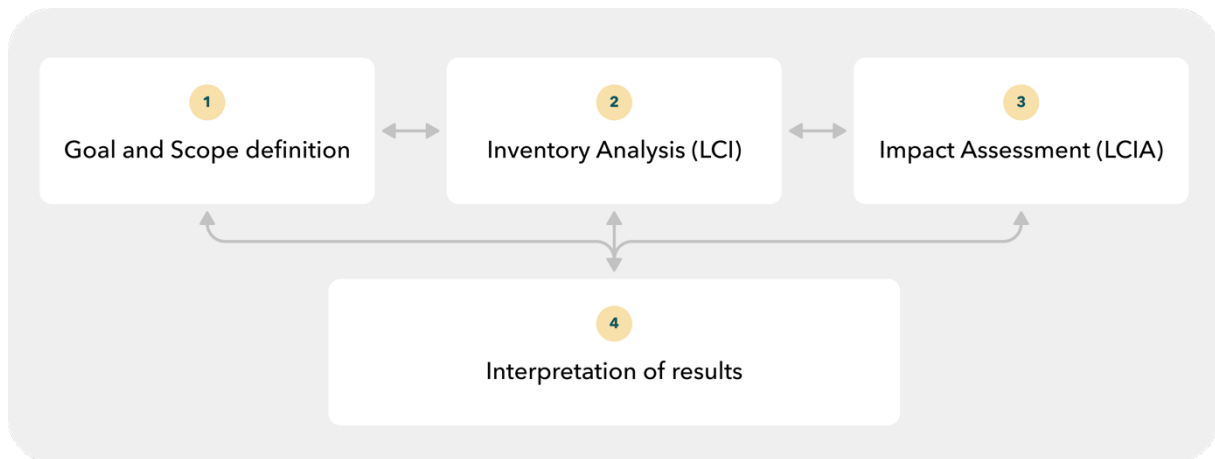
Figure 4 Illustration of the phases of the LCA methodology.

As indicated by the arrows, the different phases of LCA are not independent but rather an iterative process, where alterations to each phase are made throughout the study. The following sections provide further explanation of each phase.

2.1.1 Goal and scope

The goal and scope is the first phase of an LCA in which the fundamental framework is defined [39]. This is regarded as the most important phase, as it provides information with respect to the system under investigation, LCI and LCIA methodology, limitations of the study, and data quality. In doing so, the goal and scope facilitate the correct interpretation of the results as well as consistency and reproducibility [39].

The goal definition primarily aims to define the application, reasons for conducting the LCA, as well as the intended audience [39]. An LCA analysis can be conducted for various reasons, such as quantifying a product's environmental impacts and investigating environmental hotspots in the production chain or comparing products or processes in terms of environmental impacts. Two different modeling frameworks can be applied to an LCA: attributional and consequential. Attributional LCA models focus on the part of the global environmental burdens that should be assigned to the specific product or process [40]. In contrast, consequential LCA models account for the changes in the market and production processes that are theoretically expected to occur due to the analyzed system. Hence, it aims to reflect the impacts of the system on the global environment.

The choice of modeling framework should reflect the intended application of the LCA. This depends on whether the study will serve as decision support and the scale of the decision context [39]. For example, if the LCA aims to inform a political decision with significant consequences, the modeling framework should accurately reflect this context, and consequential modeling should be applied. Conversely, if the LCA aims to identify environmental hotspots within a production process, an attributional modeling framework would be more suitable. In short, the choice of modeling framework in an LCA study must

align with the intended application and the scale of the decision context, which is defined by the goal definition.

The scope of the study aims to identify and describe the system under investigation in detail and includes a definition of the system boundary that defines which life cycle stages, unit processes, and elementary flows are included in the LCI [39]. In addition, the scope includes the function of the product system, which forms the basis for the functional unit. If the system under investigation is not mono-functional (i.e., several co-functions exist), the scope should include the selected approach to solve the multifunctionality. The following hierarchy is established by ISO14044 [37]:

1) Subdivision
2) System expansion
3) Allocation

The first approach is subdivision, which refers to the subdivision of unit processes into mono-functional unit processes which are isolated from the extensive product system, thereby allowing the creation of an LCI specific to one product [40]. This is the preferred approach by the ISO standards as it accurately reflects the impacts caused by the studied system without any distortion from external parameters [41]. However, the complex and multifunctional nature of certain processes hinders the possibility of this approach being the sole solution. The second approach, system expansion (alternatively referred to as substitution), involves subtracting the LCI of an alternative production route of the co-function(s) from the complete LCI of the investigated system, thereby creating a mono-functional process. The third approach is allocation, which pertains to the distribution of input and output flows between the co-functions according to a selected criterion (e.g., physical properties, market value, etc.). The selected approach for multifunctionality should be based on the intended application and selected modeling framework (i.e., attributional or consequential) defined in the goal definition.

2.1.2 Life cycle inventory (LCI)

The LCI phase involves the collection and calculation of data related to the system under investigation [39]. The type of data collected is dependent on the modeling framework selected. For each unit process, input and output flows related to energy use, raw materials, ancillary materials, waste, emissions to air, and discharges to water and soil are quantified according to the defined system boundary [30]. Both numerical and descriptive data are collected and related to the functional unit, which is used to construct a model of the system using LCA software. The principle of mass balance is applied to each unit process to ensure completeness of the collected data.

The system boundary defined by the scope of the LCA can be categorized as the foreground and background system, where the foreground system refers to the processes which are specific to the product being modeled. Primary data should be collected for the processes that constitute the foreground system, as secondary LCI data cannot be used for the foreground system without compromising the quality of the LCA [39]. The background system pertains to the processes upstream or downstream of the foreground system, which indirectly affects the investigated product, process, or service. Generic- or market-average LCI data found in commercial databases, such as ecoinvent, is sufficient to represent background system processes [40].

2.1.3 Life cycle impact assessment (LCIA)

The life cycle impact assessment (LCIA) phase aims at "*understanding and evaluating the magnitude and significance of the potential environmental impacts for a product system (….)*" [30]. The interpretation of the environmental impact is achieved through several mathematical computations, for which LCA software is utilized.

The following eq. (2.1) presents the mathematical basis of LCA:

$$(I - A)^{-1} \cdot f = x \qquad\qquad (2.1)$$

Where A is the technology matrix representing each product or process in the background data, and $(I - A)^{-1}$ is the Leontief inverse of the technology matrix A [40], [42]. The Leontief matrix represents the amount of output needed for one unit of each element in the technology matrix A. The f vector represents the inventory of the product/process under evaluation, and the x vector represents the necessary amount of output needed to provide the final demand of f (i.e., the functional unit).

To calculate the total emissions related to the functional unit, the intervention matrix B is multiplied by the final demand vector x [40], [42]. The intervention matrix B consists of the individual environmental flow intensities per unit output for each background process in the technology matrix A. This is expressed by the following eq. (2.2):

$$B \cdot x = g \qquad\qquad (2.2)$$

The g vector represents all environmental flows generated from the foreground and background system for the provision of f (i.e., the defined functional unit) [40], [42]. The environmental flows are classified into impact categories depending on the environmental stressors associated with each flow. Numerous impact assessment methods exist, each with its own set of impact categories and structure. The following will focus on the ReCiPe 2016 midpoint (H) method [43], as this is the one applied in this thesis.

To translate the emissions described by vector g to impact categories, a characterization matrix C is applied, as described by the following eq. (2.3):

$$C \cdot g = h \tag{2.3}$$

The characterization matrix C aggregates environmental flows into impact categories and scales them with respect to intensity [40], [42]. For instance, dinitrogen monoxide (N_2O) is aggregated to the impact category global warming potential (GWP) and scaled as 298 more intensive than CO_2 [43]. The h vector is the final impact vector, representing the characterized environmental impacts of the functional unit [40], [42].

The classification of environmental flows into impact categories and their characterization factors are based on scientific best-guesses, which implies that some uncertainties are inherent in this framework [40]. Certain impact categories are supported by more substantial scientific evidence, such as climate change, due to the robust understanding of the effect of GHG emissions on global warming provided by the Intergovernmental Panel on Climate Change (IPCC).

Table 1 presents the 18 impact categories defined by the ReCiPe 2016 midpoint (H) method and the corresponding indicator and unit [43]. The eight impact categories highlighted in Table 1 are included in this thesis. The decision basis for this is described in Section 3.2.5.

Table 1 The 18 impact categories defined by the ReCiPe 2016 midpoint (H) method and the corresponding indicator and characterization factor. The categories included in this thesis are highlighted. Explication of the units for the remaining categories are provided.

Impact category	Indicator	Characterization factor	Unit
Climate change	Infra-red radioactive forcing increase	Global warming potential	kg CO_2eq to air
Stratospheric ozone depletion	Stratospheric ozone decrease	Ozone depletion potential	kg CFC-11eq to air
Ionizing radiation	Adsorbed dose increase	Ionizing radiation potential	kBq Co-60 eq to air[2]
Fine particulate matter formation	PM2.5 population intake increase	Particulate matter formation potential	kg PM2.5eq to air[3]
Ozone formation: terrestrial ecosystems	Tropospheric ozone increase (AOT40)	Photochemical oxidant formation potential: ecosystems	kg NO_xeq to air

---

[2] Kilobecquerels cobalt-60 isotope
[3] Kilogram particulate matter with < 2.5*10^-6 meter (μm) width

Ozone formation: human health	Tropospheric ozone population intake increase (M6M)	Photochemical oxidant formation potential: humans	kg NOₓeq to air
Terrestrial acidification	Proton increase in natural soils	Terrestrial acidification potential	kg SO$_2$eq to air
Freshwater eutrophication	Phosphorus increase in fresh water	Freshwater eutrophication potential	kg P eq to fresh water[4]
Marine eutrophication	Dissolved inorganic nitrogen increase in marine water	Marine eutrophication potential	kg N eq to marine water[5]
Human carcinogenic toxicity	Risk increase of cancer disease incidence	Human toxicity potential	kg 1,4- DCBeq to urban air
Human non-carcinogenic toxicity	Risk increase of noncancer disease incidence	Human toxicity potential	kg 1,4- DCBeq to urban air
Terrestrial ecotoxicity	Hazard weighted increase in natural soils	Terrestrial ecotoxicity potential	kg 1,4- DCBeq to industrial soil
Freshwater ecotoxicity	Hazard weighted increase in fresh waters	Freshwater ecotoxicity potential	kg 1,4- DCBeq to fresh water
Marine ecotoxicity	Hazard weighted increase in marine water	Marine ecotoxicity potential	kg 1,4- DCBeq to marine water
Land use	Occupation and time integrated transformation	Agricultural land occupation potential	m2 ×yr annual crop land
Water use	Increase of water consumed	Water consumption potential	m3 water consumed
Mineral resource scarcity	Ore grade decrease	Surplus ore potential	kg Cu eq[6]
Fossil resource scarcity	Upper heating value	Fossil fuel potential	kg oil

The following provides a brief description of the highlighted impact categories:

---

[4] Kilogram phosphor equivalents
[5] Kilogram Nitrogen equivalents
[6] Kilogram copper equivalents

2.1.3.1 Global warming potential (climate change)

The climate change impact category assesses the potential contribution of various substances to global warming through their contribution to the greenhouse effect. The intensity of each substance is defined relative to one kg CO_2.

2.1.3.2 Stratospheric ozone depletion

The stratospheric ozone depletion pertains to the amount of ozone a substance can deplete in the stratosphere relative to one kg CFC-11 (trichlorofuoromethane). CFC-gasses are chemicals that contain carbon, chloride, and fluorine atoms.

2.1.3.3 Ozone formation (human health and terrestrial ecosystems)

Ozone formation pertains to the formation of ground-level ozone that can occur in the presence of nitrogen oxides (NO_x) or volatile organic compounds (VOC) and sunlight. Exposure to ground-level ozone can influence both human health and terrestrial ecosystems. The intensity is defined relative to that of one kg NO_x.

2.1.3.4 Terrestrial acidification

The terrestrial acidification impact category pertains to the deposition of acidifying substances, primarily sulfur dioxide (SO_2) and NO_x, onto land surfaces and the subsequent effect on soil and vegetation. The intensity of these substances is related to that of one kg SO_2.

2.1.3.5 Toxicity (terrestrial, marine and human non-carcinogenic)

The impact categories related to toxicity pertain to the effect of exposure to various toxic substances on human health, marine ecosystems, and terrestrial ecosystems. The toxicity potential is related to the effect of one kg 1,4-dichlorobenzene (1,4-DCB).

The impact categories presented in Table 1 address environmental concerns at the midpoint level. The ReCiPe 2016 method enables aggregation of midpoint categories into three endpoint categories: damage to human health, damage to ecosystems, and damage to resource availability [43]. While this aggregation provides categories that can be easier to interpret, it also increases the uncertainty of the outcome. Hence, this thesis will present the results at the midpoint level. Additionally, the ReCiPe 2016 method provides three alternative value choices that affect the characterization factors: the individualist (I), hierarchist (H) and egalitarian (E) perspective. These differ in value choices made in the modeling of the effect of the substances for each impact category, such as time-horizon and included effects. This thesis employs the hierarchist perspective as it is "based on a scientific consensus regarding the time frame and plausibility of impact mechanisms" [43].

2.1.4 Interpretation

The interpretation phase aims to identify significant issues and uncertainties, assess the overall reliability of the study and interpret the results in light of the defined goal and scope [39]. Hence, the phase provides transparency to the LCA.

Identification of the most significant impact categories, unit processes, and sub-processes based on their environmental impacts is made through a contribution analysis. To evaluate the uncertainties of the LCA, a sensitivity analysis is conducted to assess the effect of the parametrical choices made regarding these processes. Additionally, the sensitivity analysis provides insights into the potential benefits and drawbacks of different measures that can be taken to improve the environmental impacts of the product or process.

In every LCA, it is important to acknowledge that the methodological choices and quality of the available data heavily influence the outcome of the analysis [39]. Hence, the representativeness, completeness, and consistency of the data should be transparently evaluated.

3 Goal and scope definition

3.1 Goal definition

This subchapter derives the goal of the LCA as a continuation of the research question presented in Chapter 1. The LCA is performed under the guidance of the ISO framework for LCA [30], [37] and the European Commission's International Reference Life Cycle Data System (ILCD) Handbook [39], and is thus consistent in its methods, assumptions and data.

As described in Section 1.1.2, the term titanium slag pertains to both chloride slag and sulfate slag. From here on, titanium slag describes both products, while titanium slag at >85 wt.% TiO_2 is referred to as *chloride slag* and titanium slag at <85% TiO_2 is referred to as *sulfate slag*.

The aim of the LCA is to analyze and compare the cradle-to-gate environmental impacts associated with titanium slag production with pre-reduction in Western Norway when coal is exchanged for hydrogen (H_2) as a reducing agent. To do so, two alternative processing routes are investigated and analyzed: Carbon-based processing route (C-PR) and hydrogen-based processing route (H-PR). Additionally, three alternative H_2 production methods are investigated: alkaline electrolysis of water using hydropower (green H_2), steam methane reforming (SMR) of natural gas utilizing carbon capture and storage (CCS) (blue H_2) and SMR without CSS (grey H_2). Figure 5 presents an overview of the analyzed system, where [a] pertains only to the C-PR and [b] pertains only to the H-PR.
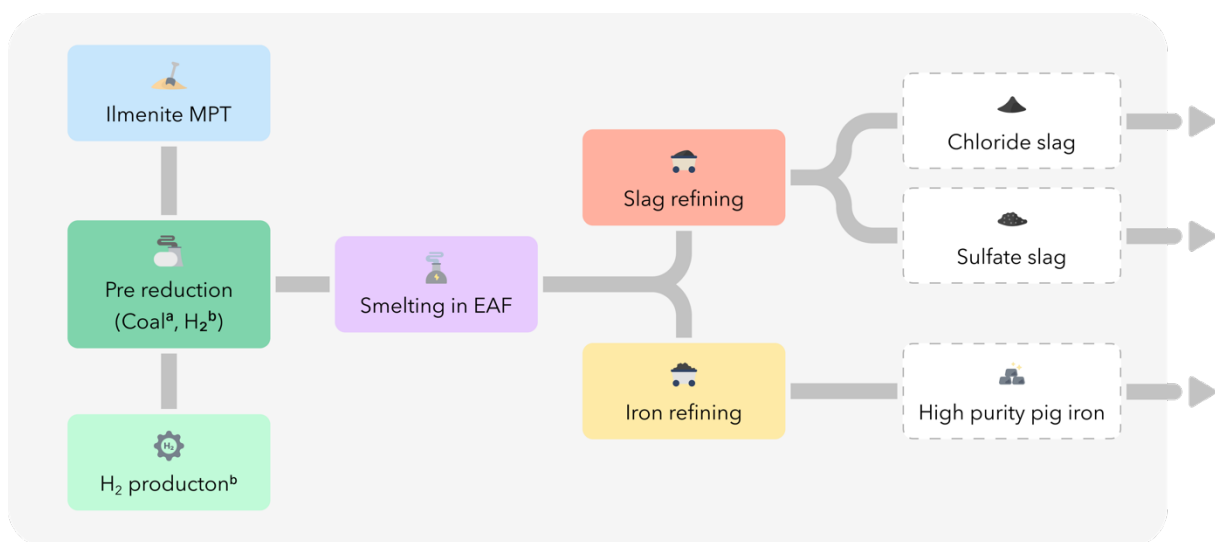
Figure 5 Overview of the process of the analyzed system. The processes market with [a] pertains only to C-PR and [b] pertains only to H-PR. EAF refers to an electric arc furnace.

This LCA is characterized as a micro-level decision support study, and the LCI modeling framework adopted is attributional in accordance with the guidelines in the ILCD handbook [39]. The basis for this decision is as follows: The provided comparison is intended to be

used as decision support by ETI on developing the H-PR in Tyssedal. Such development would have the largest impact on the consumption rate of coal and H_2. The annual consumption of coal is estimated to be reduced by 97%, from 92 thousand tons to 2.9 thousand tons. In comparison, the total consumption of coal in the EU was 449 million tons in 2021 [44]. Hence, the quantity of coal purchased by ETI to obtain the current production rate is estimated to be insignificant (0.02%) in the context of the coal market in Europe, and no large-scale structural changes beyond the investigated system are assumed to be caused. Additionally, the annual consumption rate of H_2 is estimated to be approximately 10 thousand tons for the H-PR, which is non-marginal compared to the current production rate of green H_2 in Europe, which is less than 0.3 million tons [45]. However, several reports analyzing the future H_2 market suggest that by 2030, the H_2 economy will be substantially more prominent compared to current levels [46], which is strengthened by The European Commission's proposal to produce 10 million tons of green H_2 by 2030 [20]. The same argument pertains to the production of H_2 in Norway [26]. Hence, the demand for H_2 caused by the development of H-PR is assumed to have no large-scale structural impact the H_2 market.

Therefore, the decision upon which this LCA is conducted to support is assumed to cause no significant structural changes beyond the foreground system, and an attributional modeling framework is found applicable. This decision can lead to limitations with regard to the transferability and extension of results and conclusions, which will be discussed in Chapter 7. Additional limitations result from the variance in technological maturity between C-PR (commercial) and H-PR (lab-scale). While H-PR relies on data from bench scale values and theoretical calculations, C-PR data is directly obtained from a full-scale operating facility. The largest uncertainties arising from this discrepancy in data quality are tested as part of a sensitivity analysis presented in Subchapter 7.2, where the parametrical choices made in the modeling of the main results are assessed. In the sensitivity analysis, the main results will be referred to as the *base-case results*. From this analysis, a best- and worst-case scenario is constructed.

Besides providing a comparison of specific titanium slag production paths, the results will be valuable in identifying areas for improving the overall life-cycle environmental impacts of titanium slag production for Eramet Titanium & Iron AS and other relevant stakeholders. The study is carried out as a master thesis project, completing an MSc. degree in Energy and Environment from the University of Bergen. Hence, the LCA is written with the intention to suit both a non-technical and technical audience, and the comparative assertion is planned to be disclosed to the public.

3.2 Scope definition

The following section presents the scope of the LCA in further detail, including the functional unit, system boundary, data collection, treatment of multifunctionality and chosen impact categories.

3.2.1 Functional unit

The main function of the investigated processes is to separate the titanium- and iron oxides contained in ilmenite to produce chloride slag, sulfate slag, and HPPI. The production ratio of HPPI and sulfate slag to chloride slag is approximately 0.5 kg and 0.3 kg, respectively, per 1 kg of chloride slag produced for both production routes. The following functional unit is defined for the intended comparison:

"*One kilogram chloride slag* [1 kg] with >85 wt.% TiO_2 at refinery gate".

This functional unit is chosen as it reflects the majority of the produced products, which is chloride slag with >85 wt.% TiO_2 suitable as feedstock in the chloride production process for TiO_2 pigment. Additionally, chloride slag commands a higher market value per kg than HPPI and sulfate slag, making it the primary source of revenue at ETI. Moreover, the production of chloride slag and sulfate slag is exclusively through the smelting of ilmenite, while HPPI is produced through multiple production methods [47]. This functional unit has also been used in previous LCA studies assessing titanium industries [10], thus allowing for comparison.

Hence, one kg of chloride slag is chosen as the FU, while HPPI and sulfate slag are considered co-products. The treatment of the multifunctionality of the system is further explained in Section 3.2.4.

3.2.2 System boundary

The system boundary of the study is illustrated in Figure 6. Notably, the figure illustrates both investigated processing routes (i.e., H-PR and C-PR). The unit processes and material flows market with [a] only applies to the C-PR, while [b] only applies to the H-PR.

Process flow diagram
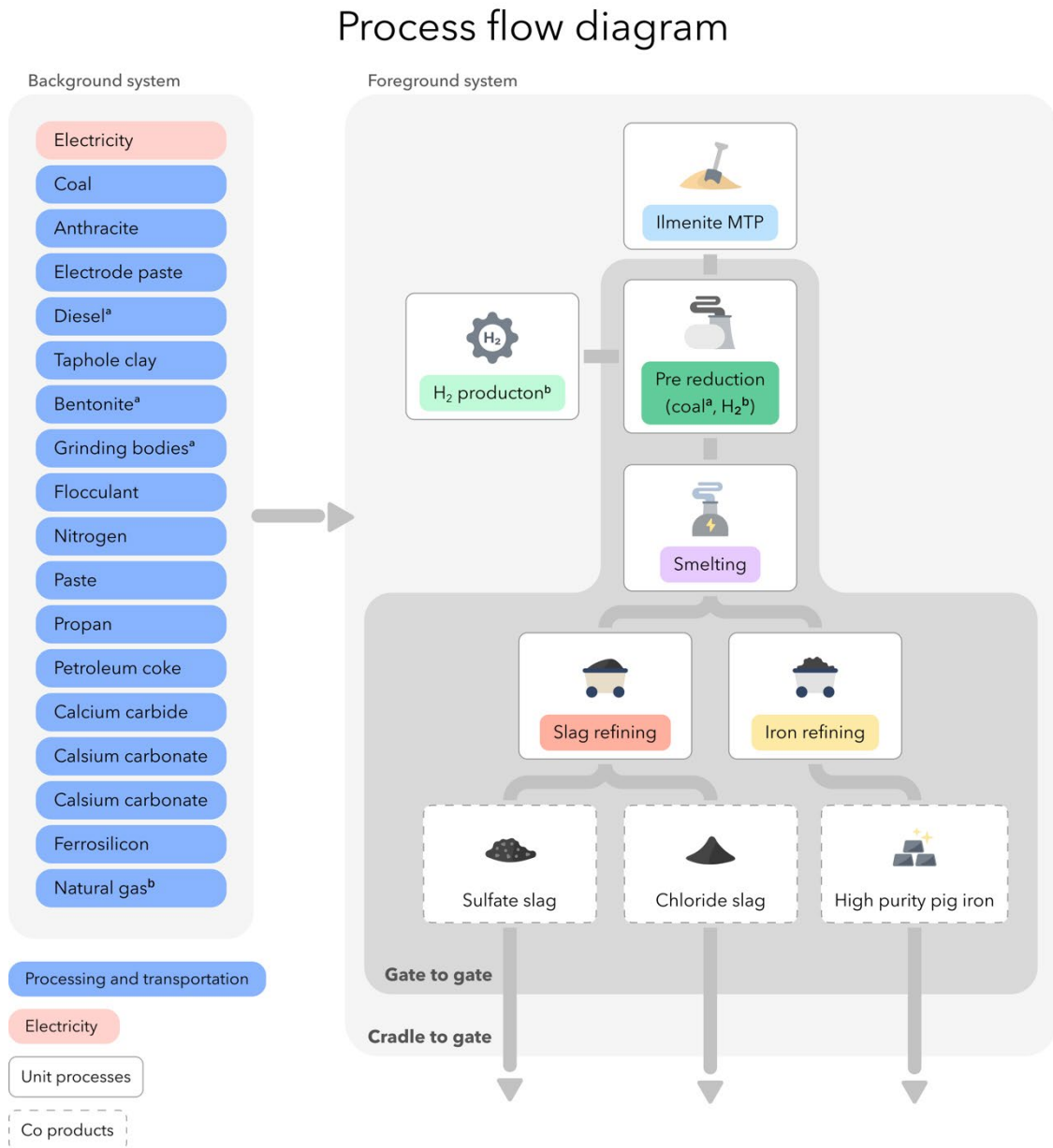
Figure 6 Process flow diagram describing the system boundary, and foreground and background system. The processes and flows market [a] pertains only to the C-PR and [b] only to the H-PR.

The study is a "*cradle-to-gate*" LCA study covering all process steps from ilmenite extraction (i.e., cradle) to the finished titanium slag and HPPI ready to be transported from ETI for further processing (i.e., gate). According to ISO 14044:2006 [37] "*the deletion of life cycle stages, processes, inputs or outputs is only permitted if it does not significantly change the overall conclusion of the study*". Given the goal of the study (i.e., to compare two alternative

21

processing routes), it is assumed that the exclusion of the "*gate-to-grave*" phase of the life cycle is in line with the stated ISO 14044:2006 requirement.

The foreground system includes the following unit processes: ilmenite mining, processing, and transportation (MPT), pre-reduction, smelting, slag refining, iron refining, and H_2 production. The "*gate-to-gate*" processes illustrated in Figure 6 refer to the on-site production process at ETI. Notably, the pre-reduction process is the only gate-to-gate unit process that differs entirely between the C-PR and H-PR. While it may be argued that assessing only this process would be sufficient for the intended comparison, the ripple effects of this alteration on subsequent processes make it necessary to evaluate the entire processing route. Subsequent downstream processing of chloride slag, sulfate slag, and HPPI, use phase, and end-of-life phase are outside the system boundary and not included in the study.

H_2 and coal are alternative reducing agents for the investigated processing routes. However, only H_2 is considered as a separate unit process, while coal MPT is aggregated to the pre-reduction process. The reason for this is that various H_2 production methods are assessed, which makes a separate unit process advantageous. For the contribution analysis, coal MPT is disaggregated from the pre-reduction to facilitate a fair comparison.

The background system is comprised of the processes related to the acquisition (i.e., processing and transportation) of the source streams, including material and energy inputs to the foreground system, as depicted in Figure 6. Transportation to Tyssedal is included for all source streams.

Capital goods have been excluded from the system boundary for all foreground processes, with the exception of H_2 production. Capital goods are, however, included in the background processes.

3.2.3 Data collection

Data for all *foreground* cradle-to-gate processes depicted in Figure 6 are provided by ETI in conjunction with its parent company Eramet AS, with the exception of H_2 production and ilmenite MPT, which is based on literature findings. All foreground data is revised by ETI.

The foreground data for the C-PR is derived from actual production data of the titanium slag production facility located in Tyssedal, collected through multiple on-site visits and interactions with industry specialists. Annual production data covering material inputs, energy use, production rates, waste streams and emissions to air and water has been obtained. The year 2021 is selected as the basis for the LCI. No extraordinary production interruptions occurred during this particular year, and thereby, it is assumed to be representative. Data covering material and energy inputs are derived from invoices and

reported consumption. Data for emissions to air and water are derived from various spreadsheets provided by ETI, which are obtained from measuring sensors and sample analysis. CO_2 emissions are determined through stoichiometric calculations by assessing the carbon mass balance of each unit process.

The foreground data for the H-PR is obtained from theoretical calculations performed by industry specialists at ETI and extrapolations of current production data. For the pre-reduction unit process, the calculations of material and energy use are based on data collected from a lab-scale test facility.

Generic background data is based on the commercial database ecoinvent v.3.8. To ensure consistency and representativeness, all background processes are ensured to be of geographical and temporal relevance. To create a complete inventory, no cut-off criteria were used during data collection.

A mass balance analysis is carried out for each unit to ensure completeness and plausibility of the collected data. For instances where mass balance was not achieved, stochiometric calculations were performed to investigate possible errors in the collected data. During data compiling, an error margin of < 2 wt.% for each unit process was aimed for. Mass balance is achieved for each unit process so that eq. (3.1) holds true for both investigated processing routes.

$$\sum m_{input} = \sum m_{output} \hspace{4cm} (3.1)$$

The assumptions made to facilitate mass balance are clearly stated for each unit process.

3.2.4 Treatment of multifunctionality

The investigated foreground process is considered multifunctional, with the primary outputs being chloride slag, sulfate slag and HPPI. In addition, ETI has undertaken several measures with the current production process (i.e., C-PR) to divert products that previously were considered waste towards becoming valuable by-products, such as skimmed slag from the iron refining, zinc dust from the pre-reduction and excess process heat. Figure 7 illustrates the multifunctionality arising from the investigated system as well as the selected approach to solve this.

23
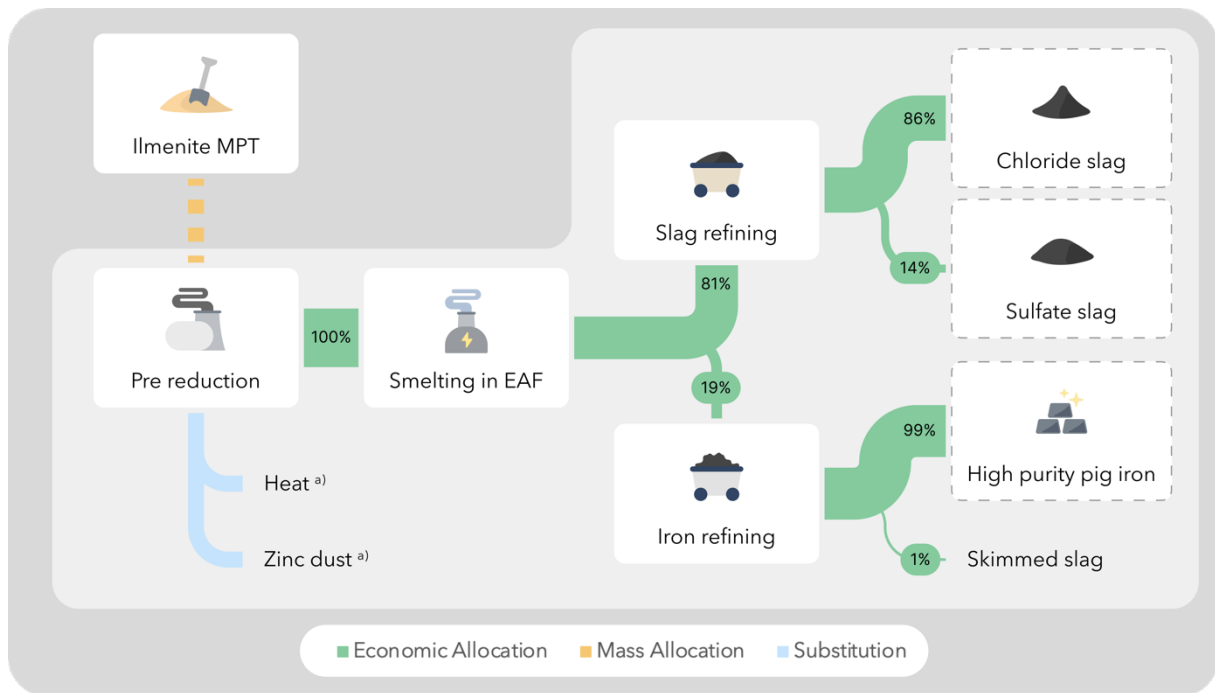
Figure 7 Treatment of multifunctionality for both processing routes, the product's market with [a] pertains only to C-PR. Allocation percentages are provided where economic allocation is applied.

The multifunctionality arising from the co-production is solved in accordance with the ILCD handbook's hierarchy for decision context A (i.e., micro-level decision support) [39]. The preferred approach of subdivision to deal with the multifunctionality was found infeasible, as no unit process can be divided into a mono-functional process due to the technical properties of the processes. As a result, alternative multifunctionality approaches located at lower levels in the ISO hierarchy were considered.

The second ISO hierarchical approach (i.e., system expansion through substitution) was found applicable to deal with the multifunctionality arising from the pre-reduction, where zinc dust and heat are produced as by-products, as illustrated by the blue line in Figure 7. However, as substitution implies that some functions provided by the process are considered secondary [41], allocation based on economic market value was found to be the most reasonable approach with respect to the co-products. This is also suggested in the "*Harmonization of LCA methodologies for the metal and mining industry*" study [48], which covers the treatment of multifunctionality in similar industries. Hence, environmental impacts are allocated to the various co-products based on their market value. In Figure 7, the green lines describe the processes to which economic allocation is applied and indicate the corresponding allocation factors. A table presenting all allocation factors and equations is provided in Appendix 1.

Additionally, economic allocation is employed to address the multifunctionality resulting from the by-production of skimmed slag from the iron refining process. The preferred

approach of substitution was initially considered for this by-product, but the lack of available LCI data for skimmed slag made economic allocation the most sufficient approach. Sensitivity to alternative allocation principles (e.g., physical causality) is tested and further discussed in Section 7.2.7. Background processes are selected based on the treatment of multifunctionality to ensure consistency.

Averaged market values are provided by ETI AS but remain disclosed due to data confidentiality.

3.2.5 Selection of the life cycle impact assessment method

Life cycle impact assessment (LCIA) is performed using the ReCiPe (H) Midpoint LCIA method [43]. The potential impact on each category will be determined using Simapro v. 9.3.0.3.

The LCIA results are presented for eight out of the 18 ReCiPe (H) impact categories presented in Table 1. The selection of impact categories is based on the contribution of the gate-to-gate unit processes depicted in Figure 6. Impact categories in which environmental flows derived from primary ETI data contribute more than 5% to the overall impact score have been included. This approach ensures that impact categories solely affected by secondary data are omitted, thus maintaining robustness and consistency in the results. The following impact categories are selected:

- Global warming potential (GWP)
- Stratospheric ozone depletion
- Ozone formation, human health
- Ozone formation, terrestrial ecosystems
- Terrestrial acidification
- Terrestrial ecotoxicity
- Marine ecotoxicity
- Human non-carcinogenic toxicity

The greatest emphasis will be given to GWP when presenting and discussing the results, as it is the impact category with the strongest scientific basis and public and regulatory interest.

4 Life Cycle Inventory (LCI)

The following chapter presents qualitative and quantitative LCI descriptions for all unit processes involved in the investigated production routes. LCI for ilmenite MPT is presented separately in Subchapter 4.1, as this is common for both production routes. The LCI for C-PR and H-PR are presented in Subchapter 4.2 and 4.3, respectively.

It should be noted that the unit processes covering the pre-reduction of ilmenite are the only significant difference between the two processing routes, in addition to H_2 production. Other unit processes (i.e., smelting in EAF and both refining processes) are broadly comparable, but modifications to input values and materials do occur. To facilitate a clear description of the processes and respective LCIs, all unit processes are described in sequential order for both production routes. A table showing complete LCI data for each unit process is presented at the end of each process description, except for ilmenite MPT and H_2 production which is included in Appendix 2.

Input materials and values are aggregated in collaboration with ETI AS to protect confidential data. The published LCIs are considered to provide sufficient transparency so as not to hinder the interpretation of this thesis and its results. Values for electrical energy are reported as a cumulative total for all unit processes in each processing route, with the exception of the pre-reduction.

4.1 Ilmenite mining, processing and transportation

The following subchapter presents the LCI for ilmenite mining, processing and transport of (MPT) ilmenite.

4.1.1.1 *Process descriptions and material inputs and outputs*

Figure 8 provides an overview of the most important inputs and outputs of ilmenite MPT. A complete LCI is presented in Appendix 2. In addition, the left part of Figure 8 illustrates an overview of the process flow by highlighting the icons used to illustrate each unit process in Figure 5 to Figure 7. This will be provided for each LCI presented.
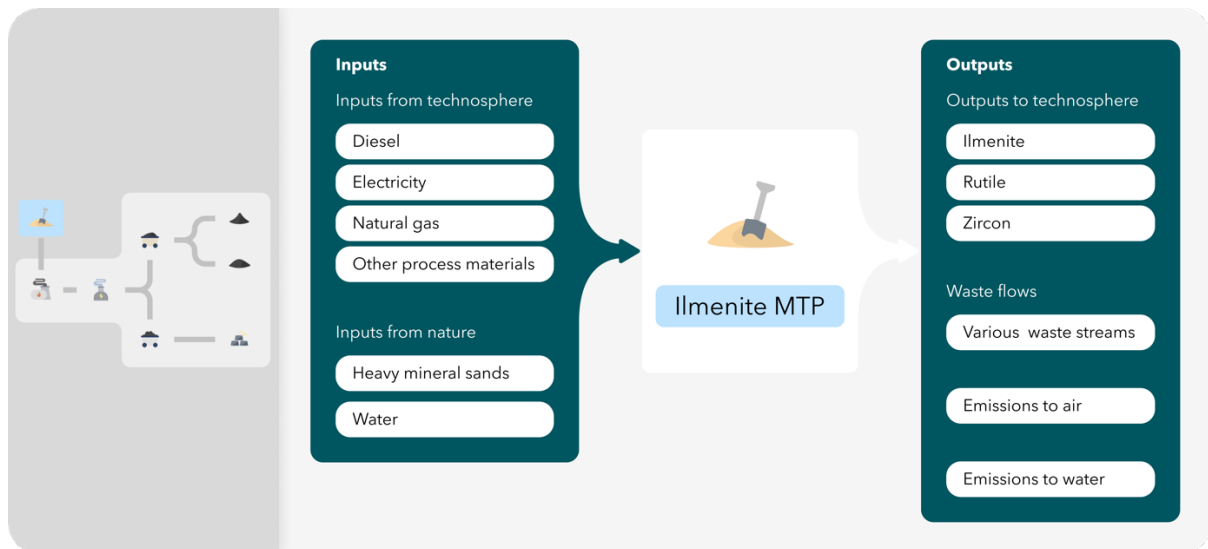
Figure 8 Overview of the most important inputs and outputs for Ilmenite MPT and an overview of the process flow.

The Ilmenite used at ETI is mined from heavy mineral sands, in which titanium minerals (e.g., ilmenite and rutile) are found together with zircon (Zr) [49]. Separating these compounds consists of three main stages: mining, beneficiation, and separation. The ilmenite processed at ETI is obtained from the Grande Côte Operation (GCO) located in Senegal, which is owned by Eramet AS. The GCO can be described as a "*mobile mine*", with a dredge constantly moving at a rate of 30 meters per day on an artificial pond [50].

The LCI for ilmenite mining and processing is primarily based on data derived from Gediga et al. [51], which has been used to construct a dataset for ilmenite in the ecoinvent database [52]. Gediga et al. present LCI data covering 77% of the global heavy mineral sand production, which is based on comprehensive data collection from ten zircon sand operations, including the GCO in Senegal. This has been confirmed by the primary author of the study through email exchanges [53]. In conjunction with ETI, it has been established that the presented LCI sufficiently represents ilmenite mining and processing at GCO.

From Gediga et al. it is found that for every one kg of zircon, 1.29 kg of ilmenite and 0.41 kg of rutile is produced [51]. The presented LCI is scaled to represent one kg of ilmenite. Multifunctionality is handled by applying mass allocation. The system boundary includes mining, beneficiation, and separation of heavy mineral sands. Several attempts to obtain site-specific LCI data for the GCO operations were made during the work period of this master thesis. Unfortunately, this was proven to be problematic due to the confidentiality of the data. However, a GCO site-specific CO_2 emission rate of 0.18 g CO_2 per kg ilmenite was obtained [54].

The LCI presented by Gediga et al. [51] was altered to be as geographically representative as achievable for the GCO operations. The following alterations were made to the LCI:

27

- o Electricity consumption has been replaced with Senegal electricity mix
- o Tap water has been replaced with 50% South African and 50% rest of world (RoW)
- o CO_2 emissions have been adjusted to the rate of GCO (0.18 g CO_2 per kg ilmenite)

Ilmenite is transported from GCO in Dakar, Senegal, to Tyssedal via a bulk carrier. Modeling of transportation is primarily based on the ecoinvent dataset for transport via bulk carrier [55]. However, given that the shipment of ilmenite involved transporting substantial amounts of ilmenite exclusively to ETI over a considerable distance, additional efforts have been put into modeling this particular transportation process. Data for fuel consumption and emission of climate gasses and pollutants during operation have been replaced by data from the NTM database [56], which provides data based on specific ship size (DWT) and load capacity. A value of six tkm (ton kilometer) per kg ilmenite was estimated based on a distance of approximately 6000 km by sea from Dakar to Tyssedal and a total of ten shipments yearly. A ship size of 40 000 DWT and a load factor of 90% is assumed for the bulk carrier. Only transportation from Dakar to Tyssedal is included in the LCI (i.e., return is not considered).

The complete LCI data for ilmenite MPT used in this study is presented in Appendix 2. Alterations are highlighted in green.

Additionally, Eramet AS has announced plans to power the GCO operations with renewable electricity generated from photovoltaic cells [57]. As the timeline for completion and full-scale implementation remains uncertain, the electricity is modeled using the dataset for the Senegalese market mix. However, the effect of employing electricity generated from photovoltaics is included as a sensitivity analysis.

4.2 Carbon-based processing route (C-PR)

The following section provides a quantitative and qualitative description of the gate-to-gate unit processes for titanium slag and HPPI production with pre-reduction of ilmenite using coal as a reductant, as described in Figure 9.
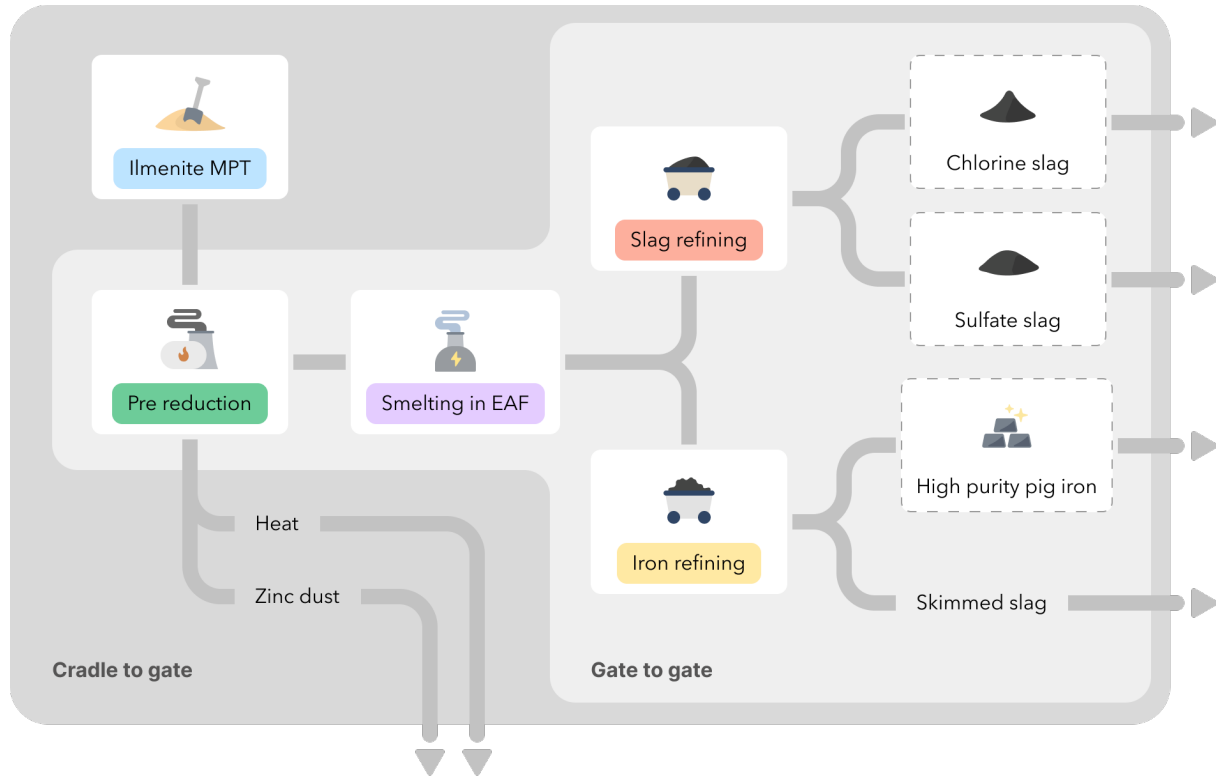
Figure 9 An overview of the C-PR, including unit processes, co-products and by-product.

The inventory is derived from annual production data provided by ETI for 2021. A mass balance analysis has been performed for each unit process. All assumptions made regarding the mass balance of the unit processes have been discussed and verified by both academic supervisors and specialists at ETI (e.g., head of environmental management).

4.2.1 Pre-reduction of ilmenite using carbon as reductant

4.2.1.1 Process descriptions and material inputs and outputs

Figure 10 illustrates the essential input and output flows of the pre-reduction process. Complete LCI is presented in Table 2.
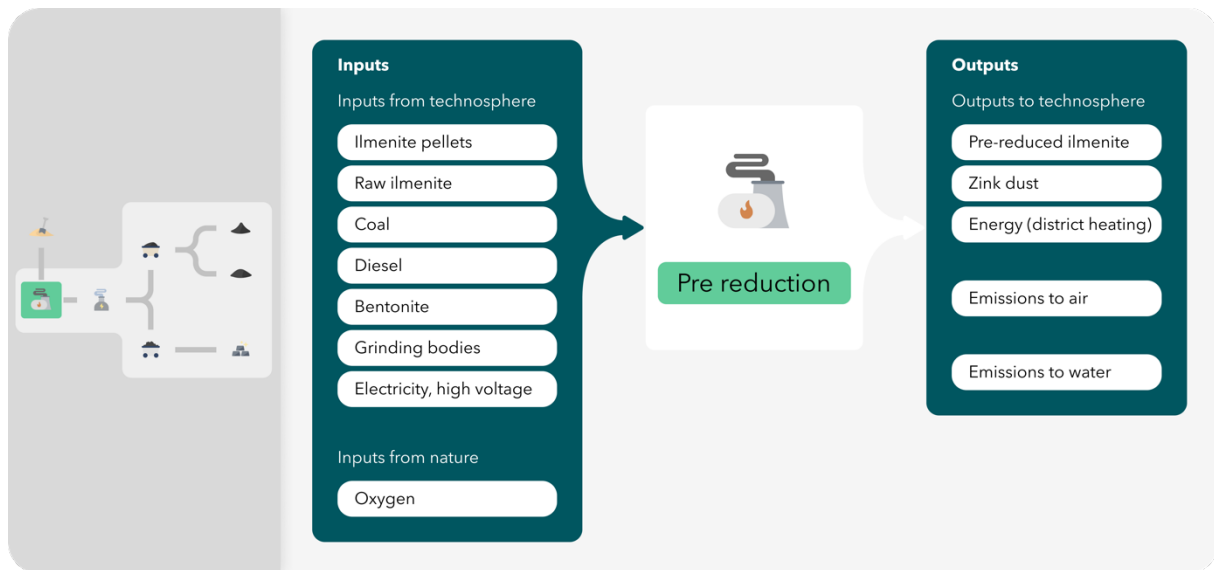
Figure 10 Overview of the most important inputs and outputs for pre-reduction (C-PR) and an overview of the process flow.

Ilmenite ($FeTiO_3$) is mainly composed of titanium dioxide (TiO_2) and iron oxides in the form of ferrous oxide (FeO) and ferric oxide (Fe_2O_3). To facilitate the separation of these compounds, ilmenite undergoes two separate endothermic reduction processes: pre-reduction and smelting. Pre-reduction is a solid-state reaction, whereas smelting is a liquid-state reaction.

Initially, raw ilmenite is pelletized to increase its metallurgical properties and withstand further thermal processing [58]. The compressive strength of the ilmenite pellets depends on their grain size and moisture level. To achieve a suitable grain size, ilmenite is subjected to a rotary mill that utilizes grinding bodies primarily made from cast iron. Approximately 1.08E-03 kg of grinding bodies are consumed per kg of ilmenite pellets produced [54]. Subsequently, 9.07E-03 kg of bentonite is added per kg of ilmenite pellet produced to enhance the compressive strength of the pellets. Finally, pellets in the 9 to 16 mm range are formed in a pelletizing drum.

The FeO contained in the raw ilmenite pellets are oxidized to Fe_2O_3 due to the following reason: firstly, oxidizing FeO to Fe_2O_3 increases the compressive strength of the pellets Secondly, Fe_2O_3 is more easily reduced to metallic iron than FeO, as Fe_2O_3 has a lower reduction potential and hence a greater tendency to be reduced. Lastly, the oxidation reaction is exothermic and thus heats the pellets [13]. Consequently, having Fe_2O_3 as the dominant iron oxide in the pellets is desirable as it increases the overall metallization degree of the subsequent pre-reduction process [23], [59]. The oxidation is facilitated using recycled CO-gas from the subsequent smelting phase.

During the oxidation, the following reaction described by eq. (4.1) occurs:

$$4FeO(s) + O_2(g) \rightarrow 2Fe_2O_3(s) \tag{4.1}$$
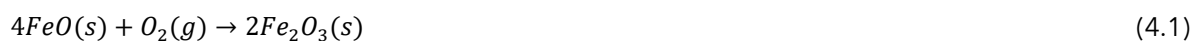
The pre-reduction of ilmenite is induced by adding heated and oxidized pellets to the rotary kiln together with reductants [13]. Oxygen atoms in the iron oxides are removed by subjecting the pellets to a compound that binds oxygen through a stronger chemical bond. In the C-PR, 0.49 kg of coal is used to reduce 1 kg of pellets.

The solid-state reduction of iron in pre-oxidized ilmenite pellets to metallic iron can be expressed by eq. (4.2), eq. (4.3), and eq. (4.4) [60]:

$$Fe_2O_3(s) + CO(g) \rightarrow 2FeO(s) + CO_2(g) \tag{4.2}$$
$$FeO(s) + CO(g) \rightarrow Fe(s) + CO_2(g) \tag{4.3}$$
$$C(s) + CO_2(g) \rightarrow 2CO(g) \tag{4.4}$$

The initial reaction (4.2) involves the reduction of Fe_2O_3 to form FeO and CO_2. FeO is then reduced to metallic iron in reaction (4.3). The CO_2 produced from reactions (4.2) and (4.3) reacts with the atomic carbon present in the coal and creates additional CO, as described by reaction (4.4). TiO_2 proceeds through the pre-reduction process unchanged.

The reactions are highly endothermic, meaning a significant input of energy is required. Sufficient temperatures are achieved by oxidizing excess CO gas to CO_2 in the presence of air within the rotary kiln [13]. A rate of 0.546 kg O_2 per kg pre-reduced ilmenite produced was obtained from ETI based on measurements of in-blown air to the rotary kiln. The efficiency of the process is such that 70-75% of the iron oxides present in the ilmenite pellets are converted to metallic iron [23]. To prevent re-oxidation of Fe to FeO, the pellets are cooled rapidly by water from 1100°C to 80°C and separated into magnetic and non-magnetic fractions so that unreacted raw carbon materials are removed [61].

Furthermore, a consumption rate of 8.67E-05 kg diesel per kg pre-reduced ilmenite is found. Diesel is explicitly used for reheating the rotary kiln in the event of a production halt where the rotary kiln is shut down and cooled and can be regarded as an ancillary input.

4.2.1.2 By-products

Zinc dust and heat are produced as by-products from the pre-reduction process. In addition to TiO_2 and iron oxides, ilmenite contains various trace-compound, such as zinc. From the pre-reduction process, zinc particles are separated from the dust created in the rotary kiln and produced as a by-product. Approximately 7.93E-04 kg of zinc dust is generated per kg of pre-reduced ilmenite. This is currently supplied to Boliden, which is a neighboring zinc alloy manufacturer. Additionally, excess heat from the rotary kiln is provided to nearby facilities, including *Tyssedal Hotel*, *Norwegian Hydropower- and Industry Museum*, and *Hardanger Fjell Fisk AS*. Based on production values from 2021, 0.0118 kWh of heat is

delivered per kg of pre-reduced ilmenite pellets, which amounts to an annual total of 2 812 MWh.

The by-production of zinc dust and heat is dealt with through substitution, as previously described in Section 3.2.4. Zinc dust is substituted using a dataset for mining and processing of zinc concentrate found in the ecoinvent database, based on an LCA of zinc production by Genderen et al. [62]. All heat (i.e., regardless of end-use) is modeled as avoided electricity used to achieve 2 812 MWh of heat from an electrical radiator with an efficiency of 100%.

4.2.1.3 *Emissions*

Before being emitted to air, the flue gas produced in the rotary kiln undergoes filtration through a waste gas treatment system where the aim is to remove particulate matter (PM) and sulfur dioxide (SO_2) [13]. PM is removed by passing the gas through electrode filters, while SO_2 and other particles are removed through an SO_2-scrubber utilizing seawater to dissolve the particles. From [7], it can be derived that 0.979 kg of CO_2 is emitted per kg of pre-reduced ilmenite pellets produced. The CO_2-emission rate is derived from the calculation of the carbon mass balance. It is assumed that all excess carbon is oxidized and emitted as CO_2.

Furthermore, NO_x, volatile organic compounds (VOC), polyaromatic hydrocarbons (PAH), PM, and various heavy metals (HM) are emitted into air during the pre-reduction. The respective values per kg of pre-reduced ilmenite pellets are listed in Table 2. Additionally, emissions of PAH, PM, and HM to water from the pre-reduction occur, as presented in Table 2. The emission rate for these compounds is based on analysis obtained by an external laboratory from the ETI facility.

4.2.1.4 *Mass balance*

An error of 0.34% was identified when compiling the LCI data for the pre-reduction process, indicating a more significant input than output. To attain mass balance within the unit process, the input value of O_2 from air is reduced by 2.4%. Given that not all the O_2 will react and form CO_2, it is found reasonable to adjust the O_2 inlet to achieve mass balance.

Input and output values for materials and emissions associated with producing one kg of pre-reduced ilmenite pellets are presented in Table 2.

Table 2 LCI for pre-reduction (C-PR), including all input and output flows and the background processes used.

Pre-reduction C-PR

Outputs to technosphere	Unit	Amount	Background process
Ilmenite pellets	kg	1.00E+00	Intermediate
Zink dust	kg	7.93E-04	Bulk lead-zinc concentrate {GLO}| zinc mine operation	Cut-off, U[7]
Energy (heat)	kWh	3.61E-03	Electricity, high voltage {NO}| Hydro, reservoir, alpine region	Cut-off, U

Input from nature

Oxygen from air	kg	5.33E-01	

Inputs from technosphere

Ilmenite pellets	kg	8.08E-01	Intermediate
Raw ilmenite	kg	1.71E-01	
Carbonaceous materials	kg	3.62E-01	Aggregated
Fuel (diesel)	kg	8.67E-05	Diesel {Europe without Switzerland}| diesel production, petroleum refinery operation	Cut-off, U
Bentonite	kg	9.07E-03	Bentonite {RoW}| quarry operation	Cut-off, U[8]
Grinding bodies	kg	3.71E-05	Cast iron {RER}| production	Cut-off, U[9]
Electricity, high-voltage	kWh	1.82E-01	Electricity, high voltage {NO}| Hydro, reservoir, alpine region	Cut-off, U[10]

Emissions to air

CO_2	kg	9.80E-01	
SO_2	kg	4.32E-05	
NO_x	kq	1.70E-04	
VOC	kg	6.81E-06	
PAH	kq	3.94E-07	
Heavy metals	kg	3.61E-05	

---

[7] Where, GLO = global, cut-off = system model, and U = unit process
[8] RoW = Rest of world
[9] RER = European
[10] NO = Norway

Particulate matter	kg	5.43E-05	

Emissions to water

Suspended solids	kg	8.87E-05	
Heavy metals	kg	7.24E-06	

4.2.2 Smelting in EAF

4.2.2.1 Process description and material inputs and outputs

Figure 11 illustrates the input and output flows associated with the smelting of pre-reduced ilmenite in an electric arc furnace (EAF).
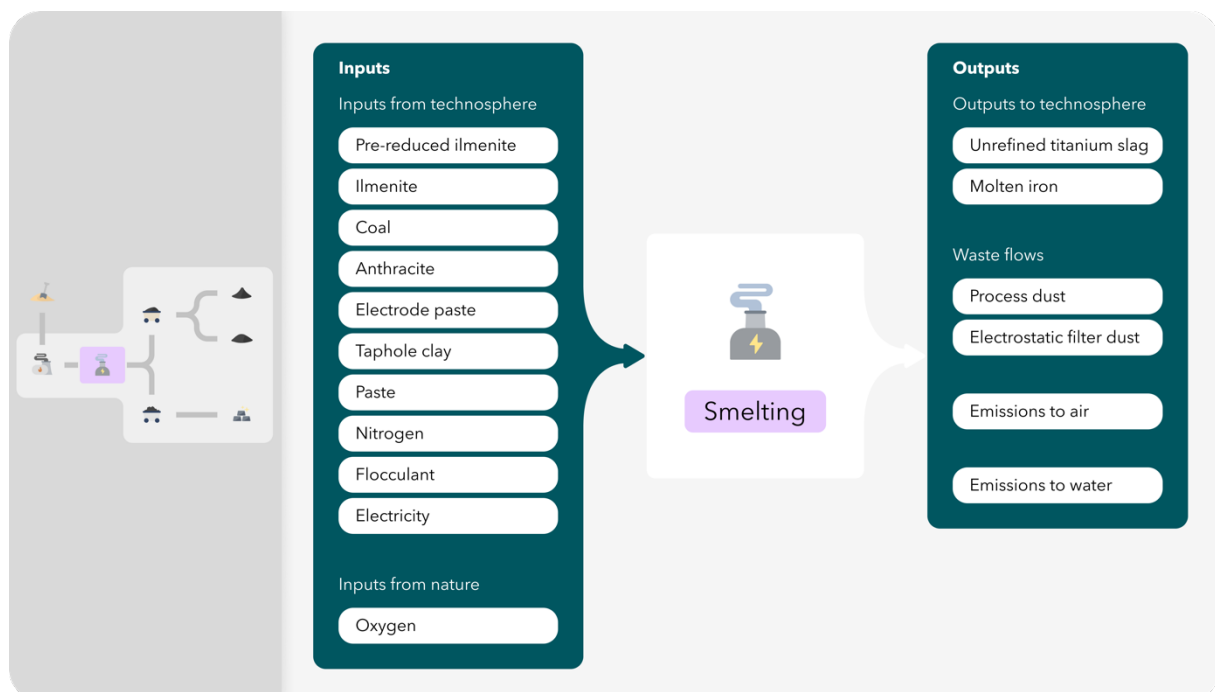
Figure 11 Overview of the most important inputs and outputs for smelting in EAF (C-PR) and an overview of the process flow.

70-75% of iron oxides are reduced to metallic iron during the solid-state pre-reduction process [13]. To facilitate the separation of TiO_2 from iron, the pre-reduced ilmenite undergoes a smelting process, where a liquid phase reduction takes place in a 40 MW EAF. The EAF operates at a temperature above the melting point of titanium (1650 °C) [63]. Per one kg of melted ilmenite (i.e., unrefined titanium slag and molten iron), 0.808 kg of pre-reduced ilmenite pellets are charged into the EAF together with 0.171 kg raw ilmenite and carbonaceous materials. Sufficient temperatures within the furnace are attained by utilizing heat generated by electrical resistance, as described by Ohm's Law [64]. An electrical current is led through three Söderberg electrodes, forming an open electric arc above the

melted material. The Söderberg electrodes are mainly comprised of carbon materials, which are continuously consumed during operation [65].

Due to data confidentiality, the carbonaceous materials and electrical energy consumption are presented as aggregated values, where electricity represents the consumption of the subsequent refining processes in addition to the smelting process.

The reactions that occur during the smelting phase can broadly be described by the following:

$$FeO\ (l) + C\ (l) \rightarrow Fe\ (l) + CO(g) \tag{4.5}$$
$$TiO_2\ (l) + C\ (l) \rightarrow Ti_2O_3\ (l) + CO\ (g) \tag{4.6}$$
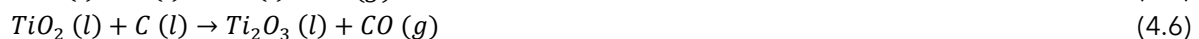
Reaction eq. (4.5) describes the primary reaction in the EAF: reduction of iron oxides to liquid metallic iron. Additionally, approximately 30% of the TiO_2 is reduced to Ti2O3, as described by eq. (4.6).

The separation of molten iron from the titanium slag occurs within the furnace due to variations in densities. To facilitate separation, tap holes are drilled into the furnace at specific heights, through which the respective liquids flow into separate ladles. Tap holes are subsequently sealed using a "*mud gun*" device, loaded with tap-hole clay. A dataset representing taphole clay was not found in the ecoinvent database. Therefore, the LCI is adopted from secondary sources in the literature [66]. As no information regarding the processing of taphole clay was provided, the adopted process only represents the upstream processing of the input materials. Additionally, a carbon-containing paste is utilized in the smelting process. No LCI data has been obtained for this material input. As the total input value is found to account for only 0.2% of the material input in the smelting process, it is assumed that excluding the upstream processing of this material input from the inventory will have a negligible effect on the overall results. Moreover, since the material input is common for both processing routes, its exclusion will not impair the intended comparison. The carbon contained in the paste is, however, included in the CO_2 emission calculations. Furthermore, a consumption rate of 9.12E-03 kg of nitrogen per kg of melted products is used to maintain an inert atmosphere and vented to air.

4.2.2.2   Emissions and waste flows

Flue gas from the EAF is treated in a waste gas treatment system that includes a venturi scrubber and a wet electrostatic precipitator to remove dust particles. Two waste flows are generated from the waste gas treatment, which are deposited in landfills. The inventory values are presented in Table 3.

Process water generated from the waste gas treatment system is led through a pressurized system that utilizes a flocculent to separate and remove the solid particulates. Aluminum sulfate ($Al_2(SO_4)_3$ is assumed as the flocculant used in this process, with a consumption rate of 2.04E-05 kg of flocculant per kg of melted ilmenite. Cleaned flue gas is partially utilized for drying the slag in the slag refining process, and the excess is combusted and released through a flue-gas stack. From ETI [54], it can be derived that 0.0993 kg CO_2 per kg of melted ilmenite is emitted. CO_2 emissions are based on mass balance calculations of carbon contained in input and output materials. In addition, the smelting of ilmenite emits SO_2, NO_x, N_2O, methane (CH_4), and PAH to air, which stems from the combustion of carbonaceous materials. PM and various HM are emitted to the atmosphere as diffuse emissions. Additionally, traces of PAH and HM are emitted to water. Inventory values for each emission flow can be found in Table 3.

4.2.2.3   Mass balance

An error of 0.21% was detected when compiling the LCI data for the smelting process from the annual production data, indicating a larger input than output. It is assumed to be likely that the discrepancy is a result of varying degrees of accuracy in the reporting data from which the LCI data was derived. Additionally, the annual production values consist of a significant number of measurements obtained from different weighing scales. This can result in a considerable cumulative deviation.

Based on these considerations, it was assumed reasonably to reduce the annual input value of pre-reduced ilmenite pellets by 0.37% to achieve mass balance. As ilmenite pellets are an intermediate product, this adjustment does not affect the overall mass balance of the process.

Table 3 LCI for smelting in EAF (C-PR) including all input and output flows and background process.

Smelting C-PR

Outputs to technosphere	Unit	Amount	Background process
Unrefined titanium slag	kg	7.06E-01	Intermediate
Molten iron	kg	2.94E-01	Intermediate
Input from nature			
Oxygen	kg	4.97E-03	
Inputs from technosphere			
Ilmenite	kg	8.08E-01	
Carbonaceous materials	kg	5.03E-02	Aggregated

Nitrogen	kg	9.12E-03	Nitrogen, liquid {RER}| air separation, cryogenic	Cut-off, U
Flocculant		2.04E-05	Aluminium sulfate, powder {RER}| production	Cut-off, U
Electricity, high-voltage	kWh	1.18E+00	Electricity, high voltage {NO}| Hydro, reservoir, alpine region	Cut-off, U

Emissions to air

CO_2	kg	9.93E-02	
SO_2	kg	9.33E-08	
NO_x	kq	9-28E-05	
N_2O	kg	3.74E-06	
CH_4	kg	8.41E-06	
Nitrogen	kg	9.12E-03	
PAH	kq	1.34E-08	
Heavy metals	kg	1.86E-05	
Particulate matter	kg	4.69E-06	

Emissions to water

Suspended solids	kg	9.45E-06	
Heavy metals	kg	4.11E-07	

Waste flows

Process dust	kg	1.24E-03	Dust, unspecified
Electrostatic filter dust	kg	6.31E-04	Electrostatic filter dust

4.2.3 Slag refining

4.2.3.1 Process description and material inputs and outputs

Figure 12 illustrates the input and output flows associated with the refining of titanium slag to chloride slag and sulfate slag.
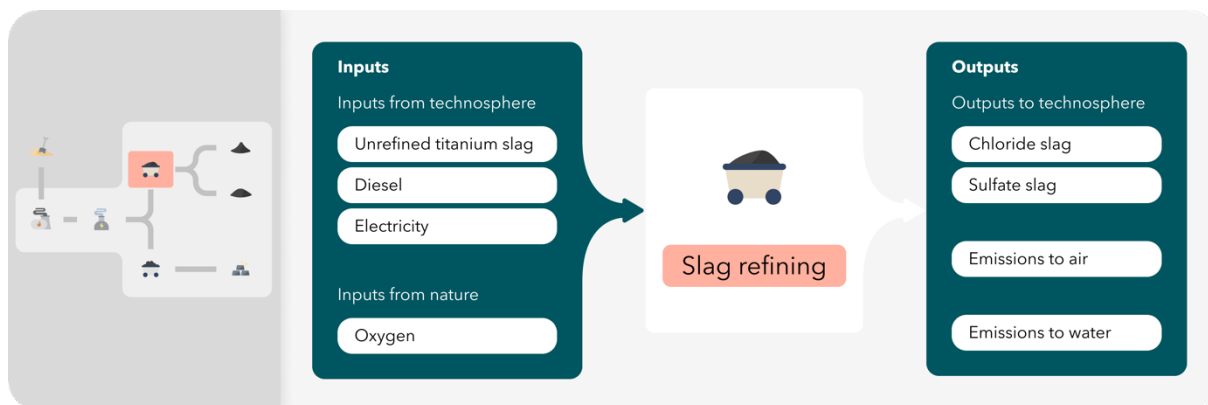
Figure 12 Overview of the most important inputs and outputs for slag refining (C-PR) and an overview of the process flow.

An important consideration in slag refining is the particle size, which must meet the specific requirements for the process in which it will be used. The unrefined titanium slag is crushed using various mechanical machinery to achieve this. For the sulfate process, the particles must be less than 12mm, while for the chloride process, the particles must be between 0.1 and 1mm and contain less than 0.1% moisture. Sulfate slag is produced from the ground titanium slag that does not meet the specifications for chloride slag after the crushing process. Due to data confidentiality, the electrical energy consumption of the crushing process is aggregated and presented as total electricity consumption in Table 3.

To achieve the required moisture level, the chloride slag is dried using heat generated by diesel combustion. For every kg of chloride slag produced, 1.11E-03 kg of diesel is consumed [54]. Drying is only applicable for chloride slag as no requirements for moisture level exist for sulfate slag. Hence, all emissions related to slag drying are allocated to chloride slag.

4.2.3.2 Emissions

Emissions from slag refining are mainly associated with the combustion of diesel, which emits CO_2, SO_2, NO_x, and VOC to air. CO_2 emissions are calculated based on carbon mass balance as previously described. SO_2 and NO_x emissions from slag refining are calculated from fixed factors of 0.05% SO_2 per L diesel and 3 g NO_x per kg diesel [54]. VOC emissions are derived from analyzed samples by ETI. PM, including several HM, are released into the environment during cooling and crushing [7].

4.2.3.3 Mass balance

When compiling the LCI data for slag refining, the total mass of inputs was found to be 0.35% higher than the outputs. Based on the reasoning for mass balance adjustments outlined in Section 4.2.2 for the smelting phase, the input value of unrefined titanium slag is reduced by the corresponding error in mass balance.

Table 4 presents the LCI data for titanium slag refining in the C-PR.

Table 4 LCI for slag refining (C-PR), including all input and output flows and background processes.

Slag refining C-PR

Outputs to technosphere	Unit	Amount	Background process
Chloride slag	kg	7.77E-01	
Sulfate slag	kg	2.23E-01	
Input from nature			
Oxygen	kg	4.97E-03	
Inputs from technosphere			
Unrefined titanium slag	kg	1	Intermediate
Diesel	kg	1.11E-03	Diesel {Europe without Switzerland}| diesel production, petroleum refinery operation | Cut-off, U
Electricity	kWh		Aggregated (See Table 3)
Emissions to air			
CO_2	kg	3.51E-03	
SO_2	kg	6.86E-07	
NO_x	kq	3.62E-06	
VOC	kg	5.00E-07	
Heavy metals	kg	4.78E-06	
Particulate matter	kg	3.30E-06	
Emissions to water			
Suspended solids	kg	1.13E-05	
Heavy metals	kg	8.66E-07	

4.2.4 Iron refining

4.2.4.1 Process description and material inputs and outputs

Figure 13 illustrates the input and output flows associated with the iron refining process.
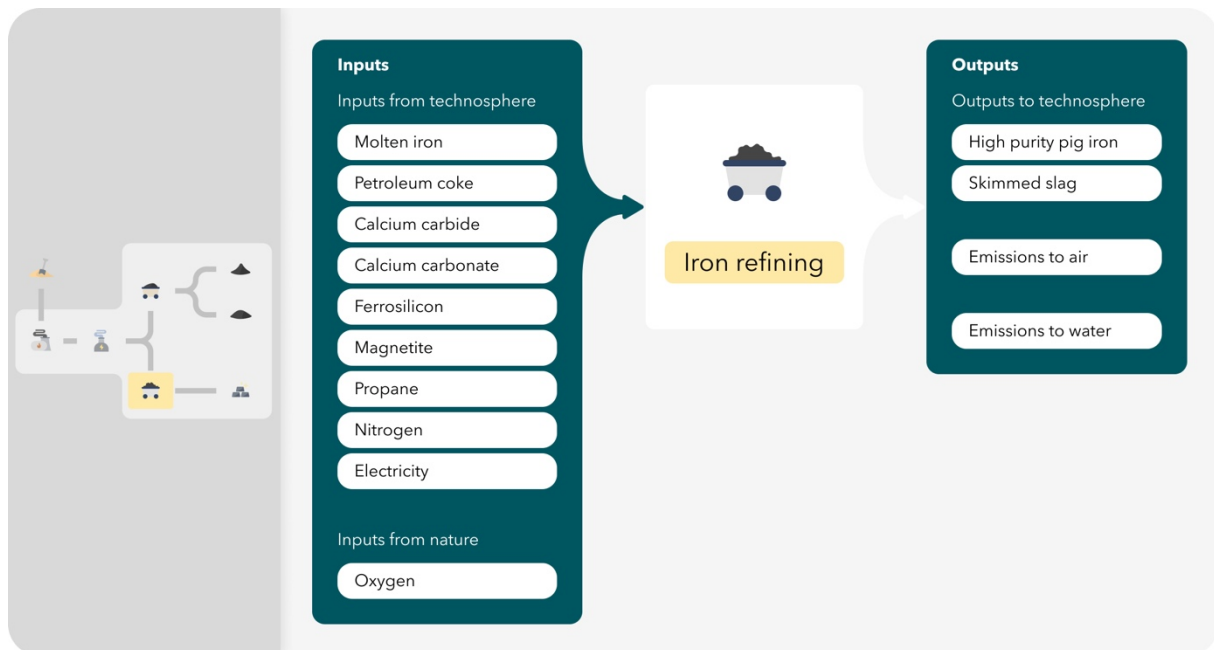
Figure 13 Overview of the most important inputs and outputs for iron refining (C-PR) and an overview of the process flow.

To produce one kg of HPPI, 0.970 kg molten iron is tapped from the EAF and subjected to additional refining, where unwanted impurities such as sulfur and phosphorus are removed, and suitable carbon and silicon content is reached.

High levels of sulfur can lead to formation of iron sulfates, which weakens the mechanical properties of the iron [13]. Consequently, the sulfur content in the molten iron is reduced by adding calcium carbide (CaC_2), which forms a stronger chemical bond with sulfur than iron. The reaction between CaC_2 and sulfur results in sulfate formation, which can be removed from the molten iron through skimming. Dephosphorization is achieved by introducing oxygen to the molten iron by adding magnetite, which reacts with the phosphorous present in the metal to form a phosphorus-oxygen compound. A slag-forming agent, such as calcium oxides (CaO), is commonly utilized to effectively remove the phosphorus-oxygen compound by creating a floating slag that is removed through skimming, similar to the removal of sulfates. The skimmed slag is sold as a by-product and utilized in landfills. For each kg of HPPI produced, approximately 0.0431 kg of skimmed slag is formed. Additionally, the silicon content in the HPPI is controlled by the addition of ferrosilicon (FeSi). Due to data confidentiality, the consumption rate of all iron refining materials mentioned is aggregated to 0.0475 kg per kg of HPPI produced.

The carbon content is adjusted from 1-1.5 wt.% to 2.5-4.5 wt.% of carbon by adding petroleum coke to the molten iron. Propane is burned to maintain an adequate temperature, so the molten iron is kept in a liquid phase. From ETI it is determined that 6.46E-04 kg of propane and 0.0408 petroleum coke are consumed per kg of HPPI produced

40

[54]. In addition, a consumption rate of 4.30E-03 kg of nitrogen per kg HPPI produced is used to maintain an inert atmosphere.

4.2.4.2 Emissions

CO_2 emissions from iron refining are calculated based on the carbon mass balance of input and output materials. A CO_2 emission rate of 0.154 kg per kg of HPPI is found. In addition, an emission rate of 4.10E-09 kg of PAH to air per kg of HPPI is obtained from the consumption of petroleum coke and combustion of propane. 9.58E-06 kg of HM are released to water per kg of HPPI produced, predominantly comprised of iron, zinc, and manganese. Data for emissions of PAH and HM from iron refining are based on ETI analysis of samples taken from the facility.

4.2.4.3 Mass balance

When compiling LCI data for the iron refining process, the mass input was found to be 1.42% higher than the output. The O_2 inlet in the iron refining is based on the assumption that all O_2 in the calculated CO_2 emission is derived from air. However, as there are several uncertainties surrounding this assumption, and it is assumed reasonable to reduce the O_2 inlet by 15% to achieve mass balance.

Aggregated LCI data for iron refining is presented in Table 5. The iron refining products consist of calcium carbide, magnetite, calcium carbonate, and ferro silicon, which can be found in the list of material inputs in Figure 6.

Table 5 LCI for iron refining (C-PR), including all input and output flows and background processes.

Iron refining C-PR

Outputs to technosphere	Unit	Amount	Background process
High purity pig iron	kg	9.57E-01	
Skimmed slag	kg	4.31E-02	
Input from nature			
Oxygen from air	kg	9.58E-02	
Inputs from technosphere			
Molten iron	kg	9.70E-01	Intermediate
Iron refining products	kg	4.75E-02	Aggregated
Propane	kg	6.46E-04	Propane {RoW}| natural gas production	Cut-off, U

Nitrogen	kg	4.30E-03	Nitrogen, liquid {RER}| air separation, cryogenic | Cut-off, U	
Petroleum coke	kg	4.08E-02	Petroleum coke {Europe without Switzerland}| petroleum coke production, petroleum refinery operation | Cut-off, U	
Electricity	kWh		Aggregated (See Table 3 LCI for smelting in EAF (C-P)	
Emissions to air				
CO_2	kg	1.54E-01		
Nitrogen	kg	4.30E-03		
PAH	kq	4.10E-09		
Emissions to water				
Suspended solids	kg	3.97E-05		
Heavy metals	kg	9.58E-06		

4.3 Hydrogen-based processing route (H-PR)

The following subchapter provides the LCI for all unit processes for the hydrogen-based processing route (H-PR), including the various H_2 production methods. This includes qualitative and quantitative process descriptions, as well as data for background processes and emissions. A mass balance analysis has been performed for each gate-to-gate unit process. All assumptions made regarding the mass balance of the unit processes have been discussed and verified by ETI. An overview of the H-PR is provided in Figure 14.
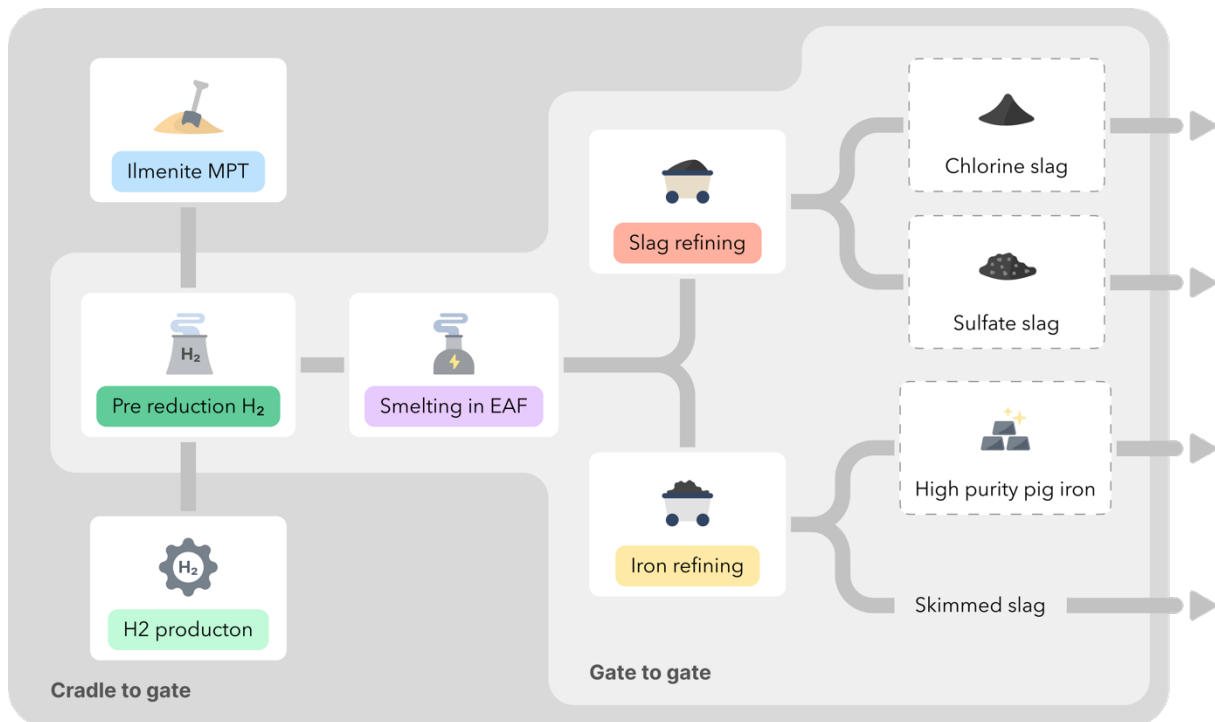
Figure 14 Overview of the H-PR, including unit processes, co-products, and by-products.

As previously mentioned, the only processes novel to the H-PR is the pre-reduction of ilmenite using H_2 (Section 4.3.1) and H_2 production (Section 4.3.5). Ilmenite MPT follows the qualitative and quantitative descriptions provided in Subchapter 4.1. The smelting of ilmenite, slag refining, and iron refining follows the qualitative description presented for the C-PR in Subchapter 4.2 to a large extent. But as the efficiency of the overall process is expected to increase with the H-PR, the consumption rate of various source streams and emissions are impacted. Therefore, this subchapter highlights the quantitative and qualitative changes that occur in these particular unit processes.

4.3.1 Pre-reduction of ilmenite using hydrogen as reductant

The pre-reduction in the H-PR differs from other unit processes in that it is based on scaled data from a laboratory facility. Representatives from ETI have scaled the consumption rates for various source streams to represent estimated annual production values for titanium slag and HPPI. As a result, direct emission rates are based on calculations and estimations.

4.3.1.1 Process description and material inputs and outputs

Figure 15 illustrates the inputs and output flows associated with the pre-reduction of ilmenite in the H-PR.
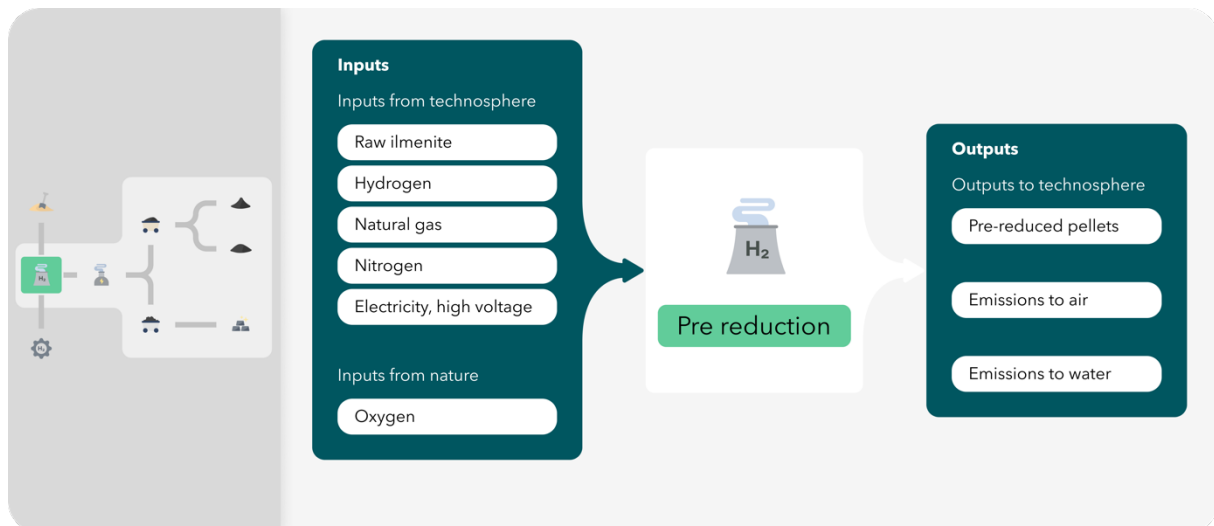
Figure 15 Overview of the most important inputs and outputs for pre-reduction (H-PR) and an overview of the process flow.

The first stage of the pre-reduction process involves heating the ilmenite to achieve sufficient temperatures for the following exothermal reduction process, similar to the C-PR. While the C-PR utilizes CO gas from the rotary kiln to oxidize FeO to Fe_2O_3, the H-PR relies on heat generated by the combustion of natural gas. A consumption rate of 0.0427 kg per kg pre-reduced ilmenite is obtained [54]. The oxidation process is exothermic and generates additional heat to the system, which is utilized to heat ilmenite to a sufficient temperature for the subsequent endothermic reduction process.

Preheated ilmenite is subjected to pressurized and reducing conditions with a surplus of H_2 gas to initiate the reduction. A consumption rate of 1.12 kg raw ilmenite per kg pre-reduced ilmenite is obtained [54]. The reduction is accomplished through a two-stage fluidized bed process. Eq. (4.7) broadly describes the reaction that occurs:

$$FeTiO_3 + H_2 \rightarrow FeTiO_2 + H_2O \tag{4.7}$$

0.0183 kg of H_2 gas is utilized to produce one kg of reduced ilmenite at a 90% reduction grade, based on estimates provided by ETI [54]. Ilmenite is exposed to pure H_2 gas in two separate fluid bed processes.

The H_2 gas utilized in the first fluid bed process is reused in the second process, where a metallization grade of approximately 90% is reached. Compared to the metallization grade of 70-75% for the C-PR, the increased metallization in the H-PR leads to increased efficiency in the subsequent smelting phase and a reduced consumption rate of carbonaceous materials and electricity.

To prevent H_2 gas leakage, an overpressure of nitrogen is maintained within the system, ensuring nitrogen leakage as opposed to H_2 in case of a deficit. A consumption rate of

0.0192 kg of nitrogen gas per kg of reduced ilmenite has been estimated. Hence nitrogen is an ancillary input, which is assumed to be vented to air.

According to estimations provided by ETI, 8.55E-05 kWh of high-voltage electricity is needed for the H_2-based pre-reduction process.

4.3.1.2 Emissions

As described by eq. (4.7) using H_2 to reduce ilmenite produces water vapor directly emitted to air. An emission rate of 0.134 kg H_2O per kg of reduced ilmenite is calculated. The combustion of natural gas generates additional emissions. To quantify these emission streams, an altered version of a dataset describing the burning of natural gas found in the ecoinvent database is utilized [67]. The process initially contained an industrial furnace and electricity to power it as inputs. However, as no other capital goods have been included within the foreground system of this thesis, the furnace was eliminated to ensure consistency. Furthermore, the electricity needed to operate the furnace has already been accounted for in the total electricity consumption and thus was subtracted from the inventory.

Emission rates of PM and HM to air and water are assumed to be equivalent to those of the C-PR, with the exception of mercury. By comparing lab analyses of ilmenite and the coal used in the C-PR, it was established that all HM are primarily derived from ilmenite, except mercury, which originates primarily from coal. Consequently, emissions of mercury to both air and water have been assigned a zero value to represent the exclusion of coal from the process. Other emission rates are kept at a constant level despite the increased ilmenite consumption rate due to an assumption that a fluid bed process will yield a reduced level of diffuse emissions compared to the coal-fired rotary kiln. Setting the diffuse emission rate of HM and PM to the same level as the pre-reduction in the C-PR is likely an overestimation. However, as it is not possible to quantify the degree of reduction at this point in the process development, the conservative estimate is selected in line with the precautionary principle. This assumption has been verified by ETI as the best starting point. Due to the significant uncertainty surrounding these emissions, the effect of varying emission rates is assessed as part of a sensitivity analysis.

4.3.1.3 Mass balance

While compiling data for the H-PR pre-reduction process, an error margin of 0.99% was detected in the mass balance. The error was likely caused by an overestimation of the O_2 inlet, which was assumed to equal the wt.% of O_2 in the calculated CO_2 emission. To restore the mass balance of the unit process, the O_2 inlet was reduced by 15%.

Table 6 LCI for pre-reduction (H-PR), including all input and output flows and background processes.

Pre-reduction H-PR

Outputs to technosphere	Unit	Amount	Background process
Pre-reduced ilmenite	kg	1.00E+00	*Intermediate*
Input from nature			
Oxygen from air	kg	6.95E-02	
Inputs from technosphere			
Ilmenite	kg	1.12E+00	
Hydrogen	kg	1.83E-02	
Natural gas	kg	4.27E-02	Natural gas, high pressure {NO}| petroleum and gas production, off-shore	Cut-off, U
Nitrogen	kg	1.92E-02	Nitrogen, liquid {RER}| air separation, cryogenic	Cut-off, U
Electricity, high-voltage	kWh	8.55E-05	Electricity, high voltage {NO}| Hydro, reservoir, alpine region	Cut-off, U
Emissions to air			
CO_2	kg	1.15E-01	
NO_x	kg	5.90E-05	
N_2O	kq	2.57E-07	
CH_4	kg	5.13E-06	
H_2O	kg	1.34E-01	
Nitrogen	kg	1.92E-02	
Particulate matter	kg	2.52E-05	
Heavy metals	kg	1.68E-05	
Emissions to water			
Suspended solids	kg	4.12E-05	
Heavy metals	kg	3.36E-06	

4.3.2 Smelting of ilmenite in an EAF

4.3.2.1 Process description and material inputs and outputs

Figure 16 illustrates the inputs and outputs of the smelting of pre-reduced ilmenite in the H-PR.
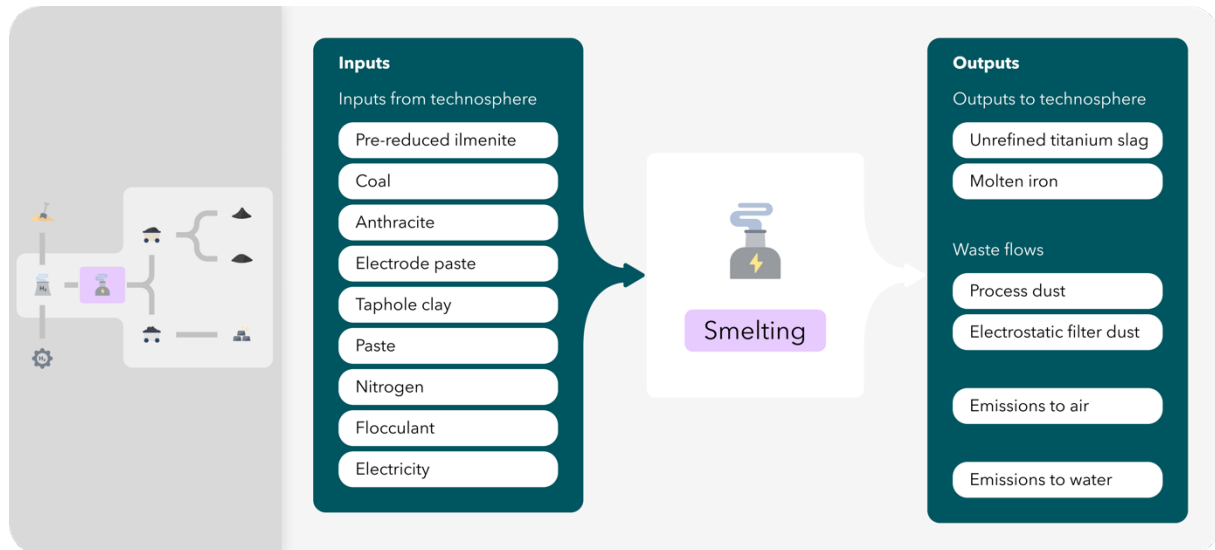

Figure 16 Overview of the most important inputs and outputs for smelting in EAF (H-PR) and an overview of the process flow.

Smelting of ilmenite in the H-PR is, to a large extent, performed as described for the C-PR in Section 4.2.2. The difference primarily lies in the initial degree of metallization of ilmenite when charged into the EAF, which is 15-20% higher for the H-PR. This leads to a lower consumption rate of reduction materials and electricity per kg of smelted ilmenite produced (i.e., increased process efficiency). A rate of 1.00 kg of pre-reduced ilmenite and 0.0200 kg of carbonaceous materials are estimated per kg of smelted ilmenite produced, based on calculations performed by ETI [54]. The waste streams delivered to landfill are scaled by a factor of 1.7 to represent the increased production rate.

4.3.2.2 Emissions

Estimations for air and water emissions have been made in the absence of measured data for ilmenite smelting in the H-PR. Emission rates of SO_2, NO_x, N_2O, and CH_4 were extrapolated from existing data from the C-PR presented in Section 4.2.2. It was assumed that these compounds are primarily associated with the combustion of carbon materials. The emission values are scaled based on the ratio of kg carbonaceous materials burned per kg of smelted ilmenite produced. As the total amount of carbonaceous materials is reduced due to increased metallization grade, the emission rate of these compounds is reduced for the H-PR compared to the C-PR.

CO_2 emissions were calculated based on carbon balance, leading to an estimated emission of 0.0190 kg of CO_2 per kg of smelted ilmenite, as presented in Table 7.

Due to a lack of reliable estimates of how diffuse emissions will be impacted by increased metallization grade and production rates, HM and PM emissions are assumed to be equivalent to the values presented for the C-PR production route in Table 3 in accordance with ETI. This assumption is made despite the increase in the amount of ilmenite processed annually, as it is likely that improved purification equipment will be installed to minimize these types of emissions due to stricter requirements from the authorities. Due to these uncertainties, a contribution analysis has been performed to assess the sensitivity of the outcomes.

4.3.2.3 Mass balance

An error margin of 0.61% was detected for the mass balance while compiling data for the H-PR smelting process. Mass balance was achieved by increasing the value of molten iron produced in the EAF by 2%. The initial value was calculated from the wt.% of molten iron produced per kg of ilmenite charged in the C-PR, which is associated with high uncertainty. As molten iron is an intermediate product, the overall mass balance of the system is unaffected.

Table 7 LCI for smelting in EAF (H-PR) including all input and output flows and background processes.

Smelting in EAF H-PR

Outputs to technosphere	*Unit*	*Amount*	*Background process*
Unrefined titanium slag	kg	6.99E-01	*Intermediate*
Molten iron	kg	3.01E-01	*Intermediate*
Input from technosphere			
Ilmenite	kg	1.00E+00	
Carbonaceous materials	kg	2.00E-02	Aggregated
Natural gas	kg	8.64E-03	Natural gas, high pressure {NO}| petroleum and gas production, off-shore	Cut-off, U
Nitrogen	kg	1.92E-02	Nitrogen, liquid {RER}| air separation, cryogenic	Cut-off, U
Flocculant	kg	1.18E-05	
Electricity, high-voltage	kWh	8.44E-04	Electricity, high voltage {NO}| Hydro, reservoir, alpine region	Cut-off, U

Emissions to air

SO$_2$	kg	3.61E-08	
CO$_2$	kq	1.90E-02	
NO$_x$	kg	3.59E-05	
N$_2$O	kg	1.45E-06	
CH$_4$	kg	3.26E-06	
Nitrogen	kg	5.27E-03	
PAH	kg	6.40E-09	
Particulate matter	kg	2.71E-06	
Heavy metals	kg	1.07E-05	
Emissions to water			
Suspended solids	kg	5.46E-06	
Heavy metals	kg	2.37E-07	
Waste flows			
Process dust	kg	1.25E-03	
Electrostatic filter dust	kg	6.35E-04	

4.3.3 Slag refining

4.3.3.1 Process description and material inputs and outputs

Figure 17 illustrates the inputs and output flows associated with the refining of titanium slag in the H-PR.
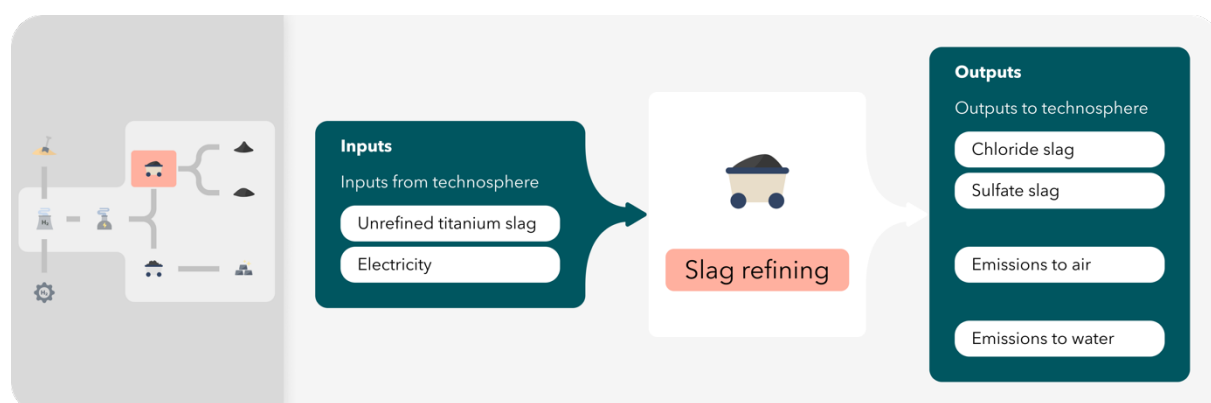

Figure 17 Overview of the most important inputs and outputs for slag refining (H-PR) and an overview of the process flow.

The refining of titanium slag in the H-PR follows the process descriptions outlined in Section 4.2.3, with one exception. In the H-PR the drying of chloride slag is facilitated by re-using

49

CO-gas from the EAF, which eliminates diesel consumption. Thus, the only input to the slag refining process is electricity used to power the machinery, which is presented as an aggregated value in Table 6.

4.3.3.2 Emissions

Since the combustion of diesel is eliminated from the process, no emissions, except PM and HM, are expected to be generated. Following the same reasoning provided in Section 4.3.2, these values are set equal to the slag refining process in the C-PR.

4.3.3.3 Mass balance

During the mass balance analysis of slag refining for the H-PR, an error of 0.01% was identified. Mass balance was restored by increasing the input value for unrefined titanium slag from the EAF by the corresponding amount. Unrefined titanium slag is an intermediate product, and the total mass balance of the unit process is not affected by this adjustment. The original value for unrefined titanium slag for the H-PR was scaled based on the ratio between pre-reduced ilmenite into the EAF and unrefined titanium slag produced from the C-PR. Considerable uncertainty is associated with this estimation, which justifies the adjustments made.

Table 8 presents the complied LCI data for titanium slag refining in the H-PR.

Table 8 LCI for slag refining (H-PR), including all input and output flows and background processes.

Slag refining H-PR

Outputs to technosphere	Unit	Amount	Background process
Chloride slag	kg	7.75E-01	
Sulfate slag	kg	2.25E-01	
Input from technosphere			
Unrefined titanium slag	kg	1.00E+00	
Electricity, high-voltage			Aggregated (See Table 7)
Emissions to air			
Heavy metals	kg	2.79E-06	
Particulate matter	kg	1.93E-06	
Emissions to water			
Suspended solids	kg	6.57E-06	

Heavy metals	kg	5.05E-07
PAH	kg	1.23E-10

4.3.4 Iron refining

4.3.4.1 Process description and material inputs and outputs

Figure 18 illustrates the inputs and outputs of the iron refining in the H-PR.
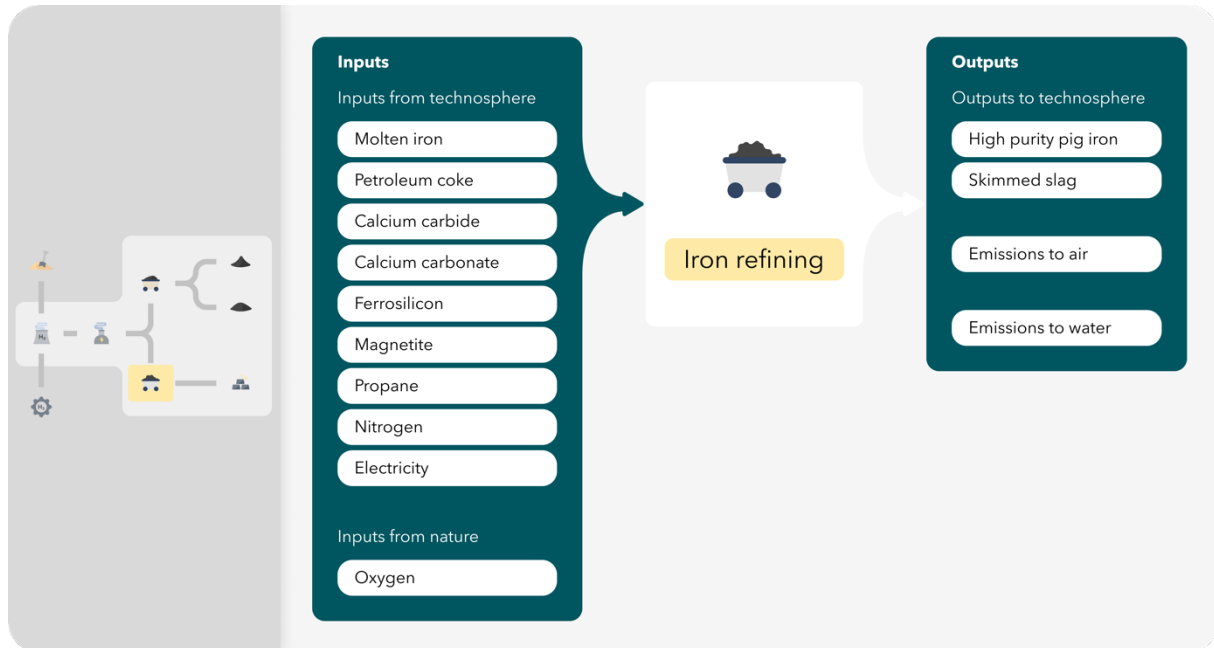

Figure 18 Overview of the most important inputs and outputs for iron refining (H-PR) and an overview of the process flow.

The iron refining process for the H-PR is comparable to the process descriptions for the C-PR outlined in Section 4.2.4. However, the quality of the HPPI produced through the H-PR is expected to increase due to less exposure to impurities. Hence, the consumption rate of iron refining products and petroleum coke per kg HPPI produced is estimated to decrease per kg HPPI. Input values have been adjusted by ETI and are presented in Table 9.

4.3.4.2 Emissions

Emissions of CO_2 and PAH to air have been adjusted to accommodate the estimated consumption of carbonaceous materials. Additionally, the values for PM and HM to water have been set equal to the corresponding values presented in Table 5 for the C-PR iron refining process, following the same reasoning as described in Section 4.3.2.

4.3.4.3 Mass balance

An error of 0.16% was identified for the mass balance when compiling the LCI data, indicating a larger input than output. The observed difference is assumed to result from an

overestimation of O_2 from air in the input values. Hence, mass balance is restored by assuming a reduced O_2 input rate.

Table 9 LCI for iron refining (H-PR), including all input and output flows and background processes.

Iron refining H-PR

Outputs to technosphere	Unit	Amount	Background process
High purity pig iron	kg	9.57E-01	
Skimmed slag	kg	4.31E-02	
Input from nature			
Oxygen from air	kg	5.87E-02	
Inputs from technosphere			
Molten iron	kg	9.79E-01	Intermediate
Iron refining products	kg	2.90E-02	Aggregated
Propane	kg	4.01E-04	Propane {RoW}| natural gas production | Cut-off, U
Nitrogen	kg	2.45E-03	Nitrogen, liquid {RER}| air separation, cryogenic | Cut-off, U
Petroleum coke	kg	2.87E-02	Petroleum coke {Europe without Switzerland}| petroleum coke production, petroleum refinery operation | Cut-off, U
Electricity, high-voltage			Aggregated (See Table 7)
Emissions to air			
CO_2	kg	9.62E-02	
Nitrogen	kg	2.45E-03	
PAH	kq	2.88E-09	
Emissions to water			
Suspended solids	kg	2.26E-05	
Heavy metals	kg	5.44E-06	

4.3.5 Hydrogen production

Three alternative H_2 production methods have been assessed for this study: H_2 produced via water electrolysis using hydropower (green H_2), H_2 produced from natural gas via steam methane reforming (SMR) utilizing CCS (blue H_2) and H_2 produced from natural gas using SMR without CCS (grey H_2). This section presents the LCIs for the investigated production methods, all of which have been adapted from the literature. To ensure representativeness, the individual LCIA results for each production method (i.e., green, blue and grey) are compared to other studies assessing the environmental impacts of H_2 production. This comparison is discussed in Section 7.2.6, as part of the sensitivity analysis.

To facilitate a fair comparison between the three H_2 production methods and between H_2 and coal as alternative reductants, capital goods have been included in all LCIs for H_2 production, despite being excluded for the rest of the foreground system.
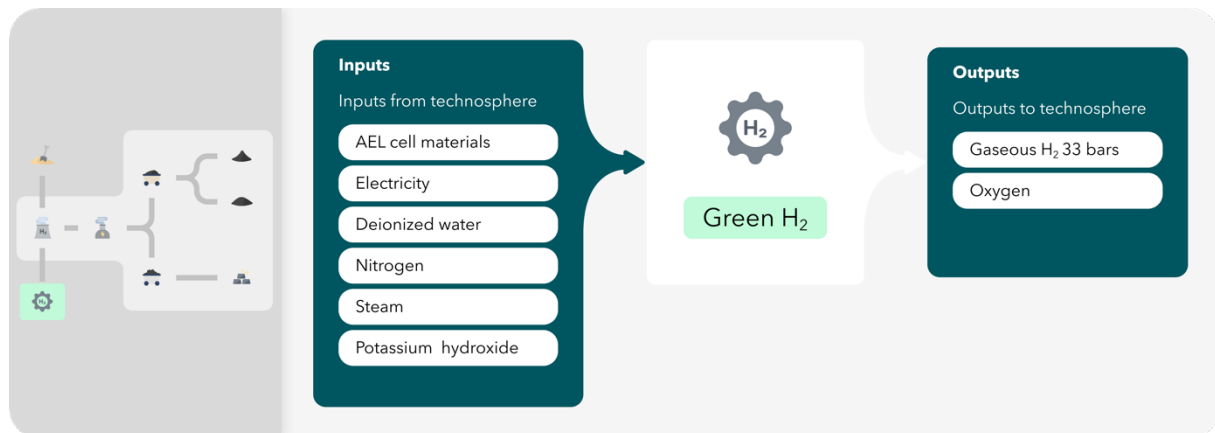
4.3.5.1 Green hydrogen production

Figure 19 Overview of the most important inputs and outputs for green H_2 production and an overview of the process flow.

LCI data for green H_2 production is adapted from Koj et al. [68] and scaled to align with the estimated annual consumption rate of H_2 provided by ETI [54]. Figure 19 describes the inputs and output flows for green H_2 production. ETI primarily intends to use Alkaline electrolysis (AEL) for on-site H_2 production. AEL is currently the most established and mature electrolysis technology available [69], particularly for stationary applications within industrial settings. Hence, AEL is assumed for this study.

Complete LCI data and technical characteristics for a 6 MW AEL are presented in Appendix 2. The LCI is found to be representative of European production for AEL [68]. The functional unit presented in the referenced study is "*one kg of gaseous H_2 at 33 bars and 40 °C*". Based on the technical data presented, an annual H_2 production rate of approximately 1 030 tons is found for the 6 MW AEL. Ten separate 6 MW AEL units are assumed to produce adequate amounts of H_2 to match the estimated annual consumption rate at ETI for the H-PR. A total lifetime of 20 years is given for the cell stack framework and ten years for the cells within the

AEL. The LCI data is adjusted to reflect a total lifetime of 20 years (i.e., one replacement of cells is accounted for). Additionally, an electricity consumption rate of 50 kWh per kg H_2 is obtained. Electricity generated from hydropower is intended to be used for one-site H_2 production at ETI.

The oxygen produced is assumed vented to air. Thus, green H_2 production is considered a mono-functional process and all associated environmental impacts are credited to the H_2.

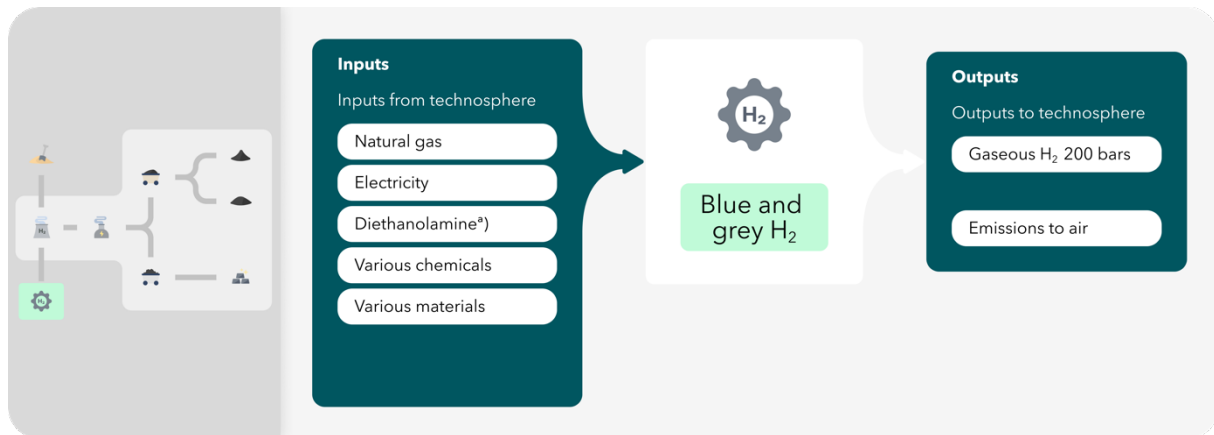### 4.3.5.2 Blue and grey hydrogen production

Figure 20 Description of the most important input and output flows for blue and grey H_2 production. Flows marked with [a] pertain only to blue H_2.

Blue and grey H_2 have been included as alternative H_2 production methods to on-site water electrolysis. The input and output flows of both production methods are illustrated in Figure 20. Notably, blue and grey H_2 rely on external production and subsequent transportation to Tyssedal. Thus, electricity for compression is included as part of the system boundary, despite not being included for the green H_2 production.

LCIs for blue and grey H_2 production have been adapted from Antonini et al. [70], which investigated the environmental impacts of H_2 production from natural gas using various carbon capture technologies and process methods. The functional unit presented is "*Production of one MJ of compressed gaseous H_2 (LHV) at a pressure of 200 bar at ambient temperature*".

Several H_2 production processes have been investigated by Antonini et al. [70]. For this study, blue H_2 production via SMR was selected, as it is currently the dominant technology for producing H_2 from natural gas [46]. Furthermore, the CO_2 capture technology applied was methyl diethanolamine (MDEA), as amine-based absorption is currently the most mature pre-combustion CO_2 capture technology [71]. Hence, these assumptions are assumed to be representative. The chosen production route also includes two water gas shift (WGS) reactors, consisting of a high- and low-temperature reactor (HT+ LT).

For the blue H_2 production, a CO_2 capture rate of 90% is assumed as a base-case scenario. In addition, a capture rate of 98% is included as part of a sensitivity analysis.

For the grey H_2, the production route is assumed to be equal to the blue H_2, with the exclusion of carbon capture (i.e., SMR with HT+LT WGS).

Complete LCI, as presented by Antonini et al. [70], for blue and grey H_2 production via SMR is shown in Appendix 2. The production facility is assumed to be located in Western Norway. To ensure geographic representativeness, alterations have been made to the background processes. More specifically, natural gas production modeled to represent European production has been replaced by offshore natural gas production based on data provided by the Norwegian petroleum industry [72]. For electricity generation, the Norwegian (NO) market process for high-voltage electricity was used to replace the European electricity market mix (ENTSO-E). The remaining background processes have been replaced to represent the European market. The altered LCI is used as a base-case for blue and grey H_2 production. However, the original LCI is included and used as part of a sensitivity analysis.

For the transportation of gaseous H_2 to Tyssedal, a distance of 350 km is assumed. Transportation is modeled using the background process "*Tanker for liquefied natural gas*", which is assumed to be an acceptable proxy.

Background processes for CO_2 transport and storage are not found in the ecoinvent database. However, their contribution to the environmental impacts have been shown to be negligible [73]. Therefore, these activities were not included in the inventory for this study, despite being part of the system boundary of Antonini et al.

5 Life Cycle Impact Assessment (LCIA)

The following chapter presents the LCIA results for all co-products. Hence, the following subchapter pertains to the primary objective of the study, as well as the first of the secondary objectives posed in this thesis.

5.1 LCIA results

The following subchapter presents characterized cradle-to-gate LCIA results for the co-production of chloride slag, sulfate slag and HPPI for both investigated processing routes (i.e., C-PR and H-PR), including the H_2 production methods assessed for the H-PR (i.e., green, blue, and grey). The results are presented for the eight impact categories described in the goal and scope (see section 3.2.5), based on the ReCiPe 2016 Midpoint (H) method.

As previously mentioned, the multifunctionality of the co-products and by-production of skimmed slag is solved by economic allocation. The allocation factors applied are presented in Figure 7 and Appendix 1. The results are presented for the co-production of one kg chloride slag, 0.29 kg sulfate slag, and 0.53 kg HPPI. The LCIA results for the by-production of 0.03 kg skimmed slag are presented separately in Appendix 3.

The results are presented in the following order: first, the eight selected impact categories are displayed separately in Figure 21 to Figure 28. The reduction potentials for the H-PR compared to the C-PR are described by the whiskers and the corresponding percentage. Then, Figure 29 and Figure 30 display relative impact scores for all impact categories for titanium slag (i.e., chloride slag and sulfate slag) and HPPI[11].

---

[11] Can also be referred to as normalized scores in the sense of rescaling the results to a 0-1 scale, not as the optional normalization step in LCA.

Figure 21 presents the LCIA results for the impact category GWP where the C-PR is represented by the orange column, and the H-PR is represented by the green, blue, and grey columns.
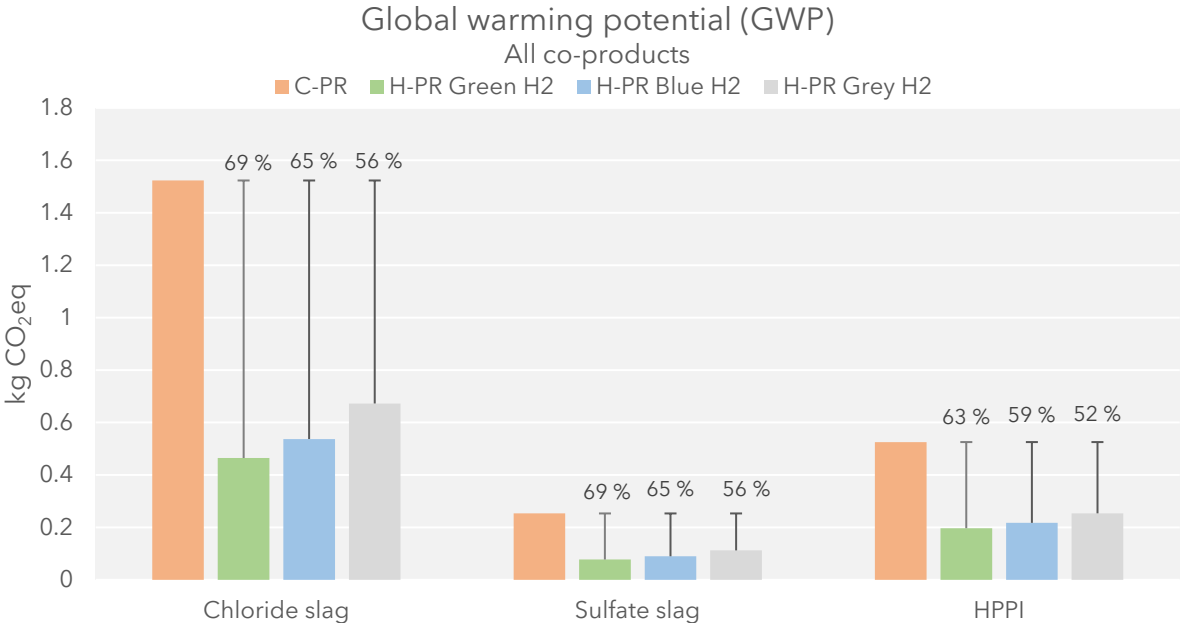

Figure 21 Characterized LCIA results for GWP using ReCiPe 2016 at the hierarchist perspective (i.e., 100 year time horizon). Results are presented for one kg chloride slag, 0.29 kg sulfate slag, and 0.53 kg HPPI. The reduction potential for the H-PR compared to the C-PR is represented by the whiskers and percentage.

From Figure 21, a GWP of 1.52 kg CO_2eq per kg chloride slag produced via the C-PR can be observed. In comparison, a GWP of 0.46, 0.54, and 0.67 kg CO_2eq per kg chloride slag is found for the H-PR using green, blue, and grey H_2 as reductants, respectively. These findings indicate that the H-PR employing green H_2 offers the most significant emission reduction potential for chloride slag compared to the C-PR (69%). The reduction potential for H-PR using blue and grey H_2 is found to be 65% and 56%, respectively.

Two additional observations can be made from Figure 21: first, the relative reduction potential for the GWP of sulfate slag is approximately equal to chloride slag when comparing the C-PR to the H-PR, regardless of the H_2 production method. Secondly, HPPI has a lower relative reduction potential than chloride slag.

Figure 22 displays the LCIA results for the impact category stratospheric ozone depletion.

Stratospheric ozone depletion
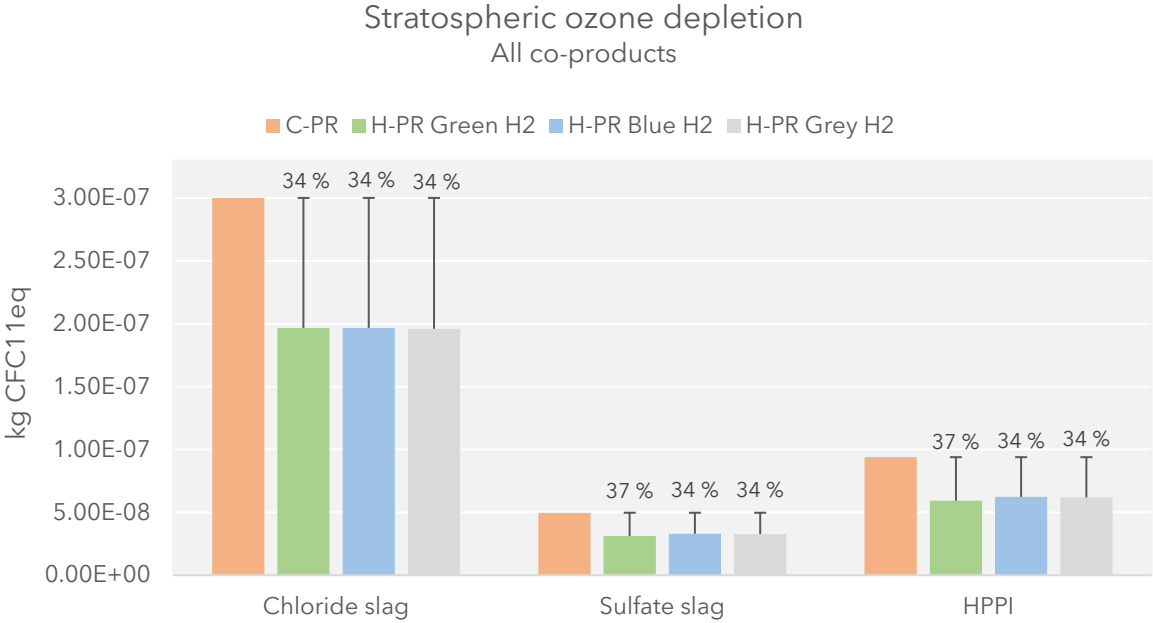All co-products

Figure 22 Characterized LCIA results for stratospheric ozone depletion using ReCiPe 2016 at the hierarchist perspective. Results are presented for one kg chloride slag, 0.29 kg sulfate slag, and 0.53 kg HPPI. The reduction potential for the H-PR compared to the C-PR is represented by the whiskers and percentage.

From Figure 22 a stratospheric ozone depletion potential of approximately 3.0E-07 kg CFC11eq per kg chloride slag for the C-PR and 2.0E-07 kg CFC11eq per kg chloride slag for the H-PR is found. Approximately equal impact scores are observed for the different H_2 production methods for the H-PR. This amounts to a 34% reduction potential for the H-PR, regardless of the H_2 production method. Similar results are found for sulfate slag and HPPI.

Figure 23 and Figure 24 display the LCIA results for the impact categories pertaining to ground-level ozone formation.
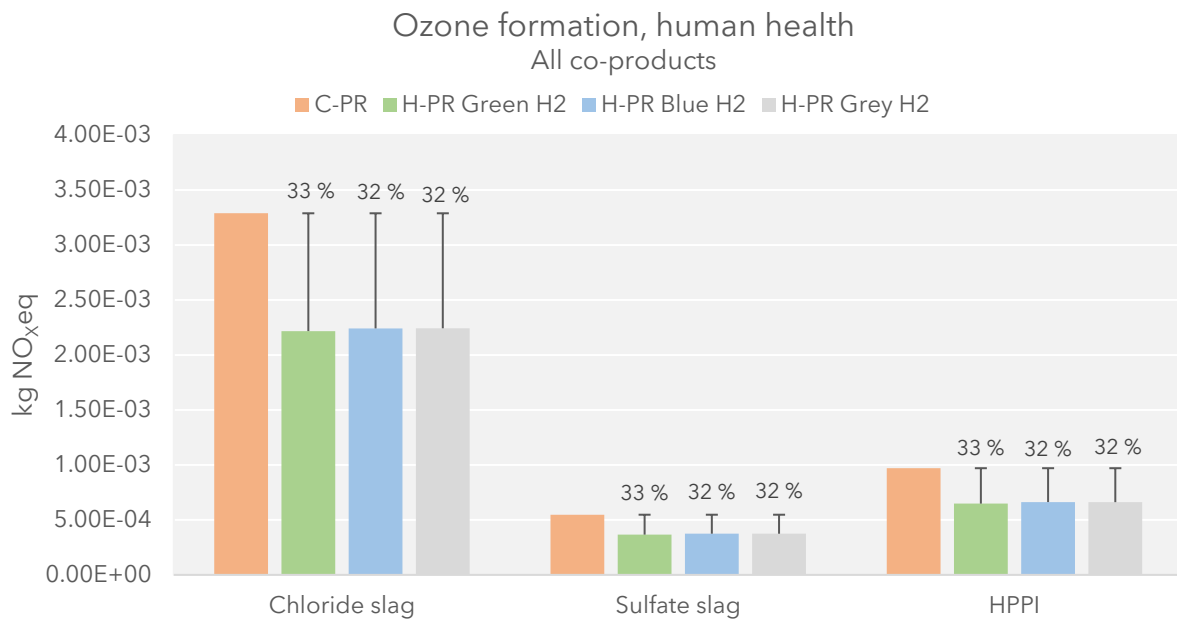

Figure 23 Characterized LCIA results for ozone formation, human health using ReCiPe 2016 at the hierarchist perspective. Results are presented for one kg chloride slag, sulfate slag and 0.53 kg HPPI. The reduction potential for the H-PR compared to the C-PR is represented by the whiskers and percentage.

From Figure 23, the impact score for ozone formation, human health is found to be approximately 3.3E-03 kg NO_xeq per kg chloride slag for the C-PR and 2.2E-03 kg NO_xeq per kg chloride slag for the H-PR, regardless of H_2 production method. The reduction potential for the H-PR is between 32% and 33% for the different H_2 production methods, with a marginally greater reduction potential for the H-PR utilizing green H_2. Similar results are found for sulfate slag and HPPI.
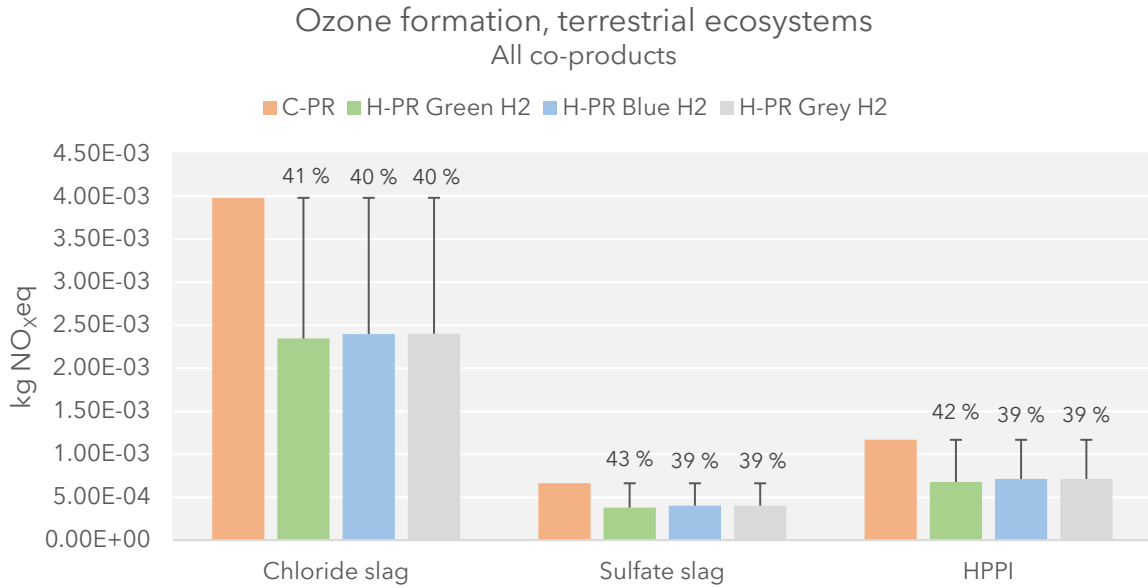
Figure 24 Characterized LCIA results for ozone, formation, terrestrial ecosystems using ReCiPe 2016 at the hierarchist perspective. Results are presented for one kg chloride slag, 0.29 kg sulfate slag and 0.53 kg HPPI. The reduction potential for the H-PR compared to the C-PR is represented by the whiskers and percentage.

From Figure 24, the impact score for ozone formation, terrestrial ecosystems per kg chloride slag is approximately 4.0E-03 kg NO_xeq for the C-PR and 2.4E-03 kg NO_x eq for the H-PR. A reduction potential between 40% and 41% can be observed for the H-PR for the different H_2 production methods. H-PR utilizing green H_2 is found to have a marginally more significant reduction potential than blue and grey H_2. Similar results are found for sulfate slag and HPPI.
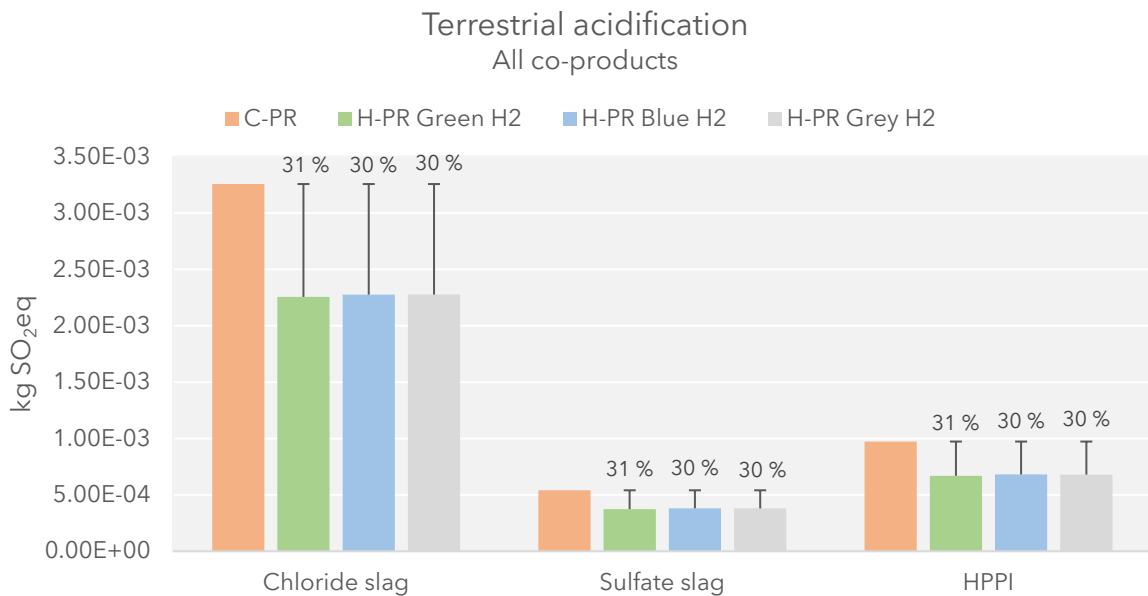

Figure 25 Characterized LCIA results for terrestrial acidification using ReCiPe 2016 at the hierarchist perspective. Results are presented for one kg chloride slag, 0.29 kg sulfate slag, and 0.53 kg HPPI. The reduction potential for the H-PR compared to the C-PR is represented by the whiskers and percentage.

As presented in Figure 25, the terrestrial acidification potential for chloride slag is found to be approximately 3.3E-03 kg SO_2eq per kg chloride slag for the C-PR and 2.3E-03 kg SO_2eq per kg chloride slag for the H-PR. In addition, the reduction potential for the H-PR is found to be approximately equivalent between the different H_2 production methods, with a 31% reduction potential for the H-PR when utilizing green H_2 and 30% when utilizing blue or grey H_2. Similar results are observed for all co-products.
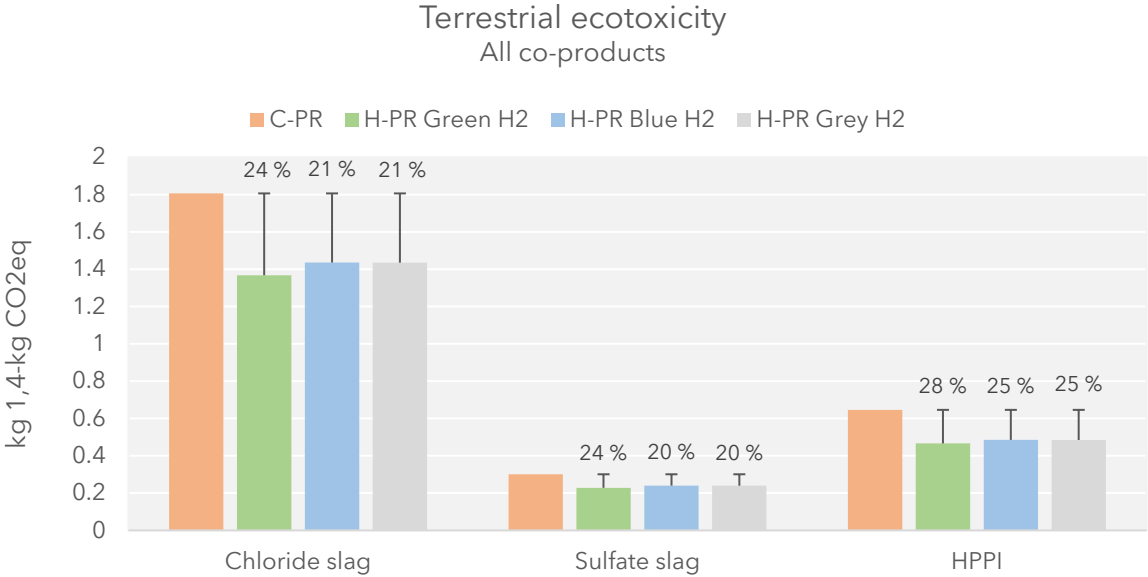

Figure 26 Characterized LCIA results for terrestrial ecotoxicity using ReCiPe 2016 at the hierarchist perspective. Results are presented for one kg chloride slag, 0.29 kg sulfate slag, and 0.53 kg HPPI. The reduction potential for the H-PR compared to the C-PR is represented by the whiskers and percentage.

As illustrated in Figure 26, the terrestrial ecotoxicity potential is approximately 1.8 kg 1,4-DCBeq for the C-PR and 1.4 kg 1,4-DCBeq per kg chloride slag. The reduction potential for H-PR is observed to be 24% when utilizing green H_2, and 20% and 21% when utilizing blue and grey H_2, respectively. Similar results are observed for sulfate slag. For HPPI, a reduction potential is between 25% and 38%, indicating a larger relative reduction potential for HPPI than chloride slag and sulfate slag.
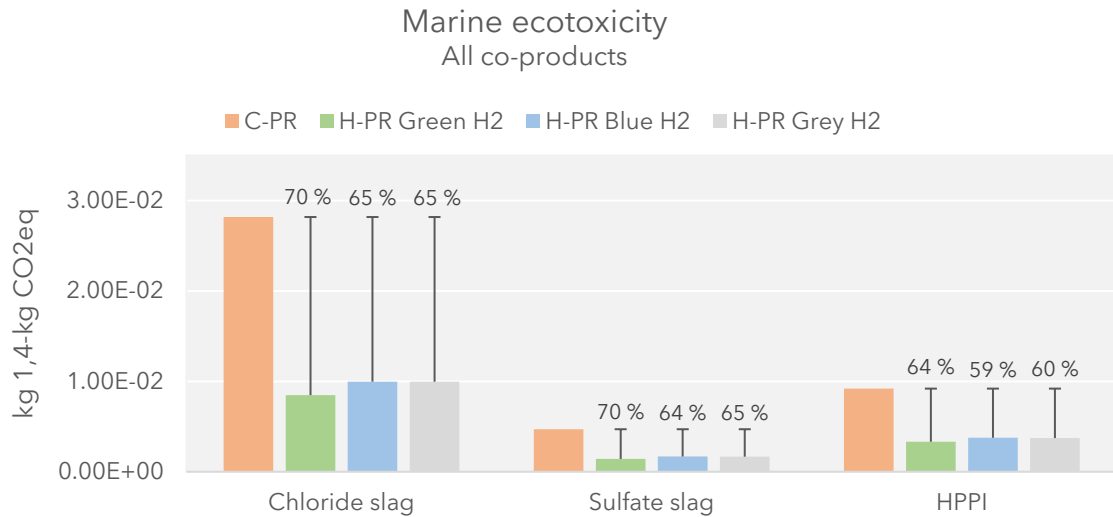
Figure 27 Characterized LCIA results for Marine ecotoxicity using ReCiPe 2016 at the hierarchist perspective. Results are presented for one kg chloride slag, 0.29 kg sulfate slag, and 0.53 kg HPPI. The reduction potential for the H-PR compared to the C-PR is represented by the whiskers and percentage.

Figure 27 displays a marine ecotoxicity potential of approximately 0.0280 kg 1,4-DCBeq per kg chloride slag for the C-PR. For the H-PR utilizing green H_2, an impact score of 8.5E-03 kg 1,4-DCBeq is found, while for H-PR utilizing blue and grey H_2, an impact score of approximately 0.0100 kg is observed for both alternatives. Hence, using green H_2 in the H-PR results in the highest reduction potential at 70%, while the reduction potential for blue and grey is 64% and 65%, respectively. Similar results are observed for sulfate slag. Conversely, the relative reduction potential for HPPI is found to be lower than for chloride slag and sulfate slag.

Human non-carcinogenic toxicity
All co-products

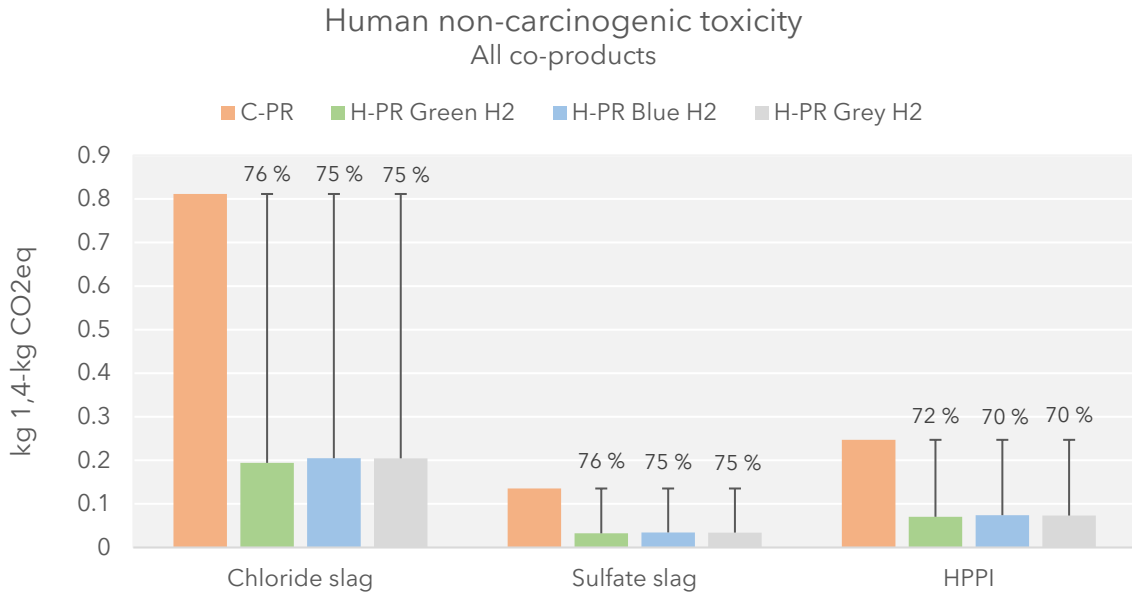■ C-PR   ■ H-PR Green H2   ■ H-PR Blue H2   ■ H-PR Grey H2

Figure 28 Characterized LCIA results for human non-carcinogenic toxicity using ReCiPe 2016 at the hierarchist perspective. Results are presented for one kg chloride slag, 0.29 kg sulfate slag and 0.53 kg HPPI. The reduction potential for the H-PR compared to the C-PR is represented by the whiskers and percentage.

As presented in Figure 28, the human non-carcinogenic toxicity potential is found to be approximately 0.8 kg 1,4-DCBeq per kg chloride slag for the C-PR. For the H-PR impact score of approximately 0.2 kg 1,4-DCBeq per kg chloride slag is observed for all H_2 production methods. The relative reduction potential for H-PR is found to be 76% for green H_2, which is marginally greater than for blue and grey H_2 (75%). Similar results are found for sulfate slag. Conversely, HPPI is observed to have a lower relative reduction potential compared to chloride slag and sulfate slag (70-72%).

Complete tables of all LCIA results for one kg chloride slag, 0.29 kg sulfate slag, and 0.53 kg HPPI are presented in Appendix 3.

Figure 29 and Figure 30 presents the relative LCIA results for all impact categories for titanium slag and HPPI, respectively. Here, titanium slag represents both chloride slag and sulfate slag, as the relative impact scores of these products are of the same order of magnitude.
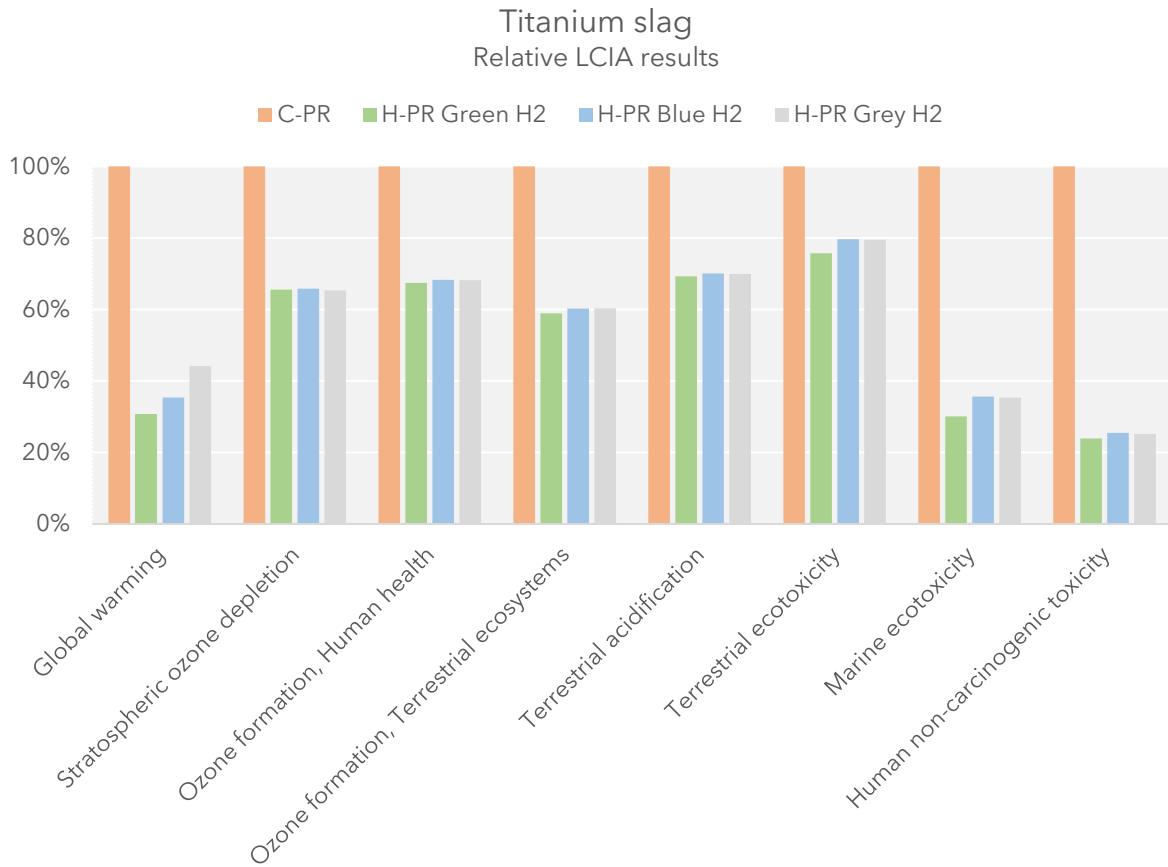
Figure 29 Relative LCIA results for the production of titanium slag (i.e., chloride slag and sulfate slag) for all eight impact categories.
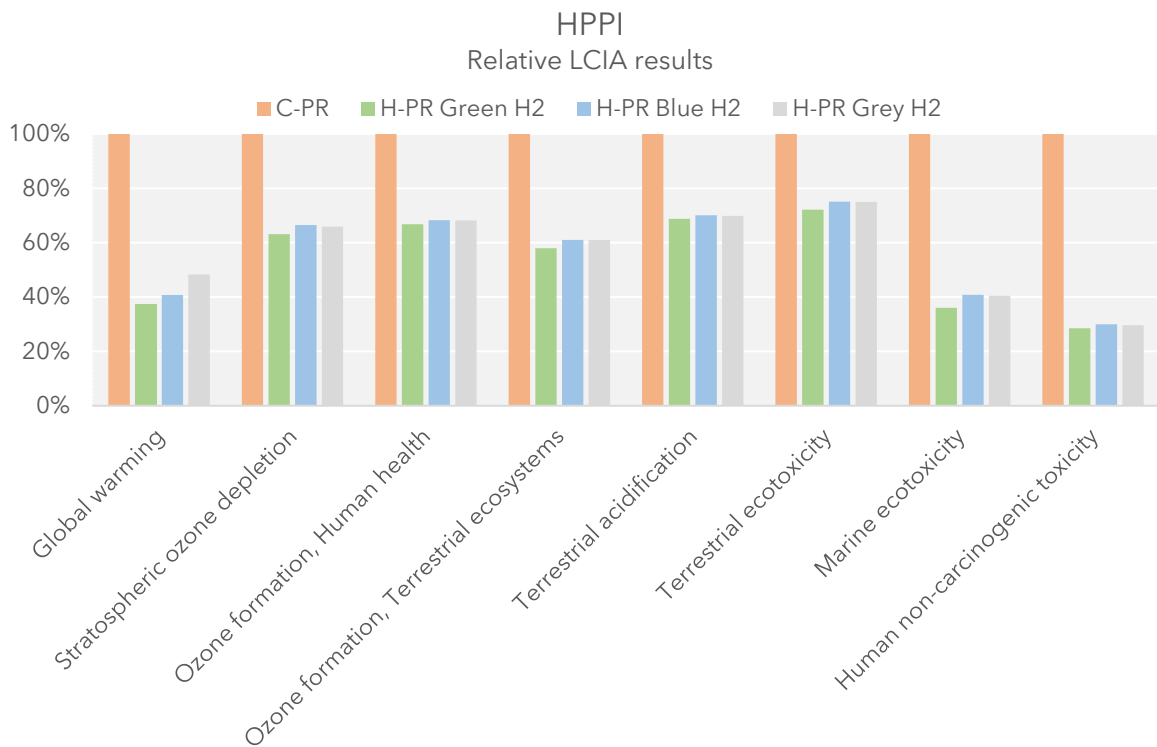

Figure 30 Relative LCIA results for the production of HPPI for all eight impact categories.

From Figure 21 to Figure 30, it is observed that the C-PR has the largest impact score for all included impact categories. The greatest reduction potential for chloride slag produced through the H-PR is observed for the following impact categories: human non-carcinogenic toxicity (76%), marine ecotoxicity (70%) and GWP (69%) when green H_2 is utilized.

When comparing H_2 alternatives for the H-PR, it is observed that using green H_2 as reductant results in a non-marginal lower impact (i.e., > 4% difference) on the following impact categories: global warming, terrestrial ecotoxicity and marine ecotoxicity. For the remaining impact categories, the difference is marginal between the investigated H_2 alternatives (i.e., < 4%). The H-PR utilizing grey and blue H_2 have approximately equal contributions to all impact categories, except GWP. These results are discussed further in the contribution analysis found in Subchapter 7.1.

The results obtained in this section pertain to the primary objective of this thesis, which is to investigate the environmental impacts of substituting coal with H_2 in the production of titanium slag. Additionally, the presented results describe the effect of employing alternative H_2 production methods and thus assess the first of the secondary objectives. These results will be further discussed through a contribution analysis and sensitivity analysis in Chapter 7. Following the sensitivity analysis, the subsequent sections will address the last objective of the study (i.e., comparison of titanium slag production with and without an additional pre-reduction phase) (see Subchapter 7.4).

6 Greenhouse Gas Protocol results

6.1 Scope 1, 2 and 3

In addition to the cradle-to-gate representation of the LCIA results presented in Chapter 5, the following chapter presents the results according to the framework of the Greenhouse gas protocol (GHG protocol) [74].

The GHG protocol is a widely used framework for reporting the carbon footprint at the corporate level [75]. To delineate direct and indirect emission sources, the GHG protocol introduces the following classification:

Scope 1	Direct GHG emissions occur from sources that are owned or controlled by the company (direct emissions)
Scope 2	GHG emissions from the generation of purchased electricity (electricity)
Scope 3	GHG emissions that occur as a consequence of the activities of the company, but from sources not owned or controlled by the company (upstream/ downstream emissions)

This classification of emission sources is typically included in sustainability reports to communicate the organization's environmental impact and progress toward sustainability goals [75]. Presenting the LCIA results obtained in this study in the classification framework of the GHG protocol is useful for interconnecting the results efficiently and is highly relevant for industrial applications as a supplement to the results presented in Chapter 5.
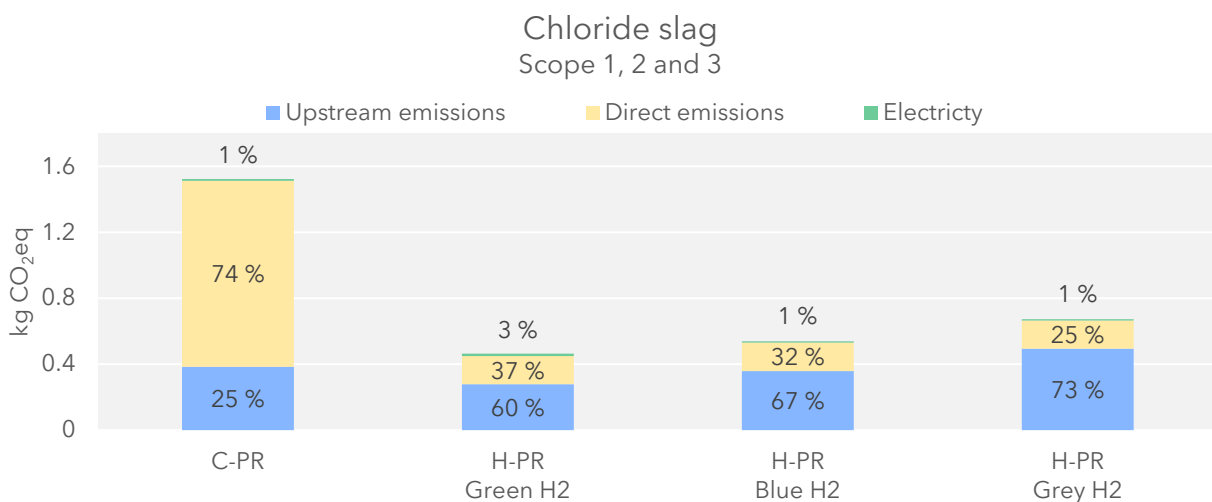

Figure 31 Results presented according to the GHG protocol as scope 1, 2 and 3 for one kg chloride slag.

Figure 31 displays GHG emissions of one kg chloride slag classified as upstream emissions, direct emissions, and electricity. Upstream emissions refer to all upstream activities from the gate at ETI's production facility in Tyssedal and comprise the production, processing, and

transportation of all source streams, including ilmenite and production of blue and grey H_2. Direct emissions include all emissions from gate-to-gate at ETI's production facility in Tyssedal. In the case of green H_2 production, electricity used for on-site electrolysis operations is displayed as electricity (i.e., scope 2), while emissions associated with material inputs for the water electrolysis are categorized as upstream emissions. Electricity comprises emissions from power generation utilized directly at ETI (i.e., not including electricity used in upstream activities).

From Figure 31, it can be observed that the direct emissions constitute the largest share of the GWP for chloride slag for the C-PR, while upstream emissions are dominating for the H-PR, regardless of the H_2 production method. Furthermore, when only considering the direct emission from the gate-to-gate unit processes, a reduction potential of 85% is observed when comparing the H-PR utilizing green H_2 to the C-PR, as opposed to the 69% found for the cradle-to-gate results (see Figure 21).

Figure 32 displays similar results for sulfate slag. Again, an 85% reduction potential per kg sulfate slag is observed for direct emissions when comparing C-PR to the H-PR utilizing green H_2.
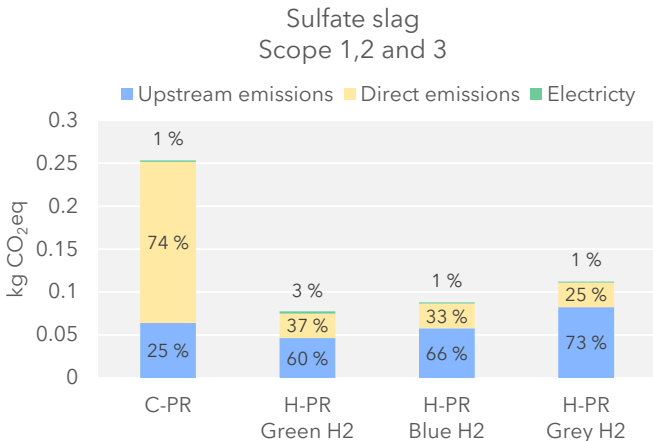
Figure 32 Results presented according to the GHG protocol as scope 1, 2 and 3 for 0.29 kg sulfate slag.

Similar results can be observed for HPPI produced via the C-PR in Figure 33. However, for the H-PR using green H_2 as a reductant, the direct emissions are found to be larger than upstream emissions. A reduction potential of 75% per kg chloride slag is found when only considering the direct emissions from the gate-to-gate unit processes in terms of GWP.

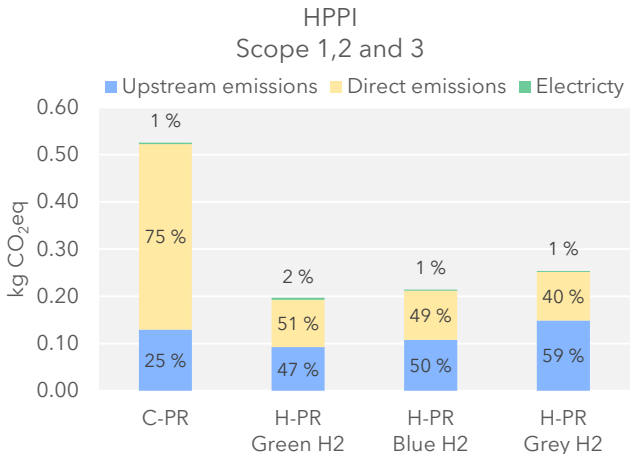*Figure 33 Results presented according to the GHG protocol as scope 1, 2 and 3 for 0.53 kg HPPI.*

6.2 Scope 3 emissions

Figure 34 displays a breakdown of the scope 3 emissions (i.e., upstream emissions from the value chain) chloride slag and HPPI. Processes contributing to less than 3% of upstream emissions are aggregated as "*other*". Scope 3 emissions from sulfate slag have not been included due to the similarity in contributing processes with chloride slag, although at a smaller scale.
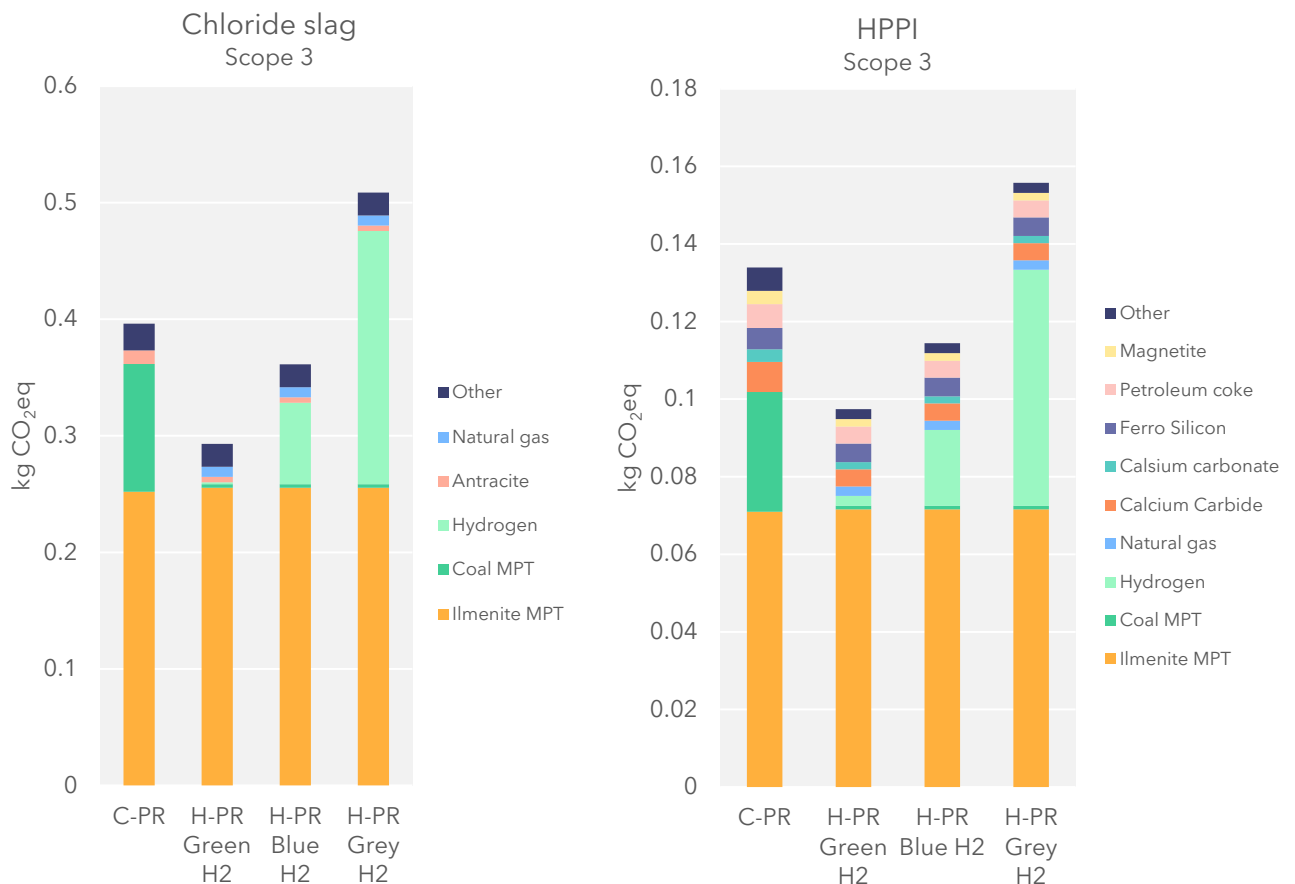
Figure 34 Breakdown of scope 3 emissions for one kg chloride slag (left) and 0.53 kg HPPI (right).

Figure 34 shows that ilmenite MPT is the upstream process with the most significant contribution to the GHG emissions for all products, regardless of processing route. For the C-PR, ilmenite MPT is followed by coal MPT. For H-PR utilizing blue and grey H_2, H_2 production is observed to be the second largest upstream contributor. In the case of the H-PR employing green H_2 as a reductant, the aggregated category labeled as "*other*" is observed to be the second largest in terms of GHG emissions. This finding can be attributed to the categorization of electricity utilized for H_2 production under Scope 2 emissions.

Additionally, it is found that the materials specific for iron refining have a significant contribution to the GHG emission intensity of HPPI. For the C-PR, iron refining products constitute 25% of the total GHG emissions of HPPI, while for the H-PR, these account for 18%, 15%, and 11% when green, blue, and grey H_2 is utilized, respectively.

7 Discussion

The following chapter presents the interpretation of the LCIA results presented in Chapter 5. It aims to provide transparency to the LCA by identifying the most important contributors, assessing the overall reliability of the results through a sensitivity analysis, and interpret the results in light of the defined goal and scope. Additionally, the data quality and limitations of the study are discussed.

7.1 Contribution analysis

A contribution analysis has been conducted to identify the most important unit processes for each impact category for chloride slag. Disaggregated LCIA results are provided for all unit processes. Notably, coal MPT for the coal used as a reducing agent is separated from the pre-reduction. This separation facilitates a fair comparison of the pre-reduction processes for C-PR and H-PR, as H_2 production is considered a separate unit process, and H_2 and coal serve the same function in the two investigated processing routes. The contribution analysis is only presented for one kg chloride slag. The results are presented in more detail for GWP, as this is the impact category of most interest.

Detailed contribution analysis results are presented in Appendix 4. Background processes contributing to more than 3% of the total impact score of each impact category are presented for each unit process in separate tables. The tables display absolute values. Additionally, a breakdown of the environmental flows contributing to the impact score of direct emissions from the gate-to-gate unit processes is provided in Appendix 4.

The results presented in Appendix 4 are referred to throughout the contribution analysis to identify the most significant contributors within the unit processes.

7.1.1 Global warming potential

Figure 35 displays the GWP of chloride slag disaggregated for all unit processes. Additionally, Figure 36 to Figure 39 show the relative contribution of background processes and direct emissions with a cut-off criteria of 3%, based on the detailed contribution analysis results presented in Appendix 4. Hence, these figures present both indirect and direct emissions. The absolute value for each unit process is displayed at the top of each column. Notably, H_2 production is the only unit process that varies within the different H-PR alternatives, and H-PR is thus presented as a singular column for the other unit processes. A separate figure for slag refining has not been included due to the relatively low contribution to the total GWP.
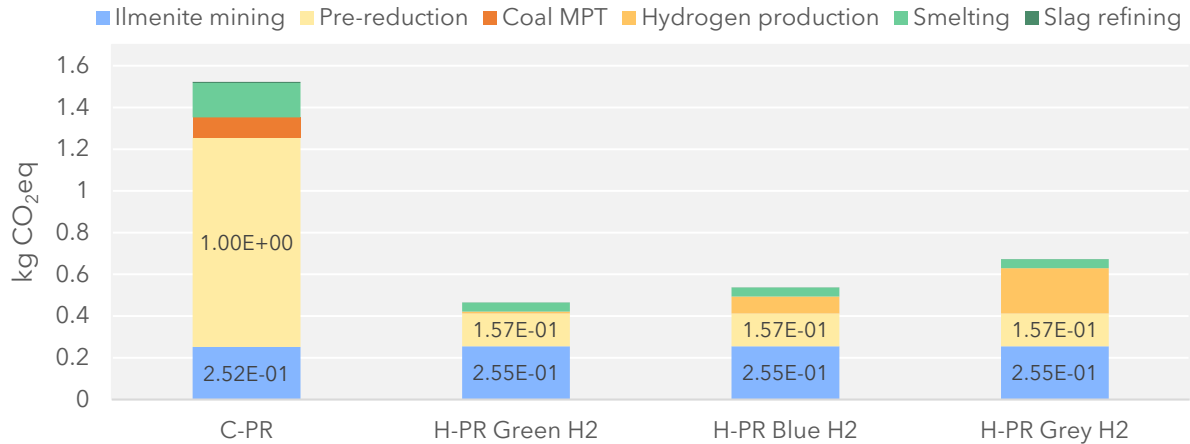
Figure 35 LCIA results disaggregated for all unit processes for the production of one kg chloride slag – GWP.

From Figure 35 it can be observed that pre-reduction is the largest contributor to the GWP of chloride slag produced via the C-PR, followed by ilmenite MPT and smelting. For chloride slag produced via the H-PR, the contribution from pre-reduction is reduced by 84% from 1.00 to 0.157 kg CO_2eq per kg chloride slag, making ilmenite the primary contributor. Pre-reduction is found to be the second largest contributor to the total GWP of the H-PR when green H_2 and blue H_2 are used as reductants. While, for H-PR employing grey H_2, H_2 production through SMR is observed to have a greater contribution than the pre-reduction. Slag refining is found to have a negligible contribution to the GWP for all processing routes.
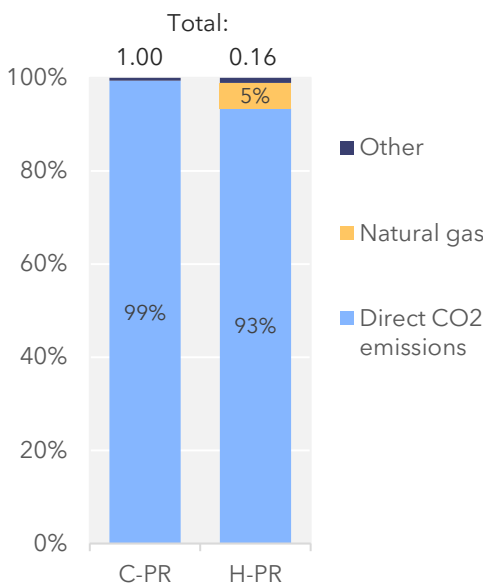
In Figure 36, the main contributors to the GWP of the pre-reduction process are displayed for both processing routes. From this it is clear that direct CO_2 emissions are the primary contributors to both the C-PR and H-PR. For the C-PR a CO_2 emission rate of 0.99 kg CO_2 per kg chloride slag is observed, while for the H-PR this is observed to be 0.15 kg CO_2 per kg chloride slag. In the case of C-PR, this is mainly due to coal combustion in the rotary kiln, while for the H-PR, it is due to natural gas combustion to heat the ilmenite. When comparing direct emissions of CO_2 from the C-PR and H-PR, an 85% reduction is observed for the H-PR per kg chloride slag.

Figure 36 Contribution analysis of pre-reduction per kg chloride slag for GWP. Figure displays the relative contribution of the largest contributors. Total value is displayed at the top of each column.

Figure 37 displays that for ilmenite MPT, the generation of electricity is the largest contributor to the GWP, accounting for 45%. The second most significant contributor is observed to be transportation to Tyssedal by bulk carrier, which contributes 18% to the GWP. The electricity utilized in the process is modeled using the dataset for Senegalese market mix for medium-voltage electricity, which is predominantly generated from oil and thus exhibits a high GHG emission rate.

Ilmenite MPT
Contribution analysis - GWP
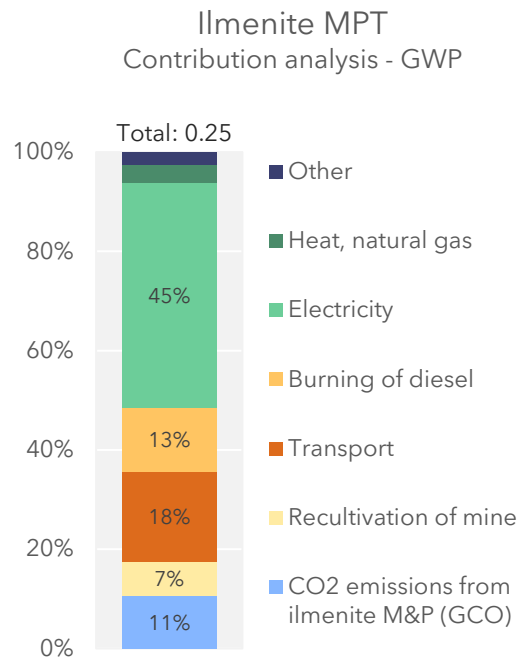
Figure 37 Contribution analysis of ilmenite mining, processing and transport (MPT) per kg chloride slag for GWP. Figure displays the relative contribution of the largest contributors. Total value is displayed at the top of each column.

From Figure 38, it can be observed that direct emissions of CO_2 from the electric arc furnace (EAF) are the main contributor to both the C-PR and H-PR from the smelting process. Additionally, two main observations can be made. Firstly, indirect emissions related to electricity consumption, coal MPT and anthracite are lower per kg chloride slag for the H-PR than C-PR. For electricity, the GWP is found to be 6.00E-03 kg CO_2eq for the H-PR and 8.00E-03 kg CO_2eq for the C-PR. Secondly, direct CO_2 emissions per kg chloride slag from the smelting phase are reduced by 81% from the C-PR to the H-PR, due to the increased efficiency of the pre-reduction process.

Smelting in EAF
Contribution analysis - GWP
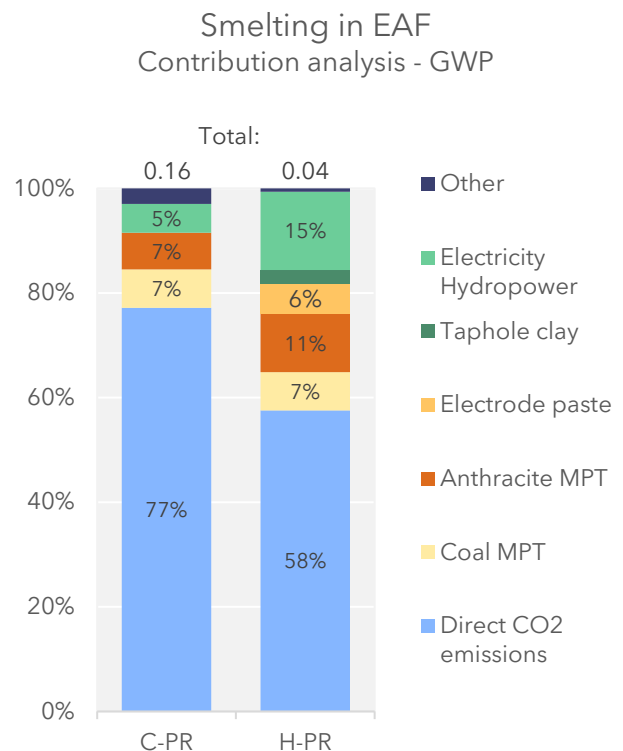
Figure 38 Contribution analysis of smelting per kg chloride slag for GWP. Figure displays the relative contribution of the largest contributors. Total value is displayed at the top of each column.

71
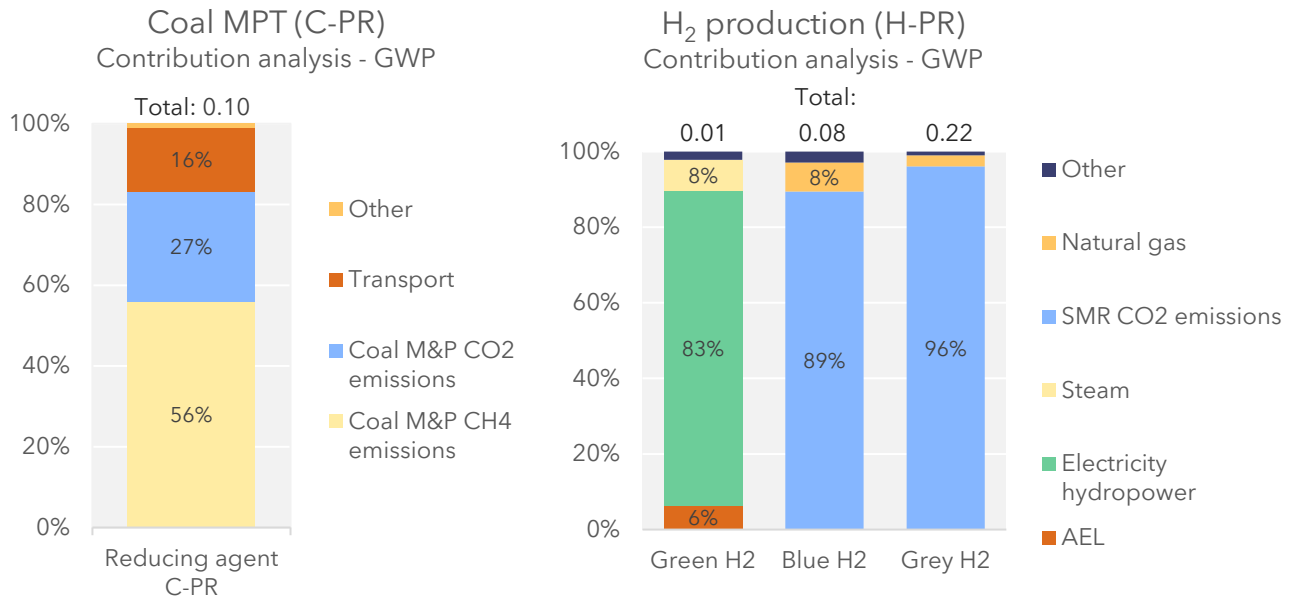
Figure 39 Contribution analysis of alternative reducing agents, coal MPT for the C-PR (left) and H₂ production for the H-PR (right) for GWP. Figure displays the relative contribution of the largest contributors. Total value is displayed at the top of each column.

Figure 39 displays the most significant contributors to the GWP of the alternative reducing agents in the C-PR and H-PR, namely H_2 and coal. It is observed that emissions of CH_4 and CO_2 from mining are the largest contributors to coal MPT (83%), followed by transportation to Tyssedal (16%). When comparing H_2 production methods, electricity is found to be the largest contributor to green H_2 production, while CO_2 emissions from steam methane reforming (SMR) is the main contributor to blue and grey H_2. The emission rate of CO_2 from SMR for blue H_2 is found to be 62% lower compared to grey H_2 due to the utilization of CCS technology.

7.1.2 Stratospheric ozone depletion
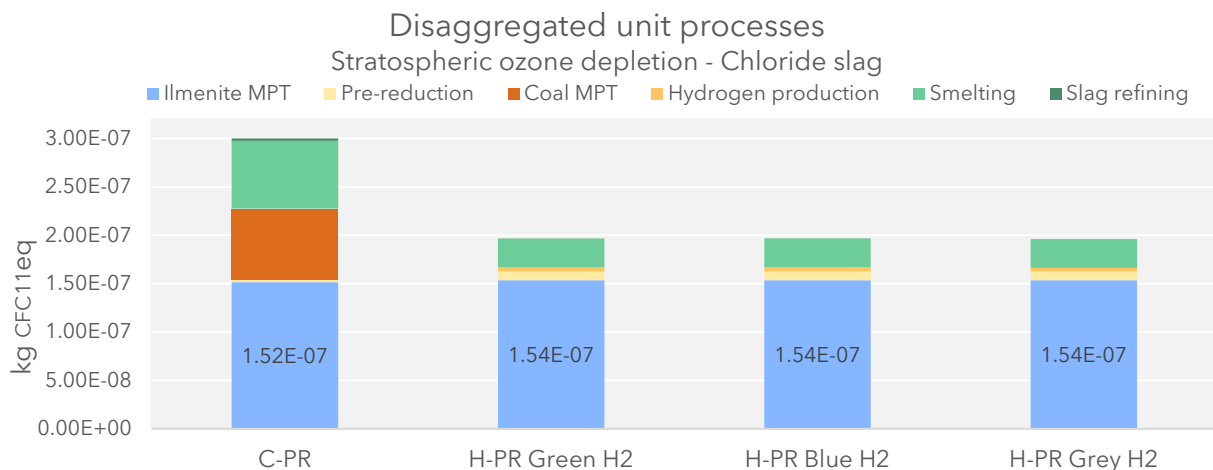
Figure 40 LCIA results disaggregated for all unit processes for the production of chloride slag - stratospheric ozone depletion.

Figure 40 displays the stratospheric ozone depletion potential disaggregated for all unit processes. From this and the complete contribution analysis results presented in Appendix 4, it can be observed that ilmenite MPT is the most significant contributor for both C-PR and H-PR, primarily due to electricity consumption (56%) and transportation of ilmenite (19%). The unit process with the second most significant contribution is observed to be smelting in the EAF for both processing routes, which is primarily caused by emissions of N_2O to air (77% for the C-PR and 58% for the H-PR).

7.1.3 Ozone formation, human health and terrestrial
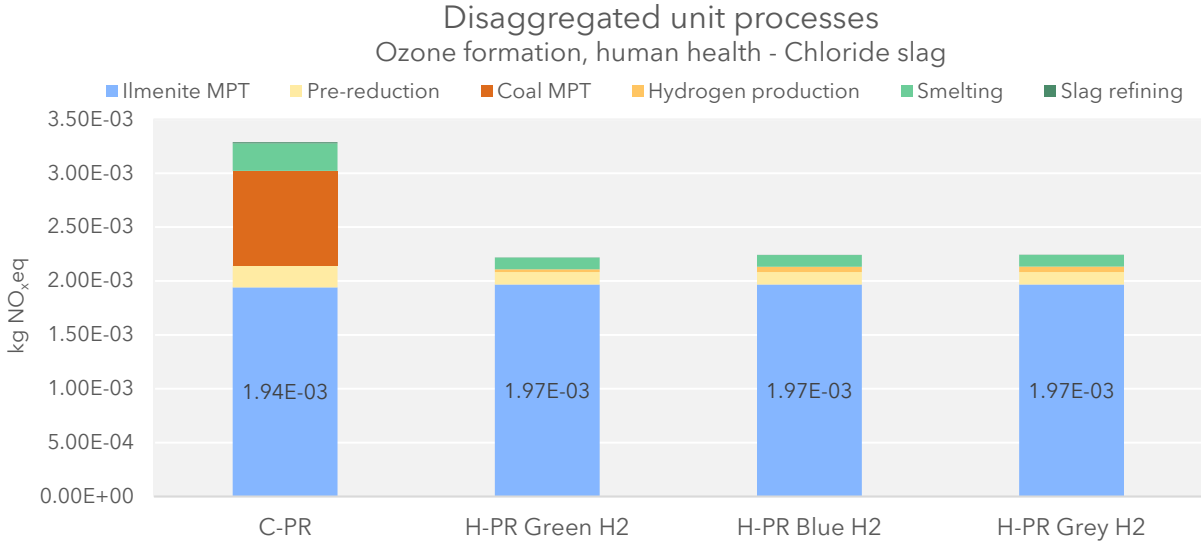
Figure 41 LCIA results disaggregated for all unit processes for the production of chloride slag - ozone formation, human health.

Figure 42 LCIA results disaggregated for all unit processes for the production of chloride slag - ozone formation, terrestrial ecotoxicity.

Figure 41 and Figure 42 display LCIA results for ozone formation human health and ozone formation terrestrial ecotoxicity disaggregated for all unit processes. From these figures, it

can be observed that ilmenite MPT is the primary contributor to both impact categories. 73% of this is found to be due to emissions of N_2O from the transport of ilmenite to Tyssedal, as presented in Appendix 4. Furthermore, the two impact categories are found to have similar results for all unit processes, with the exception of pre-reduction in the C-PR, which is observed to have a larger impact on ozone formation terrestrial ecosystems than ozone formation human health.

7.1.4 Terrestrial acidification
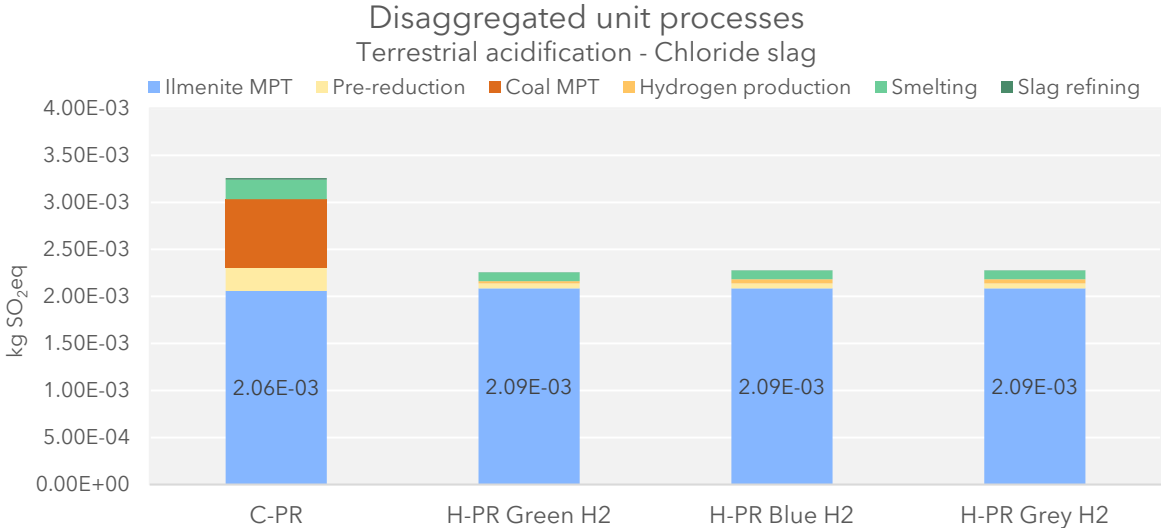
Figure 43 LCIA results disaggregated for all unit processes for the production of chloride slag - terrestrial acidification.

Figure 43 displays LCIA results for terrestrial acidification disaggregated for unit processes. The largest contributor is observed to be ilmenite MPT, primarily due to emissions of SO_2 (31%) and NO_x (16%) from transport and electricity generation (37%).

7.1.5 Terrestrial ecotoxicity

Figure 44 LCIA results disaggregated for all unit processes for the production of chloride slag - Terrestrial ecotoxicity.

Figure 44 displays LCIA results for terrestrial ecotoxicity, disaggregated for all unit processes. In the C-PR, an approximately equal contribution is observed for ilmenite MPT and pre-reduction at 37%, while for H-PR, ilmenite MPT is the primary contributor regardless of the H_2 production method, followed by pre-reduction. The primary contributors to terrestrial ecotoxicity for ilmenite MPT are found to be electricity generation (63%) and transport (22%), as shown in Appendix 4. For the pre-reduction, emissions of zinc to air account for approximately 78% of the terrestrial ecotoxicity for both H-PR and C-PR, with copper and lead to air contributing 10% and 8%, respectively.

These results are based on substitution of zinc-dust from the pre-reduction process in the C-PR, which reduces the terrestrial ecotoxicity by 2.09E-05 kg 1,4-DCBeq per kg chloride slag produced. This is equivalent to an 8% decrease per kg chloride slag.

7.1.6 Marine ecotoxicity
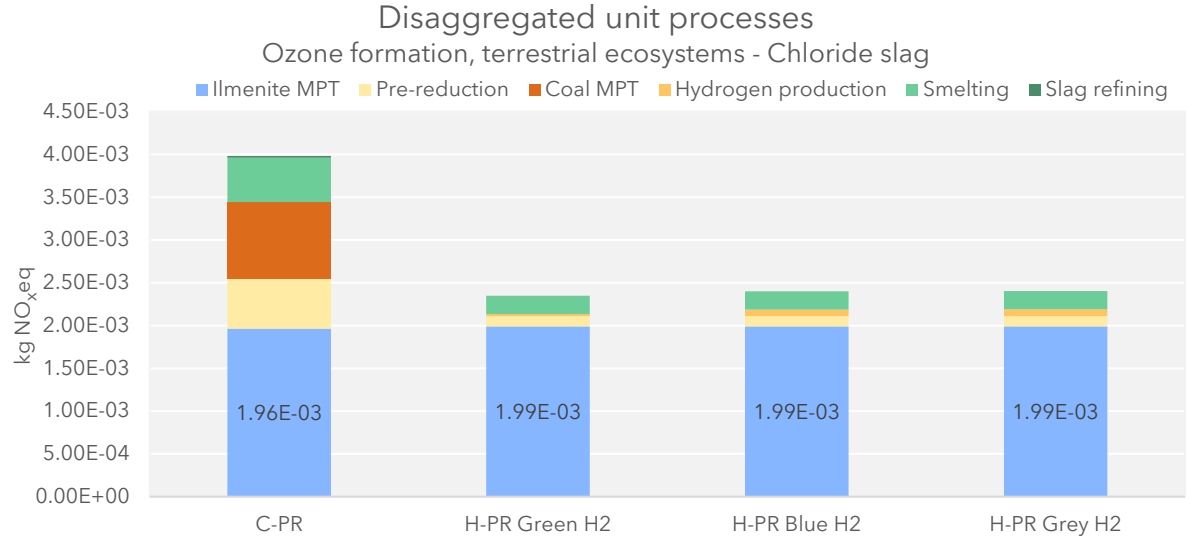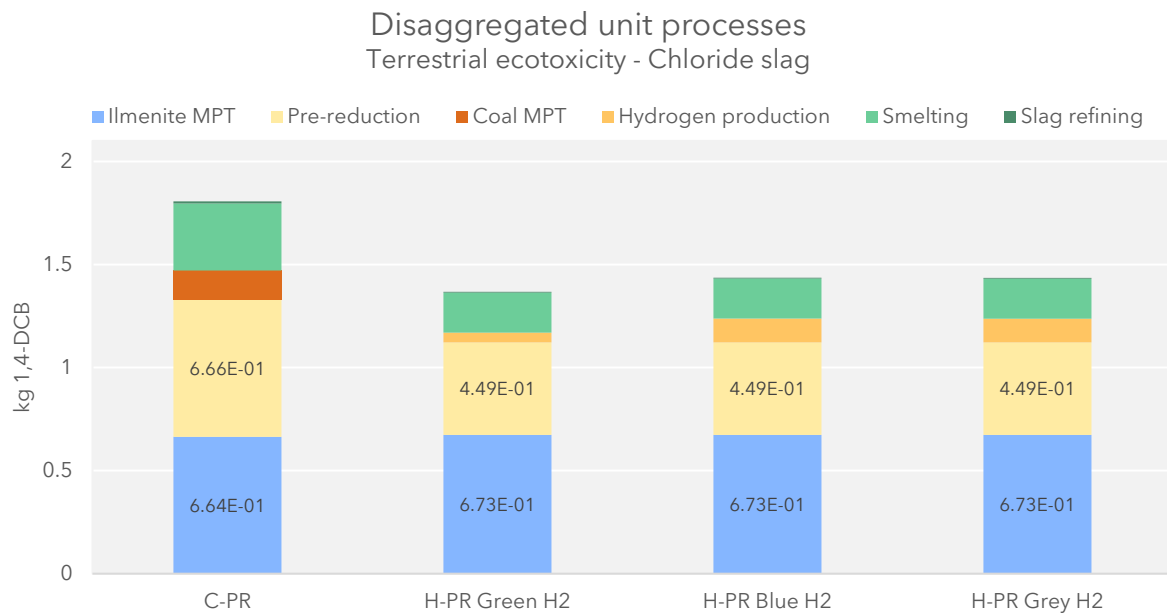

Figure 45 LCIA results disaggregated for all unit processes for the production of chloride slag - marine ecotoxicity.

Figure 45 illustrates the LCIA results for marine ecotoxicity, disaggregated for all unit processes. Marine ecotoxicity is found to be one of the impact categories with the largest reduction potential for the H-PR compared to the C-PR. From Figure 45 it is observed that this is primarily due to the exclusion of coal as a reducing agent, which contributes to 69% of the marine ecotoxicity potential for the C-PR. In the H-PR, the largest contributor to marine ecotoxicity is ilmenite MPT, accounting for 44% when green H_2 is used as a reductant and 38% when blue and grey H_2 are utilized. From the detailed contribution analysis results in Appendix 4, electricity generation is observed to be the primary contributor to the marine ecotoxicity potential of ilmenite MPT (40%), followed by transport (21%). It's worth noting that marine ecotoxicity is found to be 15% higher when blue or grey H_2 is used as a reductant compared to green H_2. This is mainly due to the emissions of copper to water from the construction of chemical factories, which have a large uncertainty and are beyond the control of ETI. Therefore, this result should be interpreted with caution. Additionally, pre-reduction and smelting contribute to approximately 20% of the marine ecotoxicity potential of the H-PR. For the pre-reduction, emissions of zinc to air and water are found to contribute to 51% of this, while the production of natural gas is the second largest contributor. For the smelting phase, only 5% is found to be due to emissions from ETI.

The substitution of zinc-dust is found to have a significant impact on the marine ecotoxicity for the pre-reduction phase for C-PR. Direct emissions from the pre-reduction result in a marine ecotoxicity potential of 1.76E-03 kg 1,4-DCBeq per kg chloride slag. However, by substituting zinc dust, this potential decreases by -1,86E-03kg 1,4-DCBeq per kg chloride slag. Hence, the contribution from the pre-reduction of C-PR is neglectable compared to the pre-reduction of the H-PR. It's important to consider that this conclusion is only valid if the production of zinc dust at ETI replaces production elsewhere.

7.1.7 Human non-carcinogenic toxicity
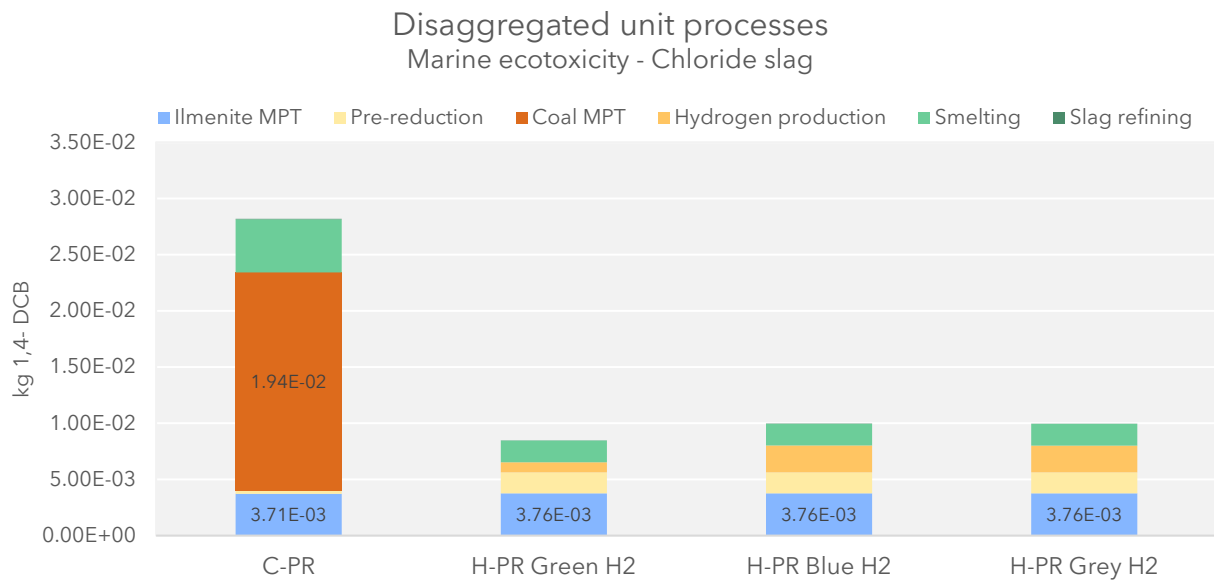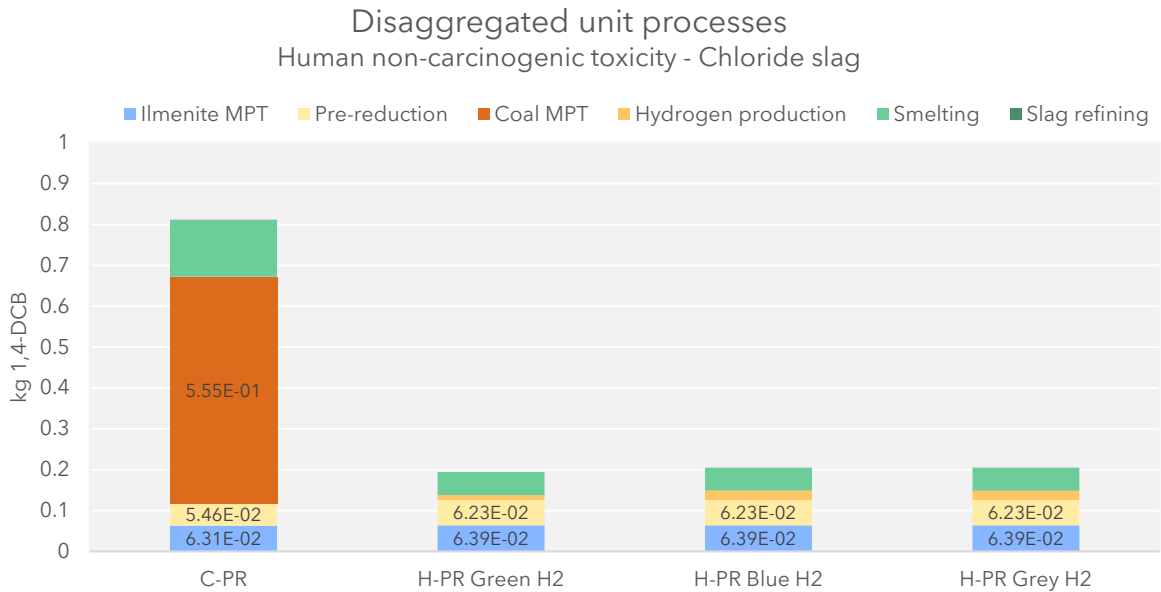

Figure 46 LCIA results disaggregated for all unit processes for the production of chloride slag - human non-carcinogenic toxicity.

Figure 46 illustrates the LCIA results for human non-carcinogenic toxicity, disaggregated for all unit processes. Similar to the findings for marine ecotoxicity, the coal used as a reductant in the C-PR exhibits the most significant contribution to the human non-carcinogenic toxicity potential for the C-PR (68%). Meanwhile, for the H-PR, the ilmenite MPT, smelting, and pre-reduction unit processes contribute approximately 30% each (+/- 3%). Specifically, for the ilmenite MPT, both electricity generation and treatment of waste are found to contribute to 30% of the human non-carcinogenic toxicity potential. For the pre-reduction process, the primary contributors are direct emissions of zinc to air and water (60%) and lead to air (25%). As for smelting, the mining and processing of coal and anthracite are the main contributors to human toxicity potential, accounting for 63% of the impact.

7.2 Sensitivity analysis

The following section presents the sensitivity analysis conducted to assess the uncertainty in the obtained results. The analysis primarily focuses on evaluating the impact of parametrical choices made regarding unit processes with a significant contribution to the overall results. Additionally, the effects of assumptions related to the H-PR with a low degree of certainty are investigated. The sensitivity analysis primarily focuses on GWP, as it is the impact category of the greatest interest. However, results are presented for other impact categories where suitable. The sensitivity analysis includes the following:

Section 7.2.1   Electricity consumption in ilmenite mining and processing (C-PR and H-PR)

Section 7.2.2   Electricity supply from solar power and consumption in ilmenite mining and processing (C-PR and H-PR)

Section 7.2.3   Emissions from the combustion of natural gas (H-PR)

Section 7.2.4   Gaseous emissions from smelting in EAF (H-PR)

Section 7.2.5   Particulate matter and heavy minerals from the pre-reduction of H-PR

Section 7.2.6   Source of electricity for green H_2 production (H-PR)

Section 7.2.6   CCS capture rate, geographical representativity and discrepancies in literature for blue and grey H_2 (H-PR)

Section 7.2.7   Treatment of multifunctionality (C-PR and H-PR)

Section 7.2.7   Effect of varying market prices on economic allocation (C-PR and H-PR)

The results of the sensitivity analysis are used to construct a best and worst-case scenario for GWP, which is presented in Subchapter 7.3. Notably, Section 7.2.5 is the only section that does not primarily pertain to the GWP, but specifically focuses on toxicity.

To facilitate a clear distinction between the LCIA results and the results obtained through the sensitivity analysis, the LCIA results presented in Chapter 5 are from here on referred to as the base-case results.

7.2.1 Sensitivity analysis - Electricity consumption ilmenite mining and processing

From the contribution analysis, it has been observed that ilmenite is a significant contributor to the GWP of chloride slag due to the electricity used for mining and processing of ilmenite. This is found to be predominantly due to CO_2 emissions caused by the generation of electricity from oil. The electricity consumption used in this study was derived from averaged values across various heavy mineral sands mining facilities, as presented by Gediga et al. [51]. However, a +/- 30% variation in electricity consumption is reported

among these facilities. As such, the effect of reduced or increased electricity consumption on the GWP chloride slag is assessed as a sensitivity analysis. Specifically, a variation of +/- 10% and +/-30% have been considered.
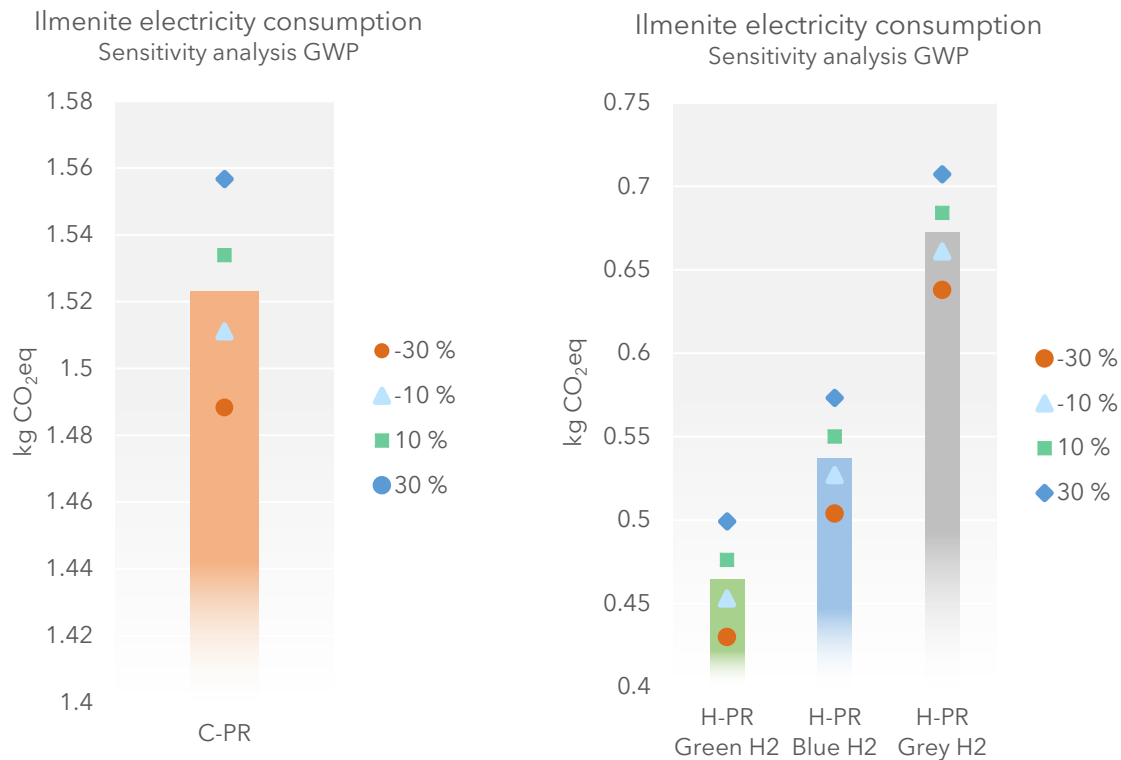
Figure 47 Sensitivity analysis for ilmenite electricity consumption for C-PR (left) and H-PR (right) for GWP, where the consumption rate is varied between +/- 30%.

Figure 47 presents the effect of varying electricity consumption in ilmenite mining and processing for both C-PR and H-PR. For the C-PR, a 30% increase in electricity consumption is found to result in a GWP of 1.56 kg CO_2eq per kg chloride slag, which amounts to a 2% increase compared to the base-case results. Conversely, a 30% decrease is found to result in a GWP of 1.49 kg CO_2eq per kg chloride slag, which amounts to a 2% decrease. For the H-PR utilizing green H_2, a GWP of 0.50 kg CO_2eq per kg chloride slag is observed when the electricity consumption is increased by 30%, and 0.43 kg CO_2eq per kg chloride slag is observed with a 30% decrease. This amounts to a variation of +/- 7% in the GWP per kg chloride slag. The corresponding results for blue and grey H_2 are found to be +/- 6% and +/- 5%, respectively.

7.2.2 Sensitivity analysis - Electricity consumption and supply for ilmenite mining and processing

Eramet AS has announced that Grande Côte Operations (GCO) in Senegal will be powered by renewable electricity generated by photovoltaic cells [57]. A 13 MW hybrid solar power station with 8 MW battery storage is scheduled to be commissioned in 2023. To assess the effect of the electricity source of ilmenite on the GWP of chorine slag, a dataset for electricity

generated by photovoltaic cells found in the ecoinvent database [76] is used to replace the Senegalese market mix. Hence, the electricity consumed is assumed to be 100% renewable.

Additionally, as it is established that the electricity consumption rate for GCO can vary between +/- 30%, this is also assessed. The outcome is presented in Figure 48.
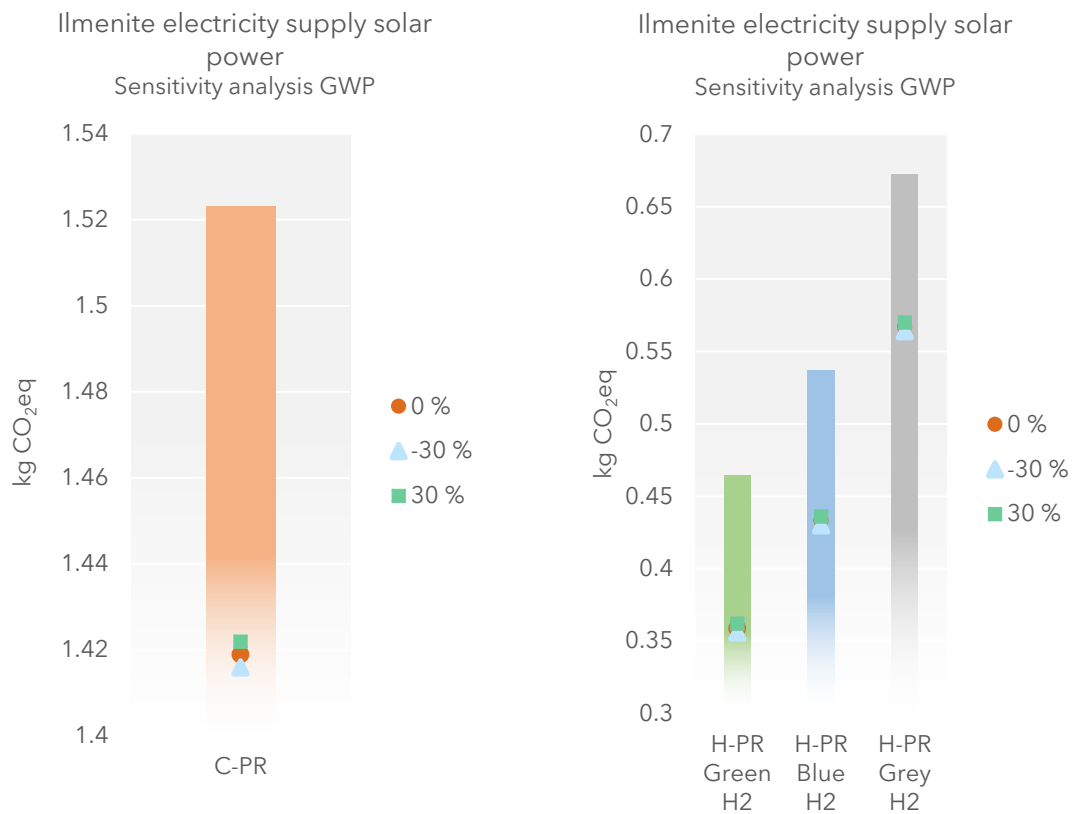
Figure 48 Sensitivity analysis for ilmenite electricity supply using solar power for C-PR (left) and H-PR (right) for GWP. Additionally, the electricity consumption rate is varied between +/- 30%.

From Figure 48, it is observed that replacing the Senegalese market mix with electricity generated by photovoltaic cells results in a GWP of 1.42 kg CO_2eq per kg chloride slag for the C-PR. This amounts to a 7% reduction in GWP compared to the base-case results. For the H-PR, a GWP of 0.36 kg CO_2eq per kg chloride slag is observed when green H_2 is utilized, which amounts to a reduction of 23% from the base-case results. For H-PR utilizing blue and grey H_2, a GWP of 0.44 and 0.57 kg CO_2eq per kg chloride slag is observed, respectively.

Additionally, it is found that varying electricity consumption has a negligible effect (<1%) on the GWP per kg chloride slag when electricity generated by photovoltaic cells is utilized.

7.2.3 Sensitivity analysis - Emissions from the combustion of natural gas

In the H-PR, natural gas is utilized to heat ilmenite prior to the reduction process. In the base-case scenario, the dataset "*Burning of natural gas*" found in the ecoinvent database [77] is used to estimate the emissions from this process. Alternatively, emission rates can be

estimated by theoretical calculations using emission factors provided by Statistics Norway (SSB) for the burning of natural gas [78], assuming a *"direct-fired furnace"*. However, the factors provided by SSB do not consider additional emission control technology for NO_x emissions and therefore overstate the emission rate. To mitigate these limitations, the SSB emission factors were employed to calculate emissions from coal combustion in the C-PR, from which a *"capture percentage"* was computed by dividing the actual measured emissions of NO_x by the calculated emissions from the C-PR based on the SSB emissions factors. The capture percentage was used to adjust the estimated emissions from burning natural gas. The performed calculations, emission factors, and estimated emission rates are shown in Appendix 5.

The effect of employing the estimated emission rates as opposed to the dataset for burning of natural gas is presented in Table 10 for the main impact categories. Results are only presented for H-PR utilizing green H_2.

Table 10 Sensitivity analysis of chloride slag produced through the H-PR utilizing green H_2 with different emission factors for burning of natural gas.

Impact category	Base-case	SSB emission factors	Difference
GWP	4.65E-01	4.63E-01	-0.32%
Stratospheric ozone depletion	1.97E-07	1.95E-07	-0.69%
Ozone formation, human health	2.22E-03	2.15E-07	-3.15%
Ozone formation, terrestrial ecosystems	2.35E-03	2.30E-07	-1.80%
Terrestrial acidification	2.26E-03	2.26E-03	-1.02%

Minor differences are observed when employing SSB emission factors. These findings support that using the ecoinvent dataset is a reasonable estimation of the emissions from natural gas.

7.2.4 Sensitivity analysis - Emissions from smelting

Several assumptions were made regarding emission rates of SO_2, NO_x, CH_4, and N_2O from the smelting process in the H-PR (see Section 4.3.2). To evaluate the impact of these assumptions, the rates have been reduced by 50%. Table 11 displays the relative changes in the GWP and terrestrial acidification for chloride slag produced via the H-PR using green H_2.

Table 11 Sensitivity analysis effect of reduced emission rates of SO$_2$, NOx, CH$_4$, and N$_2$O from smelting in the H-PR on chloride slag.

Impact category	Base-case	50% reduction	Difference
GWP	4.65E-01	4.64E-01	-0.07 %
Stratospheric ozone depletion	1.97E-07	1.87E-07	-5.15%
Ozone formation, human health	2.22E-03	2.19E-03	-1.06%
Ozone formation, terrestrial ecosystems	2.35E-03	2.27E-03	-3.16%
Terrestrial acidification	2.26E-03	2.24E-03	-0.74 %

The outcomes presented indicate a negligible effect (<1%) on the overall results of the impact categories GWP and terrestrial acidification. The greatest effect is observed for stratospheric ozone depletion and ozone formation pertaining to terrestrial ecosystems at 5.15% and 3.16% reduction.

7.2.5 Sensitivity analysis - Particulate matter and heavy metals from H-PR

From the contribution analysis, it is observed that diffuse emissions of particulate matter (PM) and heavy metals (HM) to air and water from the pre-reduction of H-PR have a significant impact on terrestrial ecotoxicity (28%) and human non-carcinogenic toxicity (30%). Due to a lack of data for diffuse emissions of PM and HM from circulating fluidized bed process in the H-PR, these emission rates were assumed to be equivalent to the emissions rates of the C-PR, with the exception of mercury which is adjusted to reflect the reduced coal consumption rate (see section 4.3.1 for further explanation). Hence, there is significant uncertainty associated with the base-case results regarding terrestrial ecotoxicity and human non-carcinogenic toxicity.

To assess the effect of these assumptions, varying emission rates of PM and HM from the pre-reduction have been applied. Specifically, a reduction rate of 50%, 30%, and 10% have been investigated, in addition to a 30% increase. As no available data on diffuse emissions of PM and HM from a circulating fluidized bed reactor has been obtained, percentages are applied. However, it is assumed that these emissions will decrease to some extent compared to the rates obtained from the pre-reduction process using the rotary kiln (C-PR), given that the circulating fluidized bed is designed as a closed system.

Figure 49 displays the results of varying emissions of PM and HM from the pre-reduction on terrestrial ecotoxicity and human non-carcinogenic toxicity.
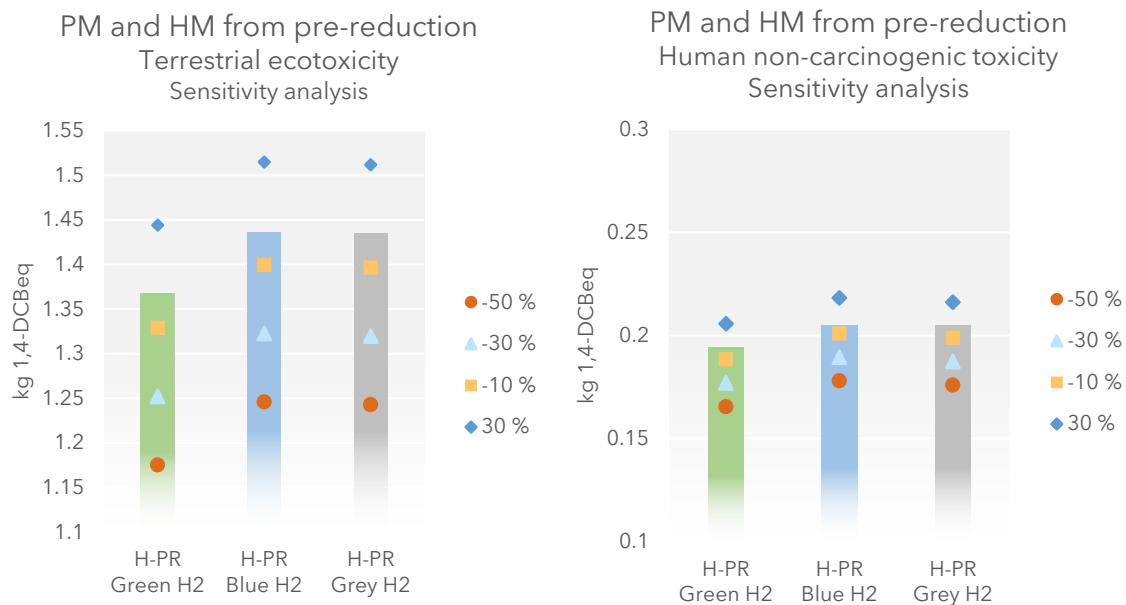
Figure 49 Effects of varying rates of PM and HM to air and water from the pre-reduction (H-PR) on terrestrial ecotoxicity (left) and human non-carcinogenic toxicity (right)

From Figure 49, it can be observed that a 50% reduction in PM and HM from the pre-reduction corresponds to a terrestrial ecotoxicity potential of 1.17 kg 1,4-DCBeq per kg chloride slag when green H_2 is utilized and 1.24 kg 1,4-DCBeq per kg chloride slag when blue and grey H_2 is utilized. For reference, the terrestrial ecotoxicity potential of C-PR was found to be 1.96 kg 1,4-DCBeq per kg chloride slag. Hence, if the emissions of PM and HM from the pre-reduction of H-PR are reduced by 50% compared to the current emissions rates with the C-PR, this amounts to a reduction potential of 40% per kg chloride slag if green H_2 is utilized. For the 30% increase, the highest terrestrial ecotoxicity potential is found for blue and grey H_2 at 1.51 kg 1,4-DCBeq per kg chloride slag, which is still lower than for the C-PR.

Additionally, a 50% reduction rate in HM and PM from the pre-reduction is found to result in a human non-carcinogenic toxicity potential of 0.17 kg 1,4-DCBeq per kg chloride slag when green H_2 is utilized, and 0.18 kg 1,4-DCBeq per kg chloride slag when blue and grey H_2 is utilized. The human non-carcinogenic toxicity potential for C-PR was found to be 0.81 kg 1,4-DCBeq per kg chloride slag. Hence, if the diffuse emissions from the pre-reduction process of the H-PR are reduced by 50%, a reduction potential of approximately 80% per kg chloride slag is obtained.

7.2.6 Sensitivity analysis – Hydrogen production

The LCIs for H_2 production used in this study have been adapted from the literature. To assess data quality and uncertainty of the three investigated H_2 production processes, the

GWP of H_2 production employed in this study is compared to findings from additional studies evaluating the environmental impacts of different H_2 production methods. In this section, the reviewed literature on all H_2 production methods and basis for the sensitivity analysis are presented, followed by the results of the sensitivity analysis.

7.2.6.1 Sensitivity analysis - Green hydrogen production

Reviewed literature on H_2 generated via electrolysis utilizing hydropower and wind power is presented in Table 12.

Table 12 Reviewed literature on the GWP of green H_2 production.

Reference	GWP [kg CO₂eq per kg H₂]	Electrolysis technology	Electricity source	LCIA method
Bhandari et al. (2014) [79]	1.80	Average	Hydropower	CML 2001
Koroneos et al. (2004) [80]	1.68	AEL	Hydropower	N/A[12]
Utgikar et al. (2006) [81]	1.7	AEL	Hydropower	N/A
Chen et al. (2019) [82]	0.11	PEM	Hydropower	CML 2001
Bhandari et al. (2014) [79]	0.97	Average	Wind power	CML 2001
Zhao et al. (2020) [83]	0.55	AEL	Wind power	ReCiPe 2016 Midpoint (H)

The GWP found in the literature range between 0.11 and 1.8 kg CO_2eq per kg H_2. The GWP of green H_2 production employed in this thesis is 0.4 kg CO_2eq per kg H_2[13], which is in the lower range compared to the values found in the literature. This discrepancy can be attributed to the temporal and geographical differences between the studies. The three studies suggesting a GWP of more than 1.6 CO_2eq per kg H_2 were all published over nine years ago, whereas the study proposing a GWP of 0.1 CO_2eq per kg H_2 is a more recent publication. This temporal disparity can impact the evaluated electrolysis technology. However, two out of the three older studies specifically focused on AEL, which is a mature technology that has undergone limited changes in the past decade. Hence, the disparity is likely attributed to geographical variations among the studies. Multiple studies have identified electricity generation as the primary driver of the GWP associated with H_2 production through electrolysis, [70], [79], [84]. This aligns with the results obtained from the contribution analysis in this LCA, which indicate that electricity generation accounts for 83% of the total GWP. From the ecoinvent database, it is found that the GWP of hydropower

---

[12] Not available
[13] Alkaline electrolysis adapted from Koj et al.

varies greatly between different geographical regions, which impacts the overall GWP per kg H_2.

In light of these findings, a sensitivity analysis has been conducted to examine the impact of different electricity sources used in the production of H_2 through electrolysis. The following electricity sources have been included: Norwegian market mix (NO market mix), Nordic market mix (NORDEL), and Average European market mix (ENTSO-E). The NO market mix contains 1% fossil-generated electricity, while the Nordic market mix contains approximately 4%. In addition, a GWP for Norwegian hydropower published by Norsus has been included. Table 13 displays the GWP per kWh.

Table 13 The GWP per kWh for the electricity sources assessed in the sensitivity analysis for H_2 production.

Alternatives	GWP [kg CO_2eq per kWh]	Source
Norsus	0.003	Norsus [85]
NO market mix	0.019	ecoinvent
NORDEL	0.058	ecoinvent
ENTSO-E	0.376	ecoinvent

Notably, H_2 produced through electrolysis using non-renewable electricity can, in theory, no longer be categorized as green H_2, as this contradicts the definition of green H_2. The result of the sensitivity analysis is presented in Figure 50.

7.2.6.2 Sensitivity analysis – Blue and grey hydrogen production

Table 14 presents the reviewed literature regarding the GWP of blue and grey H_2 production.

Table 14 Literature reviewed on the GWP of blue H_2 production.

Reference	GWP [kg CO_2eq per kg H_2]	CO_2 Capture rate [%]	CH_4 emission rate [%]	LCIA method
Khojasteh Salkuyeh et al. (2017) [86]	3.5	N/A	N/A	IPCC 2007 GWP
Kiane de Kleijne et al. (2022) [84]	3.3	93	N/A	ReCiPe 2016 Midpoint (H)
Bauer et al. (2021) [87]	2.7	93	0.2	IPCC 2021 GWP
Bauer et al. (2021) [87]	3.3	93	1.5	IPCC 2021 GWP
Bauer et al. (2021) [87]	9.0	93	8	IPCC 2021 GWP
Howards et al. [88]	15.82	90	3.5	Not an LCA

The GWP blue H_2 found in the examined literature range between 2.7-15.8 kg CO_2eq per kg H_2, as seen in Table 14. The environmental impacts of blue H_2 have been widely discussed in recent years due to contradicting results of various studies. While some studies suggest that blue H_2 can compete with green H_2 in terms of GWP [84], [86], others suggest that the GWP of blue H_2 is "*greater than burning of natural gas for heat*" [88]. From the examined literature it is observed that the main contributing factors to the disparity are the CO_2 capture rate in the CCS and emissions of methane (CH_4) from the natural gas supply chain [87], [88].

The LCI adapted for blue H_2 production in this thesis employs a 90% capture rate with a GWP 3.49 kg CO_2eq per kg blue H_2[14], which is found to be comparable to most of the reviewed literature. However, the CH_4 emissions rate used is not specified by Antonini et al., nor in the ecoinvent dataset for Norwegian natural gas employed in this LCA. Hence, the GWP of blue H_2 production with various CH_4 emission rates published by Bauer et al. have been included as part of the sensitivity analysis [70]. The work done by Bauer et al. is a continuation of the LCA conducted by Antonini et al. In the sensitivity analysis, a CH_4 emission rate of 0.2% and 8% CH_4 have been included.

---

[14] Adapted from Antonini et al., based on SMR

In addition, the effects of the CO_2 capture rate and geographical representatives of the background processes used to model blue H_2 have been assessed. As described in section 4.3.5, the adopted LCI from Antonini et al. [70] has been adjusted to represent a blue H_2 production in Norway and includes a dataset for Norwegian natural gas, while the original LCI is modeled to represent European production. The original LCI has been employed to assess the effect on the GWP of chloride slag if blue H_2 is imported from Europe. Furthermore, the effect of blue H_2 production with a 98% CO_2 capture rate is assessed by adjusting the emission rates of the original LCI of blue H_2 employed in the study, in accordance with Antonini et al.

Table 15 presents the reviewed literature on the GWP of grey H_2 production.

Table 15 Literature reviewed on the GWP of grey H_2 production.

Reference	GWP [kg CO_2eq per kg H_2]	CO_2 Capture rate [%]	CH_4 emission rate [%]	LCIA method
Khojasteh Salkuyeh et al. (2017) [86]	11.5	N/A	N/A	IPCC 2007 GWP
Kiane de Kleijne et al. (2022) [84]	11.6	93%	N/A	ReCiPe 2016 Midpoint (H)
Bauer et al. (2021) [87]	10.3	93%	0.2	IPCC 2021 GWP
Bauer et al. (2021) [87]	11.3	93%	1.5	IPCC 2021 GWP
Bauer et al. (2021) [87]	17.0	93%	8	IPCC 2021 GWP

For grey H_2, the GWP found in the literature range between 10.3 and 16.9 kg CO_2eq per kg H_2. The GWP employed in this LCA is 9.3 kg CO_2eq per kg H_2, which is lower than the values reported in the literature. However, this disparity can be attributed to the adaptations made to the original LCI adapted from Antonini et al. [70]. The original LCI is used to assess the effect of the geographical representatives, as previously outlined for blue H_2. As previously discussed for blue H_2, the CH_4 emission rate from the natural gas supply used in grey H_2 production is unknown and therefore tested using the values presented by Bauer et al. [87] in Table 15.

Notably, neither of the presented GWP values accounts for the transportation of H_2 to Tyssedal, as included in the original result. However, from the contribution analysis, transportation of H_2 is found to have a negligible contribution to the GWP and is thus unlikely to have a noteworthy impact on the overall result.

Figure 50 displays the results of the sensitivity analysis for H_2 production on one kg chloride slag. A table presenting kg CO_2eq per kg H_2 produced is presented in Appendix 6.
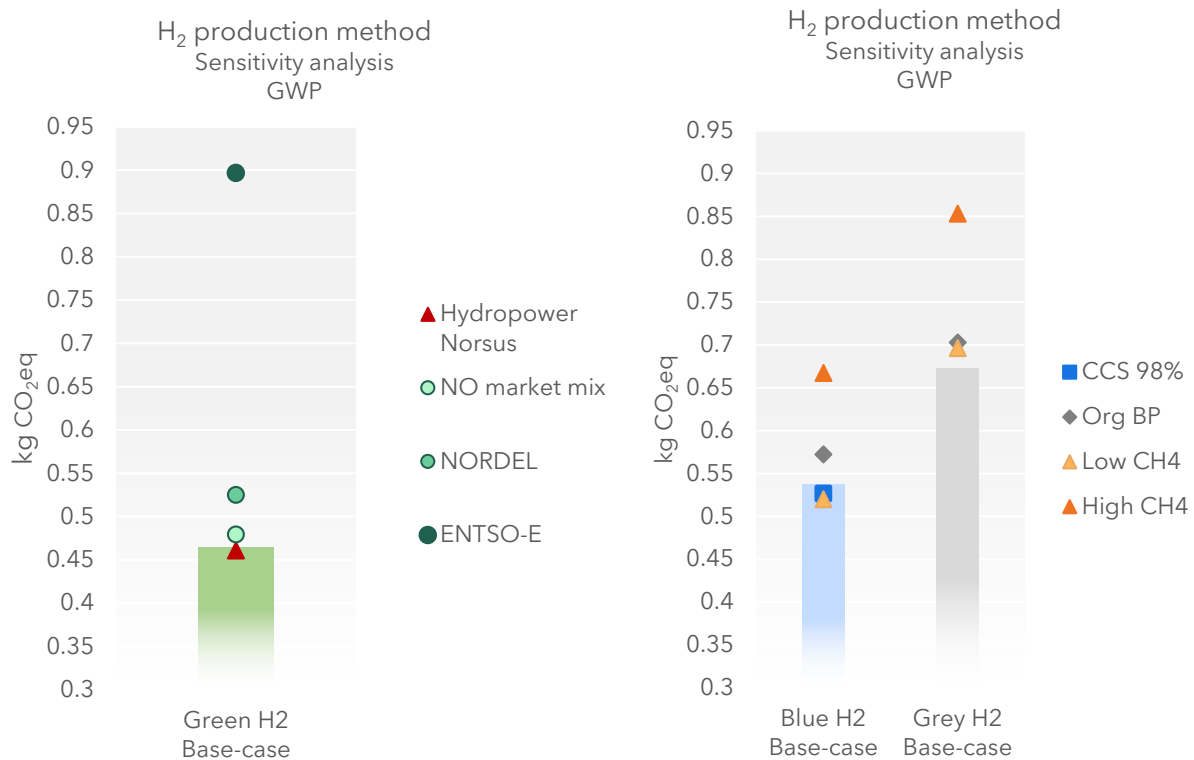
Figure 50 Sensitivity analysis of all H_2 production methods and the effect on the GWP of chloride slag. For green H_2 production, the effect of using different electricity market mixes are presented. NO = Norwegian market mix, NORDEL = Nordic market mix and ENTSO-E = European market mix. For blue and grey H_2 production, different methane emission rates are presented, as well as different CO_2 capture rated in CCS for blue H_2.

Figure 50 shows that the GWP of H-PR utilizing H_2 produced through the electrolysis of water is highly sensitive to changes in the electricity supply. A GWP of 0.90 kg CO_2eq per kg chloride slag is observed when the average European market mix (ENTSO-E) is applied, making it less favorable than all alternatives for H-PR utilizing blue and grey H_2. A minor decrease (0.8%) in the GWP of chloride slag is observed when using the GWP of hydropower determined by Norsus [89], which amounts to a GWP of 0.46 kg CO_2eq per kg chloride. When utilizing the Norwegian market mix (i.e., NO market mix) a GWP of 0.48 kg CO_2eq per kg chloride slag is observed, while for the Nordic market mix (NORDEL) the GWP is found to be 0.53 kg CO_2eq per kg chloride slag.

For H-PR using blue H_2 as reductant, the lowest GWP per kg chloride slag is observed to be 0.52 kg CO_2eq, obtained through employing a CO_2 capture rate of 93% and CH_4 emission rate of 0.2%, as suggested by Bauer et al. (i.e., low CH_4) [87]. This is found approximately comparable to utilizing the Nordic market mix to produce H_2 through electrolysis. When employing a CO_2 capture rate of 98% (i.e., CCS 98) the GWP is observed to be marginally higher compared to the low CH_4 alternative. Additionally, a GWP of 0.57 kg CO_2eq per kg

chloride slag is found when the original background processes (i.e., org BP) for the LCI presented by Antonini et al. are employed. (i.e., representing the European market). The discrepancy between the base-case result and the org BP is mainly attributed to the replacement of the European market for natural gas with Norwegian natural gas, which has a lower CH_4 emission rate.

For H-PR utilizing grey H_2, the base-case result is found to be the alternative with the lowest GWP. A 3.6% increase in GWP is observed when a CH_4 emission rate of 0.2% is employed (i.e., low CH_4), as suggested by Bauer et al. [87]. This is approximately equivalent to the GWP observed for the Org BP alternative, where grey H_2 production is modeled as European.

In this LCA, Green H_2 production is assumed to be a mono-functional process. It has been suggested that credits can be given to the co-production of oxygen through either substitution or allocation if the oxygen is utilized [84]. Parts of the heat produced in the C-PR are provided to a local fish farm in Tyssedal, which is known to also utilize large amounts of oxygen in the production. Hence, if oxygen is distributed to this fish farming operation, the environmental impacts credited to H_2 production from water electrolysis could be reduced.

Further discussion on green versus blue H_2 will be provided in Section 7.6.2.

7.2.7 Sensitivity analysis - Multifunctionality

In the following section, the impact of alternative approaches to solving the multifunctionality is assessed. For the base-case results, substitution in combination with economic allocation was used to solve the multifunctionality of the analyzed system. However, several alternative methical choices could have been made to resolve this issue, such as applying allocation factors based on physical relationships between the co-products or substitution of HPPI by an alternative production method. As such, the impact of these alternatives is evaluated.

7.2.7.1 Sensitivity analysis - Alternative multifunctionality approaches

Figure 51 displays the distribution of the GWP of each co-product and skimmed slag when physical allocation factors (orange) and substitution (blue) are applied. The physical allocation factors are solely based on the fraction of the total production mass of each co-product and skimmed slag, as opposed to the market price utilized in the base-case (green). In the substitutional approach, HPPI is subtracted from the system by using a dataset for pig iron production in Europe found in the ecoinvent database [90]. To simplify the presentation of results, only results for green H_2 are provided for the H-PR. Notably, substitution is utilized for zinc dust and heat for the C-PR when physical allocation is applied, like for economic allocation.

Treatment of multifunctionality
Sensitivity analysis GWP
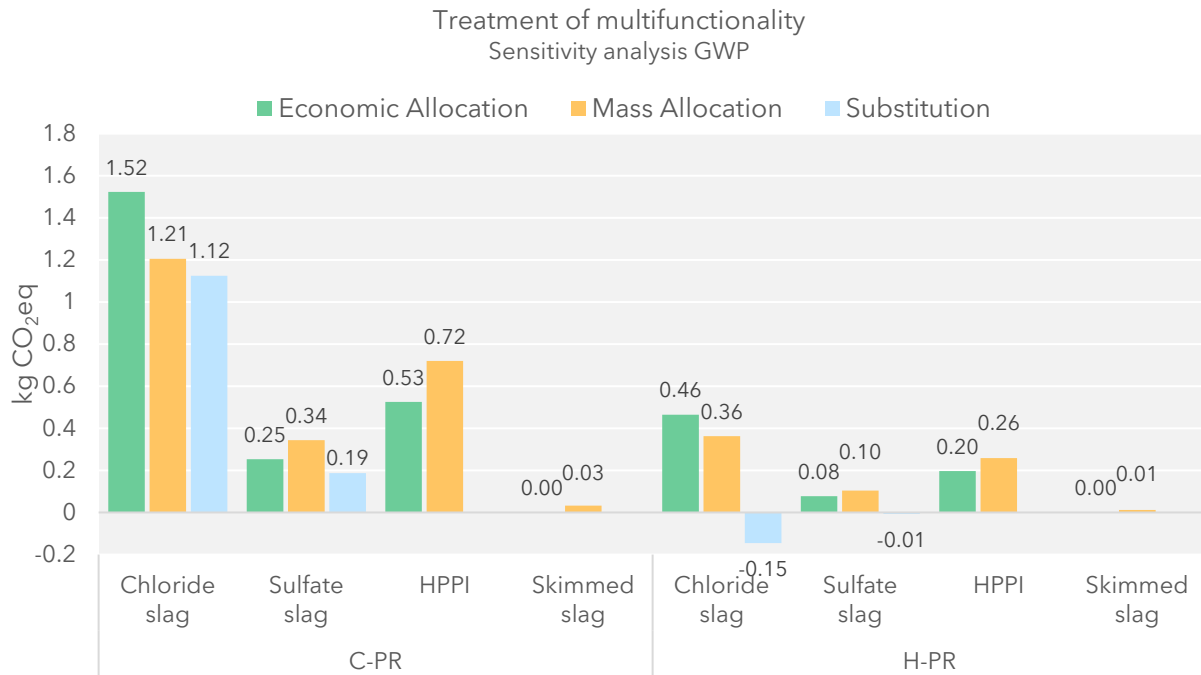
Figure 51 Effect of different methods of solving multifunctionality on the GWP. Results are presented for 0.29 kg sulfate slag and 0.53 kg HPPI. Mass allocation is based on production mass for each product. Substitution is based on substituting production of Pig Iron from the system. The base case results are based on economic allocation.

From Figure 51, it can be observed that the treatment of multifunctionality has a relatively important effect on the GWP of each co-product. Applying substitution and economic allocation is found to result in a higher GWP for chloride slag when compared to substitution and mass allocation for both production routes. Consequently, the mass allocation approach leads to an increased GWP for the remaining co-products. It is important to note that the treatment of multifunctionality only influences the distribution of environmental impacts assigned to each co-product and that the total environmental impact of the system remains unaffected.

Skimmed slag demonstrates a notably lower GWP compared to other co-products, which can be attributed to its considerably lower market value and production volume. The low impacts assigned to skimmed slag could imply that substitution would be a more suitable solution, as was the case with other by-products such as zinc dust and heat. However, a lack of LCI data for skimmed slag made allocation the preferred solution.

The substitution approach has been applied by subtracting LCI data for an alternative pig iron production process from the LCI for the smelting process. In doing so, the environmental impacts of HPPI are, in theory, cut free from the analyzed system, thereby isolating titanium slag and creating a mono-functional smelting process. This does, however, not solve the multifunctionality entirely, and economic allocation is applied to solve the issue of chloride and sulfate slag. The LCI dataset used for the substitution was a

generic dataset for European pig iron production from the ecoinvent database [90]. This dataset represents the majority of pig iron produced [91], but through a different production method than the analyzed system[15]. It's worth noting that pig iron produced at ETI contains lower levels of manganese and other impurities than conventional pig iron and is thus classified as high purity pig iron (HPPI). Consequently, the ecoinvent dataset for pig iron is not completely representative of the HPPI produced at ETI due to discrepancies in the function of the two products.

The GWP associated with producing one kg of pig iron is approximately 1.64 kg of CO_2eq, based on the ecoinvent dataset [90]. This value falls within a range of +/- 0.1 kg CO_2eq when compared to other studies investigating the environmental impacts of steel production through the BF-BOF route [92], [93]. Burchart-Korol et al. found a GWP of 1.7 kg CO_2eq per kg steel when investigating steel production in Poland and applying system expansion [92]. Findings from Renzulli, P.A et al. suggest a GWP of 1.6 kg CO_2eq per kg steel when applying economic allocation [93]. In addition, the GWP from the ecoinvent dataset for pig iron is comparable to calculations of CO_2 emissions associated with pig iron production based on EU benchmark values provided by ETI (1.61 kg CO_2eq per kg pig iron).

The substitutional approach assumes that one kg of HPPI produced at ETI replaces one kg produced from another European pig iron production facility utilizing the BF-BOF process. Thus, the total emissions do not equal the net physical GHG emissions from the process. For the C-PR, a GWP of 1.21 kg CO_2eq per kg chloride slag is observed when substitution is applied, resulting in the lowest GWP of the assessed multifunctionality methods. For the H-PR, the substitution approach yields a negative GWP for chloride slag and sulfate slag. This can be explained by a higher GHG emission rate of the LCI data for substituted pig iron than the total GHG emissions from the H-PR. It is essential to note that this negative impact does not imply a net GHG emission reduction due to titanium slag and HPPI production through the H-PR, but merely suggests that the co-production of HPPI and titanium slag via H-PR would have a net benefit compared to traditional pig iron production via BF-BOF in terms of the GWP. This argumentation is, however, only valid if the production of HPPI at ETI leads to a reduced production rate of pig iron produced via the BF-BOF route.

7.2.7.2 Sensitivity analysis - Effects of changes in the market price for economic allocation

In addition, the effect of variations in the assumed market price for chloride slag and HPPI has been assessed. The market prices used as a basis for the allocation factors are based on prices obtained from ETI, which reflect the current market for chloride slag, sulfate slag, HPPI, and skimmed slag. Hence, the allocation factors are prone to changes in market conditions. The market prices remain undisclosed due to confidentiality.

---

[15] The BF-BOF processing route

Table 16 presents the relative changes in the GWP of all products when the market price of chloride slag and HPPI varies by +/- 10%. Numerous combinations of increased and decreased market prices could have been investigated. Here, only one market price has been changed at a time, even though this is unlikely, as prices often fluctuate for more than one product simultaneously. However, the results are still valuable as they indicate how the distribution of environmental impacts can vary when economic allocation is applied.

Table 16 Effects of varying market price on the GWP of all co-products. The market price is only varied for one product at the time.

	Product	Base-case [kg CO$_2$eq]	Chloride price – 10%	Chloride price +10%	HPPI price – 10%	HPPI price +10%
C-PR	Chloride slag	1.52	-3 %	+3 %	+2 %	-2 %
	Sulfate slag	0.25	+7 %	-6 %	+2 %	-2 %
	HPPI	0.53	+6 %	-5 %	-7 %	+6 %
	Skimmed slag	7.18E-04	+6 %	-5 %	+4 %	-3 %
H-PR	Chloride slag	0.46	-3 %	+3 %	+2 %	-2 %
	Sulfate slag	0.078	+7 %	-6 %	+2 %	-2 %
	HPPI	0.20	+5 %	-4 %	-5 %	+5 %
	Skimmed slag	2.78E-04	+5 %	-4 %	+5 %	-4 %

The largest relative change is observed for sulfate slag, for which the GWP varies by approximately +/-7% if the price of chloride slag is reduced or increased by 10%. Similar variations are also observed for HPPI if the market price of HPPI is reduced or increased by 10%. The GWP of chloride slag is observed to vary between 1.47 and 1.56 kg CO$_2$eq per kg when the market price of chloride slag is decreased and increased by 10%, respectively.

7.3 Best- and worst-case scenario GWP

Based on the results of the sensitivity analysis, a best and worst-case scenario for the GWP has been constructed. Table 17 presents the complete list of alterations made to the LCI model in comparison to the base-case.

Table 17 Complete list of alterations made for the best- and worst-case scenario.

Best-case	Worst-case
Ilmenite electricity consumption reduced by 30%	Ilmenite electricity consumption increased by 30%
Ilmenite electricity supply from solar power	Ilmenite electricity supply from Senegalese market mix
Green H_2 production modeled with GWP of hydropower adopted from Norsus	Green H_2 production modeled with GWP of the European electricity mix (i.e., ENTSO-E)
Blue H_2 production modeled with 93% CO_2 capture rate and 0.2% CH_4 emission rate (i.e., low CH_4)	Blue H_2 production modeled with 93% CO_2 capture rate and 8% CH_4 emission rate (i.e., high CH_4)
Grey H_2 production modeled as base-case	Grey H_2 production modeled with a 8% CH_4 emission rate (i.e., high CH_4)

Figure 52 presents the best- and worst-case scenario for the GWP of chloride slag for both C-PR and H-PR. From this, it can be observed that the GWP of chloride slag produced through the C-PR falls within the range of 1.42 to 1.56 kg CO_2eq per kg. The variation in these results is solely attributed to the changes in electricity supply and consumption during ilmenite mining and processing. For the H-PR, a GWP in the range of 0.35 to 0.93 kg CO_2eq per kg chloride slag is obtained when green H_2 is utilized as a reductant, whereas for blue and grey H_2, the GWP is found to be in the range of 0.41 to 0.70 and 0.56 to 0.89 kg CO_2eq per kg chloride slag, respectively.
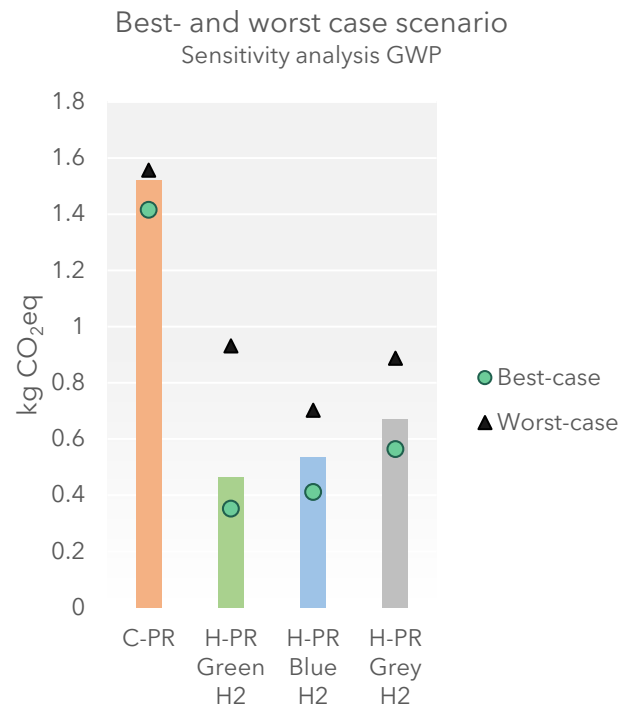

Figure 52 Best- and worst-case scenario for the GWP of chloride slag. Se Table 20 for alterations.

Additionally, it is observed that the H-PR utilizing green H_2 exhibits the most significant variation in the GWP. The best-case scenario demonstrates the lowest GWP among all the investigated processing routes, resulting in a 75% reduction compared to the best-case scenario of the C-PR, which is determined to be 1.42 kg CO_2eq per kg chloride slag. Conversely, the worst-case scenario exhibits the highest GWP among all the H-PR production routes, with only a 39% reduction compared to the worst-case scenario of the C-PR. These results highlight a comparison between the best-case outcomes for the C-PR and H-PR. Another basis for comparison would be the current GWP of chloride slag produced via the C-PR, based on ilmenite mining with the Senegalese market mix (i.e., base-case), with the possible future production of chloride slag through the H-PR, utilizing renewable electricity for ilmenite mining and processing and green H_2 produced through Norwegian hydropower (i.e., best-case). This comparison demonstrates a potential reduction rate of 77% per kg chloride slag for the H-PR, as opposed to 69% attained for the base-case.

When comparing the assessed H_2 production methods for the H-PR, a difference between chloride slag produced with green and blue H_2 of 0.0556 kg CO_2eq per kg chloride slag is observed for the best-case scenario. For the base-case results, this difference is found to be 0.0739 kg CO_2 per kg chloride slag. Hence, the best-case scenario yields a reduced difference between utilizing green H_2 and blue H_2 as a reductant in the H-PR. It is important to emphasize that these findings are specific to each kg of chloride slag produced. While the disparity may seem insignificant, it accumulates to an annual variance of 9519 tons CO_2eq, based on the assumed production rate for the H-PR in the best-case scenario.

7.4 Comparison of LCIA results to literature findings

The following sections provide a comparison of the results obtained in this study to the existing literature, and thus address the third objective of this thesis (i.e., to investigate and compare the environmental impacts of titanium slag production with and without pre-reduction of ilmenite).

7.4.1 Comparison of carbon-based titanium slag production processes

The base-case results obtained in this LCA depict a GWP of 1.52 kg CO_2eq per kg of chloride slag produced via the C-PR, based on the ReCiPe 2016 Midpoint (H) method and economic allocation. As mentioned, ETI is the only titanium slag facility currently operating with a pre-reduction phase. Hence, all findings in the literature review (see Section 1.2.1) pertain to the direct smelting of ilmenite without pre-reduction.

Only one of the assessed LCA studies provided information on the percentage of TiO_2 in the titanium slag, namely Charikinya et al. [34], which obtains a GWP of 1.56 CO_2eq per kg titanium slag >85% TiO_2 by applying mass allocation. In this thesis, economic allocation is applied to the presented LCIA results, thus hindering a fair comparison of the results.

However, mass allocation has been applied to assess the effect on the base-case results in the sensitivity analysis (see Figure 50 in Section 7.2.7.1). The sensitivity analysis demonstrated a GWP of 1.21 kg CO_2eq per kg chloride slag when applying mass allocation. When comparing this GWP to the results presented by Charikinya et al., it is observed that chloride slag produced with an additional pre-reduction phase exhibits a 22% lower GWP compared to the direct smelting of ilmenite.

Yet, three additional factors should be addressed in the comparison of these results. Firstly, the LCI presented by Charikinya et al. includes only one output stream of titanium slag, in addition to HPPI. Hence, the GWP of chloride and sulfate slag shown in Figure 50 should be allocated only to chloride slag. By doing so, a GWP of 1.55 kg CO_2eq is obtained, which is marginally lower than the results presented by Charikinya et al. Secondly, the LCI is less comprehensive than for this thesis and only includes hard coal as a material input. Hence, the system boundary is not directly comparable, indicating that the GWP presented by Charikinya et al. is naturally lower than the findings of this thesis. Thirdly, there are discrepancies in the geographical representativeness of the two LCIs. This especially pertains to the electricity mix, which is based on hydropower with a low GHG emission intensity[16] for the titanium slag produced at ETI and the South-African market mix with a high GHG emission intensity[17] for the study presented by Charikinya et al. With these additional factors addressed, one could argue that the discrepancies between the two results are too significant to facilitate a fair comparison of titanium slag produced with or without pre-reduction. It does, however, indicate that titanium slag produced at ETI has a lower GWP than the assessed facility in South Africa.

Additionally, Gao et al. [10] investigated titanium slag described as *high-grade*, implying a TiO_2 content >85%. According to Liao et al. [32], high-grade titanium slag refers to 94% TiO_2, which is of higher quality than the chloride slag assessed in this thesis. It can, however, be utilized in the chloride process and thus assumed to be comparable. Geo et al. report a GWP of 2.23 kg CO_2eq per kg chloride slag. The co-production of neither sulfate slag nor HPPI is included in the system boundary. Hence, all emissions should be allocated to chloride slag to facilitate a fair comparison of the process routes. By doing this, a GWP of 2.19 kg CO_2eq per kg chloride slag is obtained for the C-PR, which is marginally lower than the GWP reported by Gao et al. However, as with the study by Charikinya et al., discrepancies in the system boundary and geographical representativeness make the comparison of the process route with or without pre-reduction problematic. Furthermore, allocating all emissions to chloride slag does not facilitate a fair comparison, as the co-production of sulfate slag and HPPI is beneficial regarding resource utilization.

---

[16] 6.56E-03 kg CO_2eq/ kWh [94]
[17] 1.08 kg CO_2eq/ kWh [95]

Middlemas et al. [33] found a CO_2 emission rate of 2.25 kg CO_2eq per kg chloride slag. The study does not present a clear system boundary for titanium slag production nor the percentage of TiO_2, which makes comparing the results challenging. It is, however, in the same range as the GWP of 2.19 kg CO_2eq per kg chloride slag obtained if all emissions are allocated to chloride slag, which supports the findings obtained in this thesis. This is also true for the findings presented by Charikinya et al. and Gao et al.

According to these findings, it appears problematic to enable a transparent and fair comparison of titanium slag production with or without pre-reduction of ilmenite. Nonetheless, the outcomes suggest that the GWP of titanium slag produced at ETI falls within the same range as findings from LCAs of other facilities, thus increasing the validity of this LCA.

7.4.2 Comparison of hydrogen-based titanium slag production processes

For the H-PR, a GWP of 0.46 kg CO_2eq per kg chloride slag is obtained when green H_2 is utilized as a reductant. Only one study assessing the environmental impacts of utilizing H_2 as a reductant in titanium slag production is found in the literature, namely Orth et al. [24]. The process technology investigated (i.e., Circosmelt®) is similar to that employed for the H-PR in that both utilize a circulating fluidized bed process to pre-reduce ilmenite prior to the smelting phase. Orth et al. presents an emission rate of 1.54 kg CO_2 per kg titanium slag when H_2 is utilized as a reductant. Hence, a significantly lower GWP is obtained in this LCA.

This discrepancy in results could be due to several factors. Firstly, the percentage of TiO_2 in the titanium slag investigated by Orth et al. is not provided, and it remains unclear whether environmental impacts are allocated to the co-production of pig iron. Hence, the inconsistency in results could be caused by variations in the system boundary. Secondly, it is observed that electricity contributes to 53% of the CO_2 emissions presented by Orth et al., indicating a higher GHG emission intensity for electricity than what is utilized in this study. Lastly, Orth et al. do not employ the LCA methodology, which makes a fair comparison of results problematic.

7.5 Evaluation of data quality and limitations of the study

The following subchapter presents an evaluation of the data quality of the study in terms of representativeness, completeness, and consistency. Additionally, the most significant limitations are addressed.

7.5.1 Evaluation of data quality

The reliability of any LCA study is heavily dependent on the quality of the LCI data. Insufficient data quality can impose significant limitations on the study's findings and

conclusions. To address these limitations, the data quality has been evaluated in terms of representativeness, completeness, and consistency according to ISO 14044:2006 [37].

Appendix 7 displays an evaluation of the data quality for the foreground system, including comments on the largest issues. The representativeness of background processes used to model material and energy inputs is evaluated through a semi-qualitative analysis, where a set of criteria was defined to rate each background process. Appendix 7 presents the defined criteria and the context to which they apply, as well as the evaluation of each background process and alterations made.

Additionally, background processes contributing to more than 3% of the total GWP have been altered to increase the representativeness. The alterations are listed in Appendix 7.

7.5.1.1 Comments on significant issues

The following provides additional comments on some of the significant issues identified in Appendix 7.

7.5.1.1.1   Inconsistencies in modeling of hydrogen production

There is a discrepancy in the characteristics of the different H_2 production methods that can lead to inconsistency in the interpretation of the results if not addressed. While blue and grey H_2 is modeled as compressed to 200 bars, compression is not included in the green H_2 production. The reason for this inconsistency is that green H_2 is assumed to be produced on-site, while blue and grey H_2 are assumed to be transported to ETI, and the low volumetric energy density of H_2 makes compression inevitable if transported. If green H_2 is not continuously produced and utilized, electricity consumption and material inputs for compression and storage need to be incorporated into the LCI for on-site green H_2 production to be comparable.

7.5.1.1.2   Temporal representativeness of production data

For the C-PR, LCI data is derived for a one-year period, representing a potential weakness with respect to the temporal representativeness of the data. Preferably, annual production data should be collected and averaged over multiple periods.

7.5.1.1.3   Allocation factors in ilmenite MPT

The study from which the LCI of ilmenite mining and processing was adapted employed allocation factors based on wt.% (i.e., physical factors). Hence, there is an inconsistency in the basis of the allocation factors. Economic allocation factors for ilmenite and the corresponding co-products have not been obtained. However, by applying mass allocation, approximately 48% of environmental impacts are allocated to ilmenite, thus aligning with and upholding the principles of the precautionary approach.

7.5.2 Limitations of the study

7.5.2.1 General limitations

One of the greatest uncertainties for this LCA is the discrepancy between the data obtained for the C-PR and H-PR, where the H-PR data is based on estimations and theoretical calculations, which have been pointed out throughout this thesis. This is especially true for the diffuse emissions of PM and HM to air and water, which is observed to have a substantial effect on terrestrial ecotoxicity and human non-carcinogenic toxicity, making the comparison between LCIA results for the C-PR and H-PR less robust for these impact categories. However, the assumptions made regarding uncertain emission rates for the H-PR have been assessed in the sensitivity analysis by varying the input parameters within a reasonable range. Optimally, all parameters should have been based on alternative values found in the literature as opposed to percentage variations. However, as no operating hydrogen-based pre-reduction process for the production of titanium slag exists, such values are not available, and the use of percentage variations is the only practical solution to assess the sensitivity of the outcome.

The uncertainty between the data collected for the C-PR and H-PR is arguably less significant for GWP than for the other impact categories. The CO_2 emissions, which are the dominating contributor to the gate-to-gate processes, are calculated based on the carbon contained in each source stream. Hence, the calculations have the same basis for both production routes yielding a higher certainty. However, there are additional uncertainties pertaining to the GWP. Firstly, it is assumed that the CO_2 emissions from the gate-to-gate unit processes equal the difference in the carbon contained in the incoming source streams and the outgoing products. Hence, emissions of CO are assumed to be completely oxidized to CO_2. In addition, the calculations are highly dependent on accurate analysis of the carbon content in each source stream and product. Secondly, ilmenite and H_2 production are found to have substantial impacts on the total GWP, both of which are unit processes that rely on secondary data. The uncertainty of both these processes has been assessed in the sensitivity analysis, from which the best and worst-case scenario has been derived. Based on the discussion presented in the sensitivity analysis, it is assumed to be likely that the GWP is within the range of the best and worst-case scenarios for the C-PR and H-PR.

The sensitivity analysis conducted in this study primarily focuses on the GWP while providing comments on some additional impact categories. When evaluating alternative process options, such as employing solar power for ilmenite MPT in Senegal, further analysis including other impact categories should be conducted to control for problem shifting.

7.5.2.2 Limitations of the modeling framework

An attributional modeling framework has been applied for this LCA. Hence, this study seeks to quantify the total emissions from the processes and material flows used in the two

analyzed processing routes (i.e., C-PR and H-PR) by employing background processes that represent site-specific conditions to the best extent possible. The alternative modeling framework would be consequential LCA, where the main goal would be to "*identify the consequences that a decision in the foreground system has for other processes and systems of the economy*" [30]. In the context of this study, this translates to describing the overall impact of change that follows transitioning from C-PR to H-PR in a broader perspective, including indirect market effects influenced by this decision [96]. Due to these distinct differences, applying an attributional modeling framework leads to some limitations regarding transferability and extension of the results.

Firstly, the results of this LCA cannot be directly applied to inform consumers and policymakers on the total change of emissions that occurs from transitioning from C-PR to H-PR, as the indirect market effects have not been assessed [97]. The overall effect of factors such as reduced coal consumption, avoided transportation, increased demand for H_2, and future electricity mixes should be considered, among others. Secondly, the processes in this study have been modeled using geographically representative data and background processes specific to this location. For the results to be transferrable to similar production processes at other geographic locations, several adaptations would be necessary. This is especially relevant for electricity, as seen in Figure 50.

7.6 Further discussion points

7.6.1 Treatment of multifunctionality

As previously stated, economic allocation factors are applied to distribute the environmental impact of multifunctional unit processes to the resulting co-products. This approach was found to be the best option, despite being ranked lower than substitution in the ISO hierarchy. The basis for this decision is as follows: The economic value of the co-products arguably corresponds to the main reason for the process to exist. Therefore, the product that is primarily responsible for causing the environmental impacts is assigned the greatest environmental burdens. In addition, the economic allocation approach yields the highest GWP of chloride slag (see Figure 51), which is defined as the functional unit of the study. Hence, this allocation approach is in accordance with the precautionary principle.

Furthermore, several weaknesses of the substitutional approach have been identified, making this less optimal for this study. Firstly, the dataset used to substitute HPPI is not completely functionally equivalent. Consequently, the production rate of the substituted dataset cannot be assumed to be directly affected. Secondly, the results do not imply the actual environmental impact of the co-products and must be interpreted in the context it applies to. The GWP associated with substitution must, therefore, be interpreted with caution and not directly compared to the results where allocation is applied.

In the choice between economic or physical-based allocation factors, economical was chosen as it allocated the largest fractions of the environmental burdens to chloride slag, which is defined as the functional unit. Hence, the alternative that erred on the side of caution was selected. Furthermore, as the economic allocation factors are dependent on the production volume of each co-product, these two alternatives are based on the same parameter and thus co-varies to a large extent.

7.6.2 Green versus blue hydrogen

As stated in the introduction, ETI primarily intends to use green H_2 produced via local hydropower, which is found to be the best alternative in terms of GWP, terrestrial ecotoxicity, and marine ecotoxicity. In order for this to be viable, a surplus of hydropower is required, which is reliant on the availability of water in the reservoirs, a factor contingent on sufficient rainfall. Hence, in cases of inadequate power supply for green H_2 production in Tyssedal, alternative sources or methods must be utilized as a replacement, such as importing blue H_2 or H_2 produced through electrolysis employing alternative electricity sources.

From the sensitivity analysis (see Figure 50), it is found that the GWP of H-PR employing H_2 produced through water electrolysis is highly dependent on the parametrical choices made in the modeling, particularly the percentage of fossil-generated electricity in the electricity supply. It is observed that the Norwegian electricity market mix (i.e., grid mix) can be utilized in H_2 production while still maintaining a lower GWP than all assessed alternatives for blue H_2. This is, however, dependent on the GHG emission intensity of the grid mix. As Norway is part of the European power system, the GHG emission intensity varies depending on the amount of fossil-generated electricity imported. The GHG emission intensity of the Norwegian grid mix employed in the sensitivity analysis is 19.2 g CO_2eq per kWh, which is based on 5% imported electricity with 1% being fossil-generated. In 2019, the GHG emission intensity per kWh of the Norwegian grid mix was estimated to be 17 g CO_2eq, with 3.97% being imported, according to The Norwegian Water Resources and Energy Directorate (NVE) [98]. In 2021 it was estimated to be 11 g CO_2eq per kWh, with 1.84% being imported. In their short-term market analysis, Statnett predicts that by 2027 there could be a net negative balance in the Norwegian energy market [99], meaning that an increased amount of electricity must be imported. Given that the share of electricity generated from fossil sources in the European market mix was 61% in 2022 [100], this could result in an increased GHG emission intensity of the grid mix until sufficient capacity of renewable energy is installed.

From Figure 50 it is observed that utilizing the Nordic market mix (NORDEL) to produce H_2 yields a GWP equivalent to the estimate obtained for blue H_2 produced with a 98% CO_2 capture rate, as well as for a 0.2% CH_4 emission rate and a 93% CO_2 capture rate (0.53, 0.52, and 0.53 kg CO_2eq per kg chloride slag, respectively). The Nordic market mix employed in

the sensitivity analysis is based on 4% of the electricity being generated from fossil sources. This result indicates that utilizing blue H_2 produced under specific conditions in the H-PR can yield comparable results to water electrolysis when more than approximately 4.3% of the electricity is generated from fossil sources. Hence, one could argue that in a situation with inadequate amounts of renewable electricity production, blue H_2 could serve as a viable alternative in terms of GHG emissions. Moreover, utilizing blue H_2 in a transition phase until there is a surplus of renewable electricity allows for the use of this electricity in applications that rely on electricity for decarbonization. This may lead to a net positive impact in terms of reducing GHG emissions on a global scale, despite blue H_2 having a higher emission intensity than green H_2.

To the author's knowledge, blue H_2 is currently not produced on a large scale. Hence, the discussion on green and blue H_2 is also a question of availability. As mentioned in the introduction, the EU green deal and hydrogen strategy emphasize the preference for green H_2. Yet, the urgency for the independence of Russian gas in the European energy system and decarbonizing the economy has opened for blue H_2 production as a transition solution to produce enough H_2 on a short-term basis. An example of this is seen in the German steel industry, which has expressed great interest in importing blue H_2 from Norway due to a lack of available renewable power [101].

The EU taxonomy, which is a system for classifying environmentally sustainable economic activities, recognizes H_2 produced with a maximum of 3 kg CO_2eq per kg H_2 as sustainable [102]. The GWP of blue H_2 production used in the base-case results in this study is found to be 3.49 kg CO_2eq per kg H_2, which does not qualify as low emission according to the taxonomy. This is, however, attained for blue H_2 production employing Norwegian natural gas and a CO_2 capture rate of 98%, as well as when employing a 93% CO_2 capture rate and a 0.2% CH_4 emission as presented by Bauer et al. [87]. While assessing the technological readiness and feasibility of CCS is not a part of the scope of this thesis, findings suggest that the production of low-emission blue H_2, as defined by the EU taxonomy, is achievable. However, as blue H_2 production prolongs the dependence on fossil resources and relies on CCS technology, the long-term sustainability of blue H_2 is strongly debated. To properly assess this, a consequential LCA should be conducted, as well as a sensitivity analysis covering other impact categories.

7.6.3 Identified improvements measures for the H-PR

Based on the findings of this study, three measures that can contribute to a further reduction in environmental impacts from the H-PR have been identified:

- o The production of source streams to ETI needs to be decarbonized to reduce upstream emissions. This is especially true for electrode production and iron refining products: petroleum coke, ferrosilicon, and calcium carbide.

o   Replacing the natural gas used for heating ilmenite in the pre-reduction with low-emission options, such as biogas.

o   Investments in equipment that reduce diffuse emissions of PM and HM to air from the current levels.

7.7 Further work

This study has provided insights into the environmental performance of a future hydrogen-based processing route for titanium slag production using lab-scale data and estimations. The LCI developed in this study should be updated with improved data for the H-PR when the pilot scale facility is operable. Additionally, the LCI for ilmenite MPT should be updated with data specifically for the GCO in Senegal.

Furthermore, the sensitivity analysis conducted in this study is mainly focused on the impact category GWP. To control for problem shifting, the remaining impact categories should be included in an extended analysis. Further work on the LCI for green H_2 should be undertaken, such as including compression and storage of H_2. Furthermore, a separate LCA should be conducted for blue H_2 using Norwegian production data, which includes storage or utilization of the captured CO_2.

The hydrogen project undertaken at ETI is the first attempt at commercializing a hydrogen-based processing route for titanium slag production. The successful development and adoption of this technology could potentially trigger significant structural changes within the industry if additional titanium slag production facilities adopt similar processes. Consequently, an LCA employing a consequential modeling framework aligning with decision context B in the ILCD handbook [39] should be conducted.

8 Conclusion

The primary objective of this study was to investigate the environmental impacts associated with the novel process of employing H_2 as a reducing agent in the production of titanium slag in comparison to the current carbon-based production route. To do so, a life cycle model for the current (i.e., C-PR) and future (i.e., H-PR) processing route at Eramet Titanium and Iron (ETI) has been constructed based on an attributional LCA modeling framework. The system boundary includes all processing steps from the extraction of the feedstock (i.e., ilmenite) to finished titanium slag (i.e., chloride slag and sulfate slag) and HPPI at the refinery gate and thus employs a cradle-to-gate perspective. Additionally, two secondary objectives were defined. The first was to explore the environmental impacts of green, blue, and grey H_2 and incorporate this into the LCI model of titanium slag produced through the H-PR. The second was to investigate how an additional pre-reduction phase compared to the traditional titanium slag production route in terms of environmental impacts.

The key findings indicate that the H-PR demonstrates a reduced impact score across all eight evaluated impact categories compared to the C-PR. The most significant reduction potential was observed for marine ecotoxicity, human non-carcinogenic toxicity, and global warming potential, primarily associated with reduced coal consumption. Marine ecotoxicity and human non-carcinogenic toxicity were found to be associated with emissions from the background system related to coal mining and processing, while the GWP was linked to reduced CO_2 emissions resulting from the pre-reduction of ilmenite. The GWP for C-PR was found to be 1.52 kg CO_2eq per kg chloride slag, whereas H-PR utilizing green H_2 was found to be 0.46 kg CO_2eq per kg chloride slag, representing a reduction potential of 69% compared to the C-PR. The reduction potential for blue H_2 and grey H_2 was found to be 65% and 56%, respectively. Notably, green H_2 exhibited the highest reduction potential for all assessed impact categories among the evaluated H_2 production methods. From the contribution analysis, ilmenite MPT is observed to be the most significant contributor to chloride slag produced through both the C-PR and H-PR for the following four impact categories: stratospheric ozone depletion, ozone formation (human health and terrestrial ecosystems), and terrestrial acidification.

A sensitivity analysis was conducted, resulting in the development of a best and worst-case scenario for GWP. The best-case scenario considered the lowest GWP obtained for H_2 production and incorporated reduced electricity consumption and solar power in ilmenite mining and processing. The best and worst-case scenarios for the C-PR ranged between 1.42 and 1.56 kg CO_2eq per kg chloride slag, while for the H-PR utilizing green H_2, it ranged from 0.35 to 0.93 kg CO_2eq per kg chloride slag.

Additionally, this study aimed to compare the environmental impacts of the C-PR with the traditional processing routes to investigate the effect of employing an additional pre-

reduction phase. However, due to variations in system boundaries and allocation methods, a fair comparison of the results proved challenging.

Bibliography

[1]   The Norwegian Government, "Norway's new climate target: emissions to be cut by at least 55 %," *Regjeringen.no*, Nov. 2022. https://www.regjeringen.no/no/aktuelt/nytt-norsk-klimamal-pa-minst-55-prosent/id2944876/

[2]   Statistics Norway, "Emissions to air," *Statistics Norway (SSB)*. https://www.ssb.no/natur-og-miljo/forurensning-og-klima/statistikk/utslipp-til-luft

[3]   The Norwegian Environment Agency, "Measures and instruments to reduce greenhouse gas emissions from Norwegian industry." Klimakur 2020, 2010. [Online]. Available: https://www.miljodirektoratet.no/globalassets/publikasjoner/klif2/publikasjoner/2594/ta2594.pdf

[4]   The Federation of Norwegian Industries, "Roadmap for the process indusry." The Federation of Norwegian Industries, 2016. [Online]. Available: https://www.norskindustri.no/siteassets/dokumenter/rapporter-og-brosjyrer/veikart-for-prosessindustrien_web.pdf

[5]   H. E. Holmås, *Kloden Brenner - Hva må gjøres?*, 1st ed. Oslo: Res Publica, 2021.

[6]   Eramet Titanium and Iron AS, "Eramet Titanium & Iron, a pioneer of metallurgy in Norway," *Eramet*. https://www.eramet.com/en/eramet-titanium-iron-pioneer-metallurgy-norway

[7]   Norwegian Environment Agency, "The Norwegian PRTR - Pollutants to air and water and generated transfers of waste." https://www.norskeutslipp.no/no/Diverse/Virksomhet/?CompanyID=5118&ComponentPageID=180

[8]   U.S. Geological Survey, "Mineral commodity summaries 2022," U.S. Geological Survey, Reston, VA, USGS Numbered Series 2022, 2022. doi: 10.3133/mcs2022.

[9]   M. J. Gázquez, J. P. Bolívar, R. Garcia-Tenorio, and F. Vaca, "A Review of the Production Cycle of Titanium Dioxide Pigment," *Materials Sciences and Applications*, vol. 05, pp. 441–458, 2014, doi: 10.4236/msa.2014.57048.

[10]   F. Gao *et al.*, "Environmental impacts analysis of titanium sponge production using Kroll process in China," *Journal of Cleaner Production*, vol. 174, pp. 771–779, 2018, doi: 10.1016/j.jclepro.2017.09.240.

[11]   D. Filippou and G. Hudon, "Iron removal and recovery in the titanium dioxide feedstock and pigment industries," *The Journal of The Minerals, Metals & Materials Society*, vol. 61, p. 36, 2009, doi: 10.1007/s11837-009-0150-3.

[12]   W. Zhang, Z. Zhu, and C. Y. Cheng, "A literature review of titanium metallurgical processes," *Hydrometallurgy*, vol. 108, pp. 177–188, 2011, doi: 10.1016/j.hydromet.2011.04.005.

[13]   H. Elstad, K. Ure, and Ø. Tvedt, "TTI kompendiet." Eramet Titanium and Iron AS, 2021.

[14]   S. Luidold and H. Antrekowitsch, "Hydrogen as a reducing agent: State-of-the-art science and technology," *JOM*, vol. 59, pp. 20–26, 2007, doi: 10.1007/s11837-007-0072-x.

[15]   P. Pistorius, "Ilmenite smelting: The basics," *Journal of the Southern African Institute of Mining and Metallurgy*, vol. 108, pp. 35–43, 2008.

[16]   H. Krogerus, P. MÄKELÄ, J. Saarenmaa, S. PISILÄ, and P. PALOVAARA, "Method for producing titanium oxide-containing slag and pig iron from ilmenite and a plant," WO2016120529A1, Aug. 04, 2016 [Online]. Available: https://patents.google.com/patent/WO2016120529A1/en

[17]   S. Lobo, L. Kolbeinsen, and S. Seim, "Pre-reduction of Ilmenite with Natural Gas - Model Development and Use," *Efficient technologies in ferroalloy industry*, pp. 857–868, 2013.

[18]   K. Bisaka, I. Thobadi, and X. Goso, "Prereduction and DC open-arc smelting of carbon-based ilmenite pellets." Pyrometallurgy Division, Mintek, 2016. [Online]. Available: https://www.pyrometallurgy.co.za/Mintek/Files/2016Bisaka2.pdf

[19]   C. Kurrer, "The potential of hydrogen for decarbonising steel production." European Parliamentary Research Service (EPRS), 2020. [Online]. Available: https://www.europarl.europa.eu/RegData/etudes/BRIE/2020/641552/EPRS_BRI(2020)641552_EN.pdf

[20]   European Comission (EU), "A hydrogen strategy for a climate-neutral Europe." European Commission, Jul. 08, 2020. [Online]. Available: https://eur-lex.europa.eu/legal-content/EN/TXT/PDF/?uri=CELEX:52020DC0301

[21]   R. R. Wang, Y. Q. Zhao, A. Babich, D. Senk, and X. Y. Fan, "Hydrogen direct reduction (H-DR) in steel industry—An overview of challenges and opportunities," *Journal of Cleaner Production*, vol. 329, p. 129797, 2021, doi: 10.1016/j.jclepro.2021.129797.

[22]   A. Otto, M. Robinius, T. Grube, S. Schiebahn, A. Praktiknjo, and D. Stolten, "Power-to-Steel: Reducing CO 2 through the Integration of Renewable Energy and Hydrogen into the German Steel Industry," *Energies*, vol. 10, p. 451, 2017, doi: 10.3390/en10040451.

[23]   S. C. Lobo, "Experimental Investigations and Modelling of Solid-State Ilmenite Reduction with Hydrogen and Carbon Monoxide," PhD, Norwegian University of Science and Technology, Trondheim, 2015.

[24]   A. Orth, N. Anastasijevic, and H. Eichberger, "Low CO2 emission technologies for iron and steelmaking as well as titania slag production," *Minerals Engineering*, vol. 20, pp. 854–861, 2007, doi: 10.1016/j.mineng.2007.02.007.

[25]   H. Sun, J. Wang, X. Dong, and Q. Xue, "A literature review of titanium slag metallurgical processes," *Metalurgia International*, vol. 17, pp. 49–56, 2012.

[26]   Ministry of Climate and Environment and Ministry of Petroleum and Energy, "The Norwegian Government's hydrogen strategy." Jun. 03, 2020. [Online]. Available: https://www.regjeringen.no/contentassets/40026db2148e41eda8e3792d259efb6b/y-0127b.pdf

[27]   International Energy Association (IEA), "Hydrogen: A Renewable Energy Perspective–Report," *IEA*, 2019.

https://scholar.google.com/scholar_lookup?title=Hydrogen%3A%20a%20renewable%20energy%20perspective&publication_year=2019&author=IRENA

[28]   B. C. Tashie-Lewis and S. G. Nnabuife, "Hydrogen Production, Distribution, Storage and Power Conversion in a Hydrogen Economy - A Technology Review," *Chemical Engineering Journal Advances*, vol. 8, p. 100172, 2021, doi: 10.1016/j.ceja.2021.100172.

[29]   European Commission, "REPowerEU: A plan to rapidly reduce dependence on Russian fossil fuels and fast forward the green transition." European Commission, May 18, 2022. [Online]. Available: https://ec.europa.eu/commission/presscorner/detail/en/IP_22_3131

[30]   International Standardization Organization (ISO), "ISO 14040:2006 Environmental management-Life cycle assessment-Principles and framework. European Committee for Standardization." 2014. [Online]. Available: https://www.iso.org/standard/37456.html

[31]   E. Reck and M. Richards, "TiO2 manufacture and life cycle analysis," *Pigment & Resin Technology*, vol. 28, pp. 149–157, 1999, doi: 10.1108/03699429910271297.

[32]   W. Liao, R. Heijungs, and G. Huppes, "Thermodynamic resource indicators in LCA: a case study on the titania produced in Panzhihua city, southwest China," *Int J Life Cycle Assess*, vol. 17, pp. 951–961, 2012, doi: 10.1007/s11367-012-0429-4.

[33]   S. Middlemas, Z. Z. Fang, and P. Fan, "Life cycle assessment comparison of emerging and traditional Titanium dioxide manufacturing processes," *Journal of Cleaner Production*, vol. 89, pp. 137–147, 2015, doi: 10.1016/j.jclepro.2014.11.019.

[34]   E. Charikinya *et al.*, "Life Cycle Inventories of Primary Production of Precious and Scarce Metals - South Africa," *ecoinvent Association*, 2019, [Online]. Available: https://sri-lci.ecoinvent.org/ (registration required)

[35]   J. Suer, M. Traverso, and N. Jäger, "Carbon Footprint Assessment of Hydrogen and Steel," *Energies*, vol. 15, p. 9468, 2022, doi: 10.3390/en15249468.

[36]   F. Li *et al.*, "Quantifying the energy saving potential and environmental benefit of hydrogen-based steelmaking process: Status and future prospect," *Applied Thermal Engineering*, vol. 211, p. 118489, 2022, doi: 10.1016/j.applthermaleng.2022.118489.

[37]   International Standardization Organization (ISO), "ISO 14044:2006 Environmental management – Life cycle assessment – Requirements and guidelines." 2014. [Online]. Available: https://www.iso.org/standard/38498.html

[38]   H. Baumann and A.-M. Tillman, *The Hitch Hiker's Guide to LCA*, 3., vol. 50. Professional Publishing House, 2004.

[39]   European Commission. Joint Research Centre. Institute for Environment and Sustainability., *International Reference Life Cycle Data System (ILCD) Handbook: general guide for life cycle assessment : detailed guidance.* LU: Publications Office, 2010. [Online]. Available: https://data.europa.eu/doi/10.2788/38479

[40]   G. S. Gilpin, "Introduction to Life Cycle Assessment, lecture material," Bergen, Nov. 10, 2022.

[41]   F. Lai, F. Laurent, A. Beylot, and J. Villeneuve, "Solving multifunctionality in the carbon footprint assessment of primary metals production: Comparison of different

approaches," *Minerals Engineering*, vol. 170, p. 107053, 2021, doi: 10.1016/j.mineng.2021.107053.

[42]   R. Heijungs and S. Suh, *The Computational Structure of Life Cycle Assessment*, vol. 11. in Eco-Efficiency in Industry and Science, vol. 11. Dordrecht: Springer Netherlands, 2002. doi: 10.1007/978-94-015-9900-9.

[43]   M. A. J. Huijbregts *et al.*, "ReCiPe 2016 v1.1 A harmonized life cycle impact assessment method at midpoint and endpoint level." National Instutute gor Public Health and the Environment, 2016.

[44]   International Energy Association (IEA), "Coal 2022 Analysis and forecast to 2025." International Energy Association (IEA), Dec. 2022. [Online]. Available: https://iea.blob.core.windows.net/assets/91982b4e-26dc-41d5-88b1-4c47ea436882/Coal2022.pdf

[45]   European Commission, "On the European Hydrogen Bank." European Commission, Mar. 16, 2023. [Online]. Available: https://energy.ec.europa.eu/system/files/2023-03/COM_2023_156_1_EN_ACT_part1_v6.pdf

[46]   International Energy Association (IEA), "Towards hydrogen definitions based on their emissions intensity." 2023. [Online]. Available: https://www.iea.org/data-and-statistics/charts/low-carbon-hydrogen-production-2010-2030-historical-announced-and-in-the-sustainable-development-scenario-2030

[47]   A. S. Leão, D. L. Medeiros, M. A. Santiago, A. O. do Carmo Tavares, H. L. Maranduba, and E. dos Santos Almeida, "Rigorous environmental and energy life cycle assessment of blast furnace pig iron in Brazil: The role of carbon and iron sources, and co-product utilization," *Sustainable Materials and Technologies*, vol. 36, p. e00607, 2023, doi: 10.1016/j.susmat.2023.e00607.

[48]   N. J. Santero, Nicholas Santero, and J. Hendry, "Harmonization of LCA methodologies for the metal and mining industry," *International Journal of Life Cycle Assessment*, vol. 21, pp. 1543–1553, 2016, doi: 10.1007/s11367-015-1022-4.

[49]   J. L. Leal-Ayala, J. L. Martínez-Hurtado, D. Densley Tingley, A. C. Serrenho, and C. F. Dunant, "Technical handbook on zirconium and zirconium compounds 2019." Zircon Industry Association, 2019. [Online]. Available: (available at request)

[50]   Eramet AS, "Grande Côte Opérations, the specialist in mineral sands," *Eramet*. https://www.eramet.com/en/grande-cote-operations-specialist-mineral-sands

[51]   J. Gediga, A. Morfino, M. Finkbeiner, M. Schulz, and K. Harlow, "Life cycle assessment of zircon sand," *The International Journal of Life Cycle Assessment*, vol. 24, pp. 1976–1984, 2019, doi: 10.1007/s11367-019-01619-5.

[52]   ecoinvent database v.3.8, "Ilmenite, 54% titanium dioxide {RoW}| heavy mineral sand quarry operation | Cut-off, U." Switzerland, 2021.

[53]   J. Gediga, "Private communication with the main author of 'Life Cycle Assesment of Zircon Sand', employed at thinkstep AG," Feb. 08, 2023.

[54]   Eramet Titanium and Iron AS, "Communication with specialists at Eramet Titanium

and Iron AS regarding process data," 2023.

[55]   ecoinvent database v.3.8, "Bulk carrier, for dry goods {GLO}| market for bulk carrier, for dry goods | Cut-off, U." Switzerland, 2019. [Online]. Available: https://www.globallcadataaccess.org/transport-freight-sea-bulk-carrier-dry-goods-upr-ecoinvent-36-undefined

[56]   Network for Transport Measures (NTM), "NTMCalc Advanced 4.0." https://www.transportmeasures.org/ntmcalc/v4/basic/index.html#/

[57]   Eramet AS, "Hybrid solar power for Grande Côte Opérations's mineral sands production," *Eramet*, 2021. https://www.eramet.com/en/hybrid-solar-power-grande-cote-operationss-mineral-sands-production

[58]   D. Nayak, N. Ray, N. Dash, S. S. Rath, S. Pati, and P. S. De, "Induration aspects of low-grade ilmenite pellets: Optimization of oxidation parameters and characterization for direct reduction application," *Powder Technology*, vol. 380, pp. 408–420, 2021, doi: 10.1016/j.powtec.2020.11.018.

[59]   D. G. Jones, "Kinetics of gaseous reduction of ilmenite," *Journal of Applied Chemistry and Biotechnology*, vol. 25, pp. 561–582, 1975, doi: 10.1002/jctb.5020250802.

[60]   S. Lobo, L. Kolbeinsen, and S. Seim, "Reduction of Norwegian and Indian ilmenite with carbon monoxide and hydrogen gas blends," *Canadian Metallurgical Quarterly*, vol. 55, pp. 455–462, 2016, doi: 10.1080/00084433.2016.1206291.

[61]   "Method for Producing Titanium oxide-containing Slag and Pig Iron from Ilmenite and Plant"

[62]   E. Genderen, M. Wildnauer, N. Santero, and N. Sidi, "A global life cycle assessment for primary zinc production," *The International Journal of Life Cycle Assessment*, vol. 21, pp. 1580–1593, 2016, doi: 10.1007/s11367-016-1131-8.

[63]   Z. Z. Fang, F. H. Froes, and Y. Zhang, *Extractive Metallurgy of Titanium: Conventional and Recent Advances in Extraction and Production of Titanium Metal*, vol. 1. USA: Elsevier, 2019.

[64]   "Ohm's law," in *A Dictionary of Physics*, Oxford University Press, 2009. [Online]. Available: https://www.oxfordreference.com/display/10.1093/oi/authority.20110803100247443;jsessionid=BC67A8951024C8298F1CE285DA7A6798

[65]   L. Shoko, J. P. Beukes, and C. A. Strydom, "Determining the baking isotherm temperature of Söderberg electrodes and associated structural changes," *Minerals Engineering*, vol. 49, pp. 33–39, 2013, doi: 10.1016/j.mineng.2013.04.015.

[66]   Lungmuß, "Taphole Clays for Submerged Arc & Shaft Furnaces." Lungmuß Feuerfest, 2014. [Online]. Available: http://www.envicomab.com/wp-content/uploads/2014/08/Lungmuss-Taphole-Clays-for-SAF-May-2014.pdf

[67]   T. Heck, "Heat, district or industrial, natural gas {Europe without Switzerland}| heat production, natural gas, at industrial furnace low-NOx >100kW | Cut-off, U." Switzerland.

[68]   J. C. Koj, C. Wulf, A. Schreiber, and P. Zapp, "Site-Dependent Environmental Impacts of Industrial Hydrogen Production by Alkaline Water Electrolysis," *Energies*, vol.

10, Art. no. 7, 2017, doi: 10.3390/en10070860.

[69]   IRENA, "Hydrogen from renewable power: Technology outlook for the energy transition." International Renewable Energy Agency, 2018. [Online]. Available: https://www.irena.org/-/media/files/irena/agency/publication/2018/sep/irena_hydrogen_from_renewable_power_2018.pdf

[70]   C. Antonini, K. Treyer, A. Streb, M. van der Spek, C. Bauer, and M. Mazzotti, "Hydrogen production from natural gas and biomethane with carbon capture and storage – A techno-environmental analysis," *Sustainable Energy Fuels*, vol. 4, pp. 2967–2986, 2020, doi: 10.1039/D0SE00222D.

[71]   Y. Chen and H. Ahn, "Feasibility Study of Vacuum Pressure Swing Adsorption for CO2 Capture From an SMR Hydrogen Plant: Comparison Between Synthesis Gas Capture and Tail Gas Capture," *Frontiers in Chemical Engineering*, vol. 3, pp. 1–11, 2021.

[72]   M. Faist Emmenegger, "Natural gas, high pressure {NO}| petroleum and gas production, off-shore | Cut-off, U." 2017.

[73]   K. Volkart, C. Bauer, and C. Boulet, "Life cycle assessment of carbon capture and storage in power generation and industry in Europe," *International Journal of Greenhouse Gas Control*, vol. 16, pp. 91–106, 2013, doi: 10.1016/j.ijggc.2013.03.003.

[74]   The World Business Council for Sustainable Development (WBCSD) and World Resources Institute (WRI), "A Corporate Accounting and Reporting Standard," The World Business Council for Sustainable Development (WBCSD) and World Resources Institute (WRI), 2014. [Online]. Available: https://ghgprotocol.org/sites/default/files/standards/ghg-protocol-revised.pdf

[75]   L. Klaaßen and C. Stoll, "Harmonizing corporate carbon footprints," *Nat Commun*, vol. 12, Art. no. 1, 2021, doi: 10.1038/s41467-021-26349-x.

[76]   ecoinvent database v.3.8, "Electricity, low voltage {RoW}| electricity production, photovoltaic, 570kWp open ground installation, multi-Si | Cut-off, U." Switzerland, 2015.

[77]   ecoinvent database v.3.8, "Heat, district or industrial, natural gas {Europe without Switzerland}| heat production, natural gas, at industrial furnace low-NOx >100kW | Cut-off, U." Switzerland, 2010.

[78]   Statistics Norway (SSB), "Emission factors used in the estimations of emissions from combustion." Statistics Norway, Nov. 2021. [Online]. Available: https://www.ssb.no/_attachment/404602/

[79]   R. Bhandari, C. A. Trudewind, and P. Zapp, "Life cycle assessment of hydrogen production via electrolysis – a review," *Journal of Cleaner Production*, vol. 85, pp. 151–163, 2014, doi: 10.1016/j.jclepro.2013.07.048.

[80]   C. Koroneos, A. Dompros, G. Roumbas, and N. Moussiopoulos, "Life cycle assessment of hydrogen fuel production processes," *International Journal of Hydrogen Energy*, vol. 29, pp. 1443–1450, 2004, doi: 10.1016/j.ijhydene.2004.01.016.

[81]   V. Utgikar and T. Thiesen, "Life cycle assessment of high temperature electrolysis for hydrogen production via nuclear energy," *International Journal of Hydrogen Energy*,

vol. 31, pp. 939–944, 2006, doi: 10.1016/j.ijhydene.2005.07.001.

[82]   Y. Chen, X. Hu, and J. Liu, "Life Cycle Assessment of Fuel Cell Vehicles Considering the Detailed Vehicle Components: Comparison and Scenario Analysis in China Based on Different Hydrogen Production Schemes," *Energies*, vol. 12, Art. no. 15, 2019, doi: 10.3390/en12153031.

[83]   G. Zhao *et al.*, "Life cycle assessment of H2O electrolysis technologies," *International Journal of Hydrogen Energy*, vol. 45, pp. 23765–23781, 2020, doi: 10.1016/j.ijhydene.2020.05.282.

[84]   K. de Kleijne, H. de Coninck, R. van Zelm, M. A. J. Huijbregts, and S. V. Hanssen, "The many greenhouse gas footprints of green hydrogen," *Sustainable Energy Fuels*, vol. 6, pp. 4383–4387, 2022, doi: 10.1039/D2SE00444E.

[85]   M. Silva and I. S. Modahl, "The inventory and life cycle data for Norwegian hydroelectricity," Norsus AS, Kråkerøy, Open memo AR 01.19, May 2019. [Online]. Available: https://norsus.no/publikasjon/the-inventory-and-life-cycle-data-for-norwegian-hydroelectricity/

[86]   Y. Khojasteh Salkuyeh, B. A. Saville, and H. L. MacLean, "Techno-economic analysis and life cycle assessment of hydrogen production from natural gas using current and emerging technologies," *International Journal of Hydrogen Energy*, vol. 42, pp. 18894–18909, 2017, doi: 10.1016/j.ijhydene.2017.05.219.

[87]   C. Bauer *et al.*, "On the climate impacts of blue hydrogen production," *Sustainable Energy Fuels*, vol. 6, pp. 66–75, 2021, doi: 10.1039/D1SE01508G.

[88]   R. W. Howarth and M. Z. Jacobson, "How green is blue hydrogen," *Energy Science & Engineering*, vol. 9, pp. 1676–1687, 2021, doi: 10.1002/ese3.956.

[89]   "The inventory and life cycle data for Norwegian hydroelectricity," *Norsus*. https://norsus.no/publikasjon/the-inventory-and-life-cycle-data-for-norwegian-hydroelectricity/

[90]   ecoinvent database v.3.8, "Pig iron {RER}| pig iron production | Cut-off, U." Switzerland, 2020.

[91]   World Steel Association, "World Steel in Figures 2021," World Steel Association, 2021. [Online]. Available: https://worldsteel.org/world-steel-in-figures-2021/

[92]   D. Burchart-Korol, "Life cycle assessment of steel production in Poland: a case study," *Journal of Cleaner Production*, vol. 54, pp. 235–243, 2013, doi: 10.1016/j.jclepro.2013.04.031.

[93]   P. Renzulli, B. Notarnicola, G. Tassielli, G. Arcese, and R. Capua, "Life Cycle Assessment of Steel Produced in an Italian Integrated Steel Mill," *Sustainability*, vol. 8, 2016, doi: 10.3390/su8080719.

[94]   ecoinvent database v.3.8, "Electricity, high voltage {NO}| Hydro, reservoir, alpine region | Cut-off, U." Switzerland, 2012.

[95]   ecoinvent database v.3.8, "Electricity, medium voltage {ZA}| market for | Cut-off, U." Switzerland, 2014.

[96]   M. Brander, R. Tipper, C. Hutchison, and G. Davis, "Consequential and Attributional

Approaches to LCA: A Guide to Policy Makers with Specific Reference to Greenhouse Gas LCA of Biofuels," *Ecometrica. Technical Paper TP090403A*, vol. 44, 2009.

[97]   M. Brander and C. Wylie, "The use of substitution in attributional life cycle assessment," *Greenhouse Gas Measurement and Management*, vol. 1, pp. 161–166, 2011, doi: 10.1080/20430779.2011.637670.

[98]   The Norwegian Water Resources and Energy Directorate (NVE), "Where does the electricity come from?," *NVE*, Apr. 2023. https://www.nve.no/energi/energisystem/kraftproduksjon/hvor-kommer-stroemmen-fra/ (accessed May 13, 2023).

[99]   Statnett, "Long-term Market Analysis 2020-2050," Statnett, 2021. [Online]. Available: https://www.statnett.no/globalassets/for-aktorer-i-kraftsystemet/planer-og-analyser/lma/lma-update-2021.pdf

[100]   Our World in Data, "Share of electricity production from renewables," *Our World in Data*. https://ourworldindata.org/grapher/share-electricity-renewables

[101]   O. A. Øvrebø, "Hydrogen: Tyskland får stort importbehov – Norge kan bli viktigste leverandør," *Energy and Climate*, Jan. 18, 2023. https://energiogklima.no/nyhet/hydrogen-tyskland-far-stort-importbehov-norge-kan-bli-viktigste-leverandor/ (accessed May 12, 2023).

[102]   European Commission, "EU Delegated Acts on Renewable Hydrogen," European Commission, Brussel, 2023. [Online]. Available: https://ec.europa.eu/commission/presscorner/detail/en/qanda_23_595